Preparation and characterization of kaolinite-based nanocomposite materials.

Anna Czarnecka

Thesis submitted to the
Faculty of Graduate and Postdoctoral Studies
in partial fulfillment of the requirements
For the M.Sc. degree in Chemistry

Department of Chemistry
Faculty of Science
University of Ottawa

Acknowledgements

I would like to express my gratitude to my research supervisor in Canada, Professor Christian Detellier for his endless patience and help throughout this project. His enthusiasm, incomparable professionalism and outstanding knowledge of the subject have made my studies an enjoyable and truly informative experience.

I would especially like to thank my supervisor in Portugal, Professor Fernando Rocha for his strong support and professional advice concerning chapter 3 of my thesis.

It would not have been possible to realize this research without participation in the Erasmus Mundus program, International Master in Advanced Clay Science (IMACS).

I would like to thank all the members of the Detellier research group, especially Rola Mansa and Gustave Kenne for help and professional discussions.

I would like to thank the members of my committee for taking the time to examine my thesis and partake in my defense.

For my parents, Maria and Andrzej Czarnecki who introduced me to the joy of science from birth, enabling such a study to take place today and supported me each step of the way.

Abstract

A kaolinite-nylon 6 composite was prepared by a polycondensation reaction from 6-aminohexanoic acid (AHA) intercalated in the kaolinite interlayer space. The basal spacing of kaolinite-AHA was 1.47 nm and the basal spacing of the heated products decreased to 1.16 nm. The signals attributed to nylon 6 were detected in the ^{13}C CP/MAS NMR spectra of the heated products. Formation of nylon 6 in kaolinite was confirmed by appearance of IR band due to amide I and amide II.

Sarcosine was intercalated in kaolinite for the first time by guest displacement with methanol from the kaolinite-methanol precursor. The basal spacing of kaolinite-sarcosine was 1.27 nm. This intercalation compound was characterized by NMR, TGA, XRD, and IR.

The physical and chemical properties of natural clay sample from Mirandela formation (Portugal) were determined in terms of external skin treatment. The low CEC 4,45meq/100g is consistent with high content of kaolinite in the sample.

Index of the figures

Abbreviations

AHA- 6- aminohexanoic acid
ATR - Attenuated Total Reflectance
BET-Brunauer- Emmett- Teller method of measuring specific surface area of materials
BSE- Back Scattered Electron
CEC- Cation Exchange Capacity
CP- Cross Polarisation
DMSO- Dimethyl Sulfoxide
DSC- Differential Scanning Calorimeter
DTA- Differential Thermal Analysis
DTG - Differential Thermogravimetric
EDS- Energy Dispersive Spectrometry
FTIR- Fourier transform infrared spectroscopy
FWHM- Full Width at Half Maximum
IA- Index of Abrasiveness
IR- Infrared
IR-TGA- Infrared- Thermogravimetric Analysis
KAHA- Kaolinite- 6-aminohexanoic acid
KAHA STANDARD –Kaolinite -6 – aminohexanoic acid heated under TG
KAHA100°2H- Kaolinite-6-aminohexanoic acid heated under vacuum condition at 100°C for 2h
KAHA150°2H- Kaolinite-6-aminohexanoic acid heated under vacuum condition at 150°C for 2h
KAHA150°C17H- Kaolinite-6-aminohexanoic acid heated under vacuum condition at 150°C for 17h
KAHA180°C18H- Kaolinite-6-aminohexanoic acid heated under vacuum condition at 180°C for 18h
KAHA180°C2H- Kaolinite-6-aminohexanoic acid heated under vacuum condition at 180°C for 2h
KAHA240°C2H- Kaolinite-6-aminohexanoic acid heated under vacuum condition at 240°C for 2h
KAHA250°C- Kaolinite-6-aminohexanoic acid heated under nitrogen condition at 250°C for 2h
KAHA250°Cex- Kaolinite-6-aminohexanoic acid heated under nitrogen condition at 250°C with excess of the acid
KBr-Potassium bromide
kGa-1- Georgia kaolinite from repository
LL- Liquid Limit
MAS- Magic Angle Spinning
Mi- Mirandela
NMR- Nuclear Magnetic Resonance
PI- Plastic Index
PL- Plastic Limit
SE- Secondary Electron
SEM- Scanning Electron Microscopy
SPA- balneotherapy
SSA- Specifc Surface Area

TGA- Thermogravimetric Analysis
TO- tetrahedra and octahedra packet
TOT – tetrahedra- octahedra- tetrahedra packet
WDS- Wave Dispersive Spectrometry
XRD- X- Ray Diffraction

1 Introduction

1.1 Chemistry of clay minerals

Clay minerals are traditionally classified as silicates with layered structure belonging to phyllosilicates group (Bailey, 1980). As an alternative classification, clays belong to hydroxides of silicon, aluminium or magnesium, because content of oxygen in the structure of clays is higher than Al, Si, Fe and Mg (Bergaya and Lagaly 2006). In the past, particle size criteria was taken into consideration as one of the methods to differentiate clay minerals (Pinnavaia 1983). The layered structure of clay minerals is one of the major properties that allows them to be classified as a separate group of silicates. The basic structure of the layer of clay minerals is defined in terms of sheets composed of octahedra or tetrahedra. The sheets may be arranged in several ways to create layers with different compositions and chemical properties. The tetrahedral sheets are composed of tetrahedra consisting of atoms coordinated to four oxygen atoms. Usually the atoms that are coordinated in the tetrahedral sheet are Si^{4+}, Al^{3+} and Fe^{3+}(Brigatti *et al.,* 2006). The tetrahedra are arranged in the sheets in the form of hexagonal nets, which may be deformed. The distance between free oxygen in a net is close to 0.13 nm and this value is close to the O-O distance of a coordination of octahedron 0.14 nm. Therefore the tetrahedral layer fits almost perfectly on the top of octahedral layer. The tetrahedral sheet is connected to the octahedral sheet by apical oxygen atoms. In the octahedral sheet, Al^{3+}, Fe^{3+}, Fe^{2+} and Mg^{2+} are coordinated by hydroxyls and oxygen. The Octahedral sheet is created by edge-shared octahedron.

The different arrangements of the sheets in the layers are the decisive factor in classifying the minerals in groups according to their structural features. In

accordance with the classification proposed by Martin *et al.,* (1991), layers consisting of one tetrahedral sheet and one octahedral sheet are commonly known as TO structured minerals, classified as a 1:1 type of structure. On the other hand, minerals ascribed to the group 2:1 are built from the repetition of TOT units, where octahedral sheets are linked with tetrahedral sheets from the apical and bottom part of the sheets.

1.2 Structural features of kaolinite

Kaolinite, dickite, and nacrite are polymorph which belong to the dioctahedral 1:1 layer structure of clay minerals, with a general composition of $Al_2Si_2O_5(OH)_4$. As a representative of the 1:1 layer structure, kaolinite is built by sequence of layers consisting of tetrahedral sheets and octahedral sheets. Predominance of Al^{3+} in the octahedral sites of kaolinite and low amount of substitutions by Fe^{3+} or divalent ions like Mg^{2+} is the major reason for a low layer charge, which is close to zero (Brigatti *et al.,* 2006). The kaolinite layer is essentially neutral and two continuous layers are linked by hydrogen bonds Al- O-H….Si-O-H. The strength of hydrogen bonds is related to the position and orientation of OH groups in the interlayer space of kaolinite. In kaolinite primitive cell four OH groups connected with octahedral sheet are distinguished. Three of them are located at the inner surface of the layer and one inside the layer (Brigatti *et al.,* 2006). These inner surface OH groups almost perpendicular to the tetrahedral sheet of the next layer form strong hydrogen bonds. If the OH groups are parallel to the layer, they are not involved to the H-bonding with basal oxygen atoms of the adjacent kaolinite layer Akiba *et al.,*(1997).

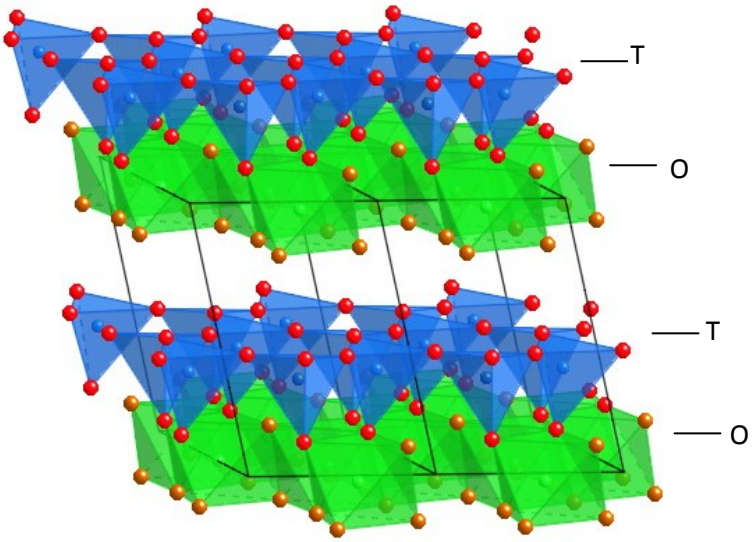

Figure 1 The structure of kaolinite (Si blue, O red, Al green, OH groups light brown, T- tetrahedral, O-octahedral).

Due its structure, kaolinite has some unique properties, such as a small specific surface area (SSA) in comparison to other clay minerals and a low cation exchange capacity (CEC). These two properties influence the adsorption capacity of metals onto kaolinite plates, and relates to the difficulties associated with the modification of pure kaolinite by many organic compounds.

The modification of kaolinite by intercalation or grafting is much more problematic than in smectites due to the low layer charge of the mineral and to the strong interactions, such as dipole-dipole interaction, hydrogen bonds and van der Waals forces between octahedral and tetrahedral sheets. Also, the loss of structural order in kaolinite due to the presence of stacking faults or defects along the *ab* plane and *c* axis is important in terms of future modifications to kaolinite.

1.3 Therapeutic applications of clay minerals

There are a number of health applications of clay minerals. Mixtures of clay minerals or raw materials are used in spa treatments. In aesthetic medicine, some clay minerals are applied, for example, as a treatment of lipodystrophies in their

initial state. In the pharmaceutical industry, clay minerals are used as active substances or excipients. The oral application of clay minerals as gastrointestinal protectors, osmotic oral laxatives and antidiarrhoeaics are examples of the usage of clay as active substances. Additional examples include their use as dermatological protectors or cosmetic agents in their topical application. Kaolinite, smectite, talc and palygorskite are often used as excipients to improve the physical - chemical properties of pharmaceutical agents or to improve drug release properties. Using clays as inert basis' or emulsions in the cosmetic industry is a very well known practice. Moreover, the degradation of drugs in the presence of clay minerals has been observed. Clay minerals mixed with water are used in geotherapy processes in many spa centers. Mixtures of clays with paraffin are called paramuds and are also used in aesthetic medicine. Clay mixed with salty sea water or mineral- medical water and then matured (mixture is prepared for several months before usage) are used in paleotherapy. Even though there are many applications to clay minerals such as in spa treatments and aesthetic medicine, there are still many uncertainties in terms of the classification of materials for potential use in health applications.

1.4 Objectives

Nowadays, spa treatments, natural medicine and eco friendly pharmaceutical products are strongly observed world-wide. However, for many years, the examination and investigation of clay minerals used in natural medicine as geophagy or SPA treatments was not uniform and regulated by international agencies. In the first part of this thesis, the characterization of a clay mineral mixture which may be potentially used for cosmetic applications is thoroughly discussed. The

methods of investigating natural mixtures applied for dermatological use are presented. The results are described with reference to existing publications.

The preparation of a composite material based on nylon- 6 and kaolinite is presented in the second part of this thesis. Many nanocomposites are produced using clays from the smectite group of clay minerals for various applications. Due to difficulties in the modification of kaolinite, examples in literature of composite materials prepared with this particular mineral are significantly lower. Nanocomposites prepared with nylon-6 and montmorillonite have excellent properties allowing for applications in many industries, including the car industry. Therefore, the preparation of such a material using kaolinite as filler may have a future prospective in terms of technological applications.

1.5 Content of the thesis

The thesis present three different aspects connected with application of kaolinite. In the chapter 3 application of raw natural sample which consists mostly of clay minerals including kaolinite is described. The procedures described in that part of the thesis allow to classify the raw mineral sample in terms of usage in external skin treatment. This aspect of the thesis is not related with experimental part concerning modification of kaolinite.

Modifications of Georgia kaolinite KGa-1 sample by intercalation of organic molecules is presented in chapter 4. In this part of the thesis attention is paid for the preparation and characterisation of precursors which may be useful for future polymerization of nylon 6 in the interlayer space of kaolinite.

The third part of the thesis is focused on polymerization of nylon 6 between kaolinite interlayer space. In chapter 5 detailed description of the heating experiments and interpretation of the results are included.

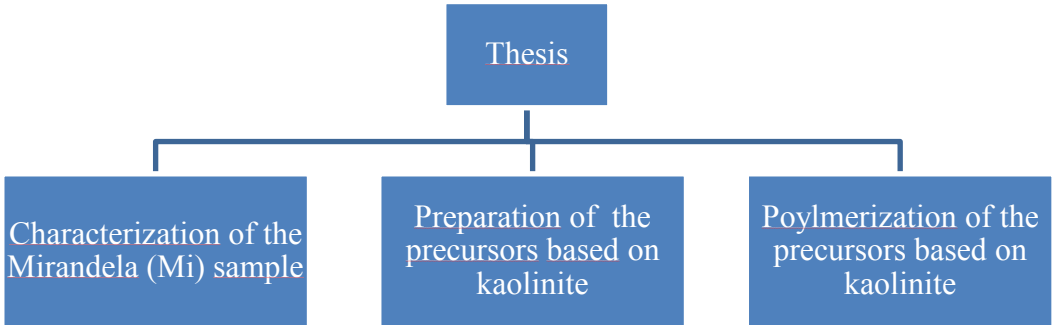

1.6 Contribution of the Author

The XRD patterns and XRF results presented in the chapter 3 were collected by Denise Lara Andrade Gomes de Faria Terroso and Ana Cláudia Moreira Dias. In the SEM investigation presented in chapter 5 Yun Liu, Rola Mansa and Gustave Kenne are involved. The other procedures including collecting of the sample from the outcrop were prepared by the author.

2 Major techniques of characterisation

2.1 X-Ray Diffraction Method

XRD is a basic method for identification of the crystal structure. In this method, powder samples and monocrystals can be identified. The phenomenon which allows for the identification of a variety of materials is the diffraction of X-ray waves on the crystal atom where there can be increased or decreased intensities. This observation is connected with wave theory and has been the starting point for the Bragg equation. Bragg assumed that a crystal consists of some planes of atoms. X-ray waves are reflecting from planes; however, distances between the X-ray source and plane 001 and 002 are different. Due to that, it is possible to define from a geometric equation the distance between plane 001 and 002. This distance is called d-spacing and is characteristic for planes of crystal. Visualisation of the measurements is the diffractogram with reflections from planes. The intensity of those reflections depends on the type of atoms in the plane, diffraction angle, temperature and distribution of atoms in a crystal cell.

XRD is a powerful method for the identification of minerals and other materials, which are characterised by crystal structure (for ex narcotics). The spectra can be obtained from powdered specimen or from a single crystal. In the case of clays, powdered samples are used. Generally, two types of spectra of clays can be obtained. The first is from randomly oriented samples and the second is from oriented samples. Qualitative analysis of clays is possible from both types of samples; however, it is harder to identify clays from randomly oriented powder samples (especially the natural soil samples). Therefore, oriented samples are used for a qualitative analysis. Those spectra provide more detailed information about clay materials. From glycolated oriented spectra, information about the type of materials can be obtained (whether it swells or not, which

can be connected with the chemical composition of material).The heated spectra are also helpful for the identification of clay, because due to high temperature, the crystallinity of the investigated phase changes (ex. kaolinite is transformed to mullite and the peak of the previous phase is not present on the spectra anymore). Moreover, oriented specimens are used for the quantitative analysis of clay samples. The ratio between different types of clay in a specimen is calculated. In some spectra, quantification of di- and trioctahedral types of smectites and micas are possible. Mixture layer of clay minerals are investigated by using the the XRD powder oriented method. To sum up, X-ray diffraction is a method which gives crystallographic data of clay that is needed to perform a detailed identification and quantification.

2.2 Infrared spectroscopy

In spectroscopic techniques the energy differences between ground and excited states are analyzed. In the infrared technique, energy transitions due to the vibration of molecular groups are investigated. The principle of this method is related to changes in the vibration energy level affected by adsorption and emission of incident beam radiation. The energy is related to the frequency or wavelength according to the Planck equation:

$$E = h\vartheta = \frac{hc}{\lambda}$$

Where:

h- Planck constant

λ- wavelength

υ- frequency

c- velocity of the light in the vacuum

In the infrared adsorption spectroscopy, radiation of IR is passed through the investigated sample and the intensity of the transmitted light is measured as a function of wavelength. The adsorption occurs in specific frequencies or wave numbers which correspond to the energy differences between vibration energy levels.

The vibrational behaviors of the crystals, like bond stretching or rotations of molecules are determined by using the infrared technique. Generally, the spectra are in the approximate energy range 0-80 kJ/mol. From the infrared spectra, information concerning structural properties like symmetry, bond lengths, angles, and coordination of polyhedral are given. It is also a helpful technique for the identification of molecules.

2.3 Thermal Analysis

Thermal analysis is the general name for several methods, which are used for the investigation of the thermal properties of material. TGA (thermal gravimetric analysis) measures the amount of the rate of change in the weight of material as a function of temperature or time in a controlled atmosphere (N_2, He, air). The method is used primarily for the determination of the chemical composition of material, because different reactions (such as an oxidation or dehydration) during the heating process up to a temperature of 1000°C can occur. From that method, the thermal stability of the material, chemical composition of clay, oxidative stability and kinetics of the decomposition of clay can be obtained. In addition, the nature of evolving gases can be investigated. TGA is a qualitative and a quantitative method. The changes in weight of the samples during the heating process are related with the emission or absorption of energy and are visualized by endothermic or exothermic peaks of the DTA (differential

thermal analysis) graph. Endothermic peaks are related with the emission of energy to the system (for ex. loss of water during heating), while exothermic peaks are related with needing energy from the system (for ex. phase transition). DTA is a qualitative analysis and changes in the sample are compared with the reference under the same heating conditions. DTA is useful for examining the degradative pathways of a material as both physical and energetic transformations are detectable. The third method is Differential Scanning Calorimetery (DSC), which is used for the determination of organic compounds in the sample. This technique monitors the thermal flux variation of material in comparison to the inert reference (conditions for sample and reference are the same). It is a qualitative and quantitative method. Thermal analysis is an important method for clay identification. The clay composition can be detected from the TGA when percentage weight loss is measured and from the DTA peaks, which are related with different processes during heating. The temperature for changes in the structure of clay and phase transitions will be specified (kinetic of decomposition). The determination of the organic compounds in a clay hybrid material will be possible by DSC.

2.4 Nuclear Magnetic Resonance

The physical phenomena of NMR are connected with the behaviour of magnetic nuclei in a magnetic field. The electrons and neighbouring nuclei in molecules perturb the applied magnetic fields experienced by the nucleus. In the magnetic field, absorption and reemission of electromagnetic radiation from magnetic nuclei take place. Energy in that process is in a specific resonance frequency, which is strictly connected with the strength of the magnetic fields and magnetic properties of investigated isotopes of the atoms. Through that technique, the observation of the quantum mechanical magnetic

properties of the atomic nucleus is possible. In that method, all of the isotopes of elements, which are characterised by non-zero spin quantum number, can be investigated because non-zero magnetic spin isotopes are always associated with non-zero magnetic moments. Therefore, it is possible to produce NMR absorption spectra which are caused by transition between the nuclear spin level (numbers of that level are connected with spin value). However, resonance absorption is only possible when an electromagnetic radiation of the correct frequency is applied to match the energy difference between the nuclear spin levels in a constant magnetic field of the appropriate strength. For obtaining high resolution NMR spectra of solids, magic-angle spinning is applied. The time in which nuclei return to the thermodynamic equilibrium state in the magnet is called T1. T2 is the time in which nuclei stop to produce a signal after returning to the magnetization vector. That time is reversibly related to the width of NMR signal; therefore, if relaxation time is long, sharp NMR spectra will be obtained. Two types of NMR experiment for clay minerals can be done. Liquid NMR method is applied when the chemical relationship between investigated elements (by using isotope) has to be described, or in other words, the type of bonding in which an element participates in. Therefore, that method gives information which depends on the chemical structure of the compound. The second type of NMR experiment is solid-state NMR where the number of lines on the spectra are related to crystal symmetry of the investigated compound. If one element is present on two different positions in the crystal structure, both NMR patterns are present on the spectra. Width of the lines in solid method are sensitive to molecular rotations. Therefore, solid state NMR of clay sample is helpful for the determination of structural tetrahedral or octahedral position of elements (mostly Si and Al) in crystal, which are helpful for clay identification. The cross polarization magic angle spinning (CP MAS NMR) is a major technique used for

acquisition of solid state spectra. In the cross polarization technique, the abundant nucleus is excited, and its energy is then transferred to the nucleus chosen for observation (for example ^{29}Si). This method gives stronger signals than direct excitation.

2.5 Scanning Electron Microscopy

In electron microscopy, the sample is scanned line by line by a focused electron beam, which is emitted by source. During that bombarding by electron beam, the sample emits several types of signals, for example, secondary electrons, backscattered electrons, or X-rays. The electron beam excites atoms of the sample on the surface and below it. Signals, which come from the sample, are registered by detectors and processed as images or spectra. Secondary electrons are punched from external electron layer by electron beam. Those are characterised by low energy, up to 5 eV; therefore, emission takes place from the external layer of sample. SE signal is used for high-resolution imaging and contrast is connected with the topography of the sample. Due to fact that the excitation area is close to the surface, a higher amount of secondary electrons can be obtained from atoms located near to the electron beam. Therefore, the convex part of sample is bright and the concave parts are dark on the image. Backscattered electrons are characterised by high energy from 50eV up to speed voltage of sample. There are beam electrons, which are reflected by sample due to elastic collision with atoms nuclei of sample. In BSE images, contrast is dependent on average atomic number between areas in the sample. More electrons are dispersed by heavy atoms nuclei; consequently, they are visualised as bright spots on the image. X- Ray is created by dispersion of electron beam on atom nuclei or by ionisation of internal electron layers of atoms. Two different methods, which are based on X-ray detection,

can be used for microanalysis: Energy Dispersive Spectrometry (EDS) or Wave Dispersive Spectrometry (WDS). For clay investigation by SEM, secondary electron images can be created. It is possible to present by that method, shape, size, and orientation of clay crystals to compare with scale. That type of imaging is helpful for initial identification of clay. BSE images can be useful if the goal of the experiment is connected with the modification of clays by heavy particles for ex. gold. It is also useful for the investigation of heavy minerals in the clay sample. The microanalysis simplifies the identification of the mineral phase by providing information about the chemical composition of the sample in selected points.

3 Therapeutic application of kaolinite from Mirandela (Mi) formation

3.1 Introduction

Humans have used clays in healing applications for ages. In 1949, the International Society of Medical Hydrology accepted the term 'peloid' which refers to different types of sediments or deposits of mineral substances (ex sulphates or carbonates, clays) and variable amounts of organic substances (Carretero and Lagaly,2007) mixed with spring or sea water for obtaining paste consistency and therapeutic properties (Legido *et al.,* 2007). Nowadays, we can observe a strong trend of the return to natural solutions in the cosmetics industry. Natural muds are popular in spa therapy. They are an important ingredient of facemasks, exfoliation cosmetics, for example feet peeling, anti acne preparations and the majority of mud masks (Carretero and Lagaly, 2007). The use of clays and muds are dependent on their physical and chemical properties like plasticity, grain size, viscosity, abrasiveness, cation exchange capacity, specific surface area, and non-toxic chemical composition (Fakhfakh *et al.,* 2005). This paper presents the properties of the Mirandela (Mi) sample from NE part of Portugal, in comparison to other Portuguese clay samples, which can be used in spa centres.

3.2 Geological setting

Sampling was made near Vila Nova das Patas from the soil bank IP4 motorway (41°30'43''N 7°10'58''W). The outcrop is located in the Bragança district in the NE part of Portugal. This area belongs to Mirandela Depression, which is filled with Cainozoic sediments. (Sample had been taken from the Mirandela formation.) It is not evident that this depression has a simple tectonic origin; it could be created by the lateral erosion of two rivers, Rabaçal and Tuela. However, neotectonic movement was detected on this area (Cabral et al., 1986). These movements are responsible for graben phase. The primary structure of this depression is NS fault of Mirandela, secondary

faults with NNE-SSW directions are in accordance with flow direction of these two rivers and extend of depression. The main rocks, which were eroded or blocked by the tectonic processes, belong to Ordovician quartzites and granites.

Figure 2 Localization of Mirandela sample

The more detailed description of the evolution of the Mirandela depression was prepared by Pereira in her PhD thesis (1997). She suggests that firstly, the formation of the tectonic ridge took place. After very intense sedimentation of Bragança formation in active tectonic conditions, the top part of this formation – Castro layers, had deposited in stable conditions. Due to tectonic tilt, which could be the impulse for the opening of small basins, a new type of sedimentation was started. Mirandela formation had deposited in humid conditions and the thickness was greater than 30m. In the episode, the tectonic tilt was not detected, only the regional uplift had taken place. In the end, depression was balanced by extension and deposition of Avelada formation.

In the Mirandela Depression, Cainozoic sediments are represented by three formations. The oldest one, the Bragança formation (Miocene/Pliocene), consists of two units: bottom Castro and top Atalaia (Pais et al., 2010). It is a red, sandy, and conglomeratic formation with subangular clasts. The sandy matrix is characterized by polimictic coarse grains whereas in the clay fraction, smectite is present (Pereira 1997). In the middle formation of Mirandela, Pliocene age (Pais et al., 2010) has been represented by conglomeratic with quartz clasts, rolled moderately, mainly sandy matrix, quartz-feldspar, mostly pink or brownish color, almost exclusively kaolinite and illite in the clay fraction (Pereira 1997).The thickness greater than 30m suggests strong river environment which had been responsible for deposition. Moreover, a significant amount of kaolinite in the clay fraction can be the result of a strong chemical weathering at the source, which replaced feldspars by clays. The youngest formation in Mirandela depression is Avelada formation (Pliocene/Pleistocene) (Pais et al., 2010). This formation is very thick and difficult for characterization; it was a mostly conglomerate, reddish-brown, predominately quartz and kaolinitic-illitic clay fraction.

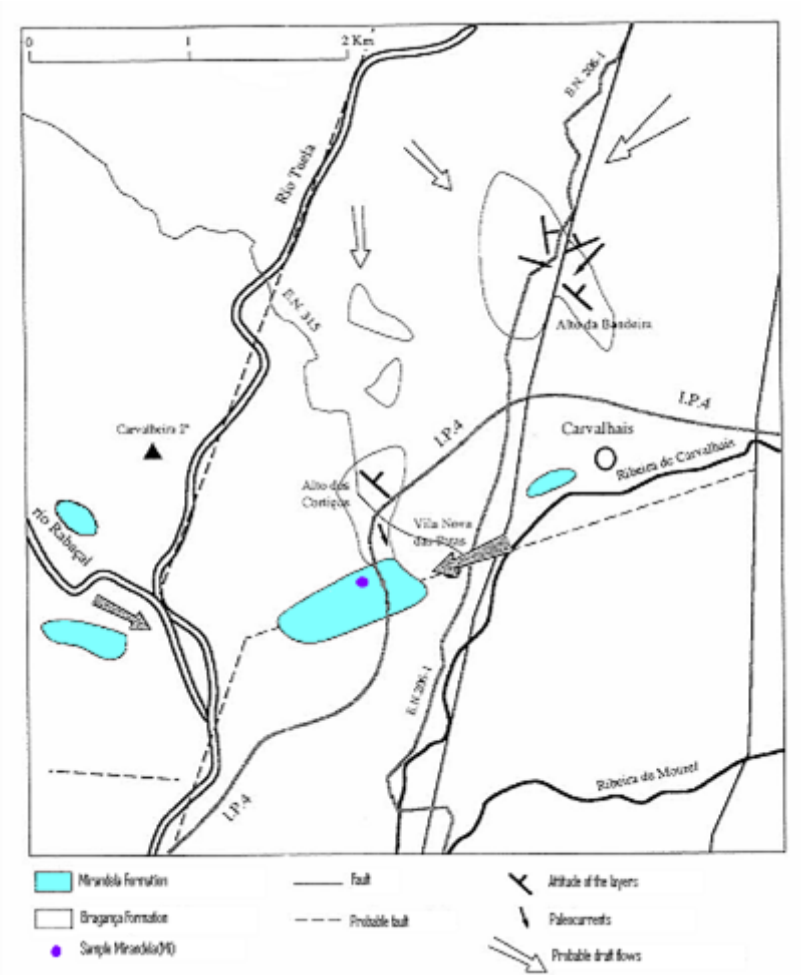

Figure 3 Map of the present localization of sediments from Mirandela Formation in Mirandela depression. (Pereira 1997).

Figure 4 Photo of outcrop Mirandela, formation of Mirandela (Mi).

3.3 Methods, techniques of preparation and procedures

3.3.1 Sieving

Sample was separated into two fractions through wet sieving. At the beginning, 500g of bulk sample is mixed with distilled water until the sample is well disaggregated. Separation of the fine fraction <63µm, from the coarse fraction >63µm, was made by using 63µm sieve. Each obtained fraction was dried and weighed. Consequently, it will be possible to measure the percent content of the fine fraction in bulk sample. The fine fraction was used for all of the chemical and physical analysis. The dried and sieved sample was milled by hand using a ceramic mortar. Attention was paid to using an optimal power and time of grinding.

3.3.2 Grain size distribution

X-ray beam particle size analyzer- Micromeritics® Sedigraph 5100, which measures the gravity-induced settling rates of different particles in a liquid with known properties, was used for determining the grain size distribution. 3g of <63µm fraction and water suspension for the measurement was prepared.

3.3.3 pH measurements

The pH measurement was realised in suspension of clay fraction in water. 10g of clay was mixed with 25ml of distilled water. After one hour with stirring from time to time, the pH value was obtained at room temperature of suspension by using pH meter HANNA HI 9126.

3.3.4 Cation Exchange Capacity

CEC was determined by using the ammonium acetate method. This method should not be applied for samples with acidic pH. 10 g of fine fraction sample was mixed and saturated with 150mL of 1N ammonium acetate by twenty-four hours. After that, the mixture was filtered through Macherey-Nagel MN 640 d filter in vacuum

conditions. Ethanol was used to wash the sample from an excess of ammonium. The sample should be washed to remove any trace of ammonium in suspension, which may have passed through the filter. For detection of ammonium, Nessler reagent is used. Then, the sample was distilled with 2g of magnesium oxide and 200ml of distilled water.100g of distillate is collected in the beaker which is filled by 50ml of boric acid and 4 drops of marker (bromocresol green). The obtained solution is titrated by 0,1N of hydrochloric acid drop by drop with continuous stirring up to the point when the blue color turns into green. The amount of HCl which was used for titration is approximately the CEC value:

$$\mathrm{CEC} = \frac{\mathrm{X} \times [\mathrm{HCl}]}{\mathrm{m}} \times 100$$

X -quantity of HCl used for titration (ml) [HCl] -concentration of hydrochloric acid

m -weight of sample (g)

3.3.5 Specific Surface Area

Determination of SSA provides an idea about the size of particles of clay and possible adsorption. Specific surface area was determined by the methylene blue method. This method is ideal for light samples; however, for the reddish brown Mirandela (Mi) sample, this can also be applied. Firstly, a suspension of 3g of clay and 100ml of distilled water was prepared. After using ultrasound for 2 minutes, 5 ml of suspension was measured by pipette 3 times and put into 3 beakers, which were put into the oven for drying and obtaining an average mass of 5ml of suspension. Into 3 test tubes, 5ml of suspension and 1 drop of ethylene blue (0,01M) were placed. Ultrasound was used to homogenize the suspension by 30 seconds. Test tubes were centrifuged for 10 minutes at 3000 rpm. Next, examination of the color was made. If water was clear the test had to be repeated, but when the water was bluish the test was over. SSA is calculated from formula:

$$SSA=\frac{V_{mb}}{M_{average}}\times 6{,}45[m^2/g]$$

Where:

V_{mb} -volume of methylene blue measured by pipette (one drop 0, 05 ml)

$M_{average}$ -average mass of 5ml of clay suspension

3.3.6 X-Ray Diffraction

X- Ray diffraction patterns were obtained by using a Phillips X'pert diffractometer. In the measurements, Cu-Kα radiation was utilized. Randomly oriented spectra were prepared from <63μm fraction. This type of preparation allowed for the identification of mineral composition. For a better inspection of clay minerals, oriented spectra were prepared. The method which was used for obtaining oriented slides with the <2μm fraction consisted of the preparation of clay water suspensions. After stirring by ultrasound (approximately for 2 minutes) and a 20 minute break (time for the sedimentation of bigger grains from fraction <63μm), sample was deposited carefully on glassy plate, by using pipette. Three types of oriented sample spectra are obtained: air dried, saturated by glycol, and heated at 500°. Orientated spectra were used for the quantitative analysis of the clay fraction. The obtained oriented spectra were quantified by measuring diagnostic peak areas, which were determined by considering the full width at half maximum (FWHM), and then weighted by empirically estimated factors by Chung (1974).

3.3.7 X-Ray Fluorescence

Determination of the chemical composition of samples that were formed into pills by a press was obtained by a Philips PW1404 X-ray fluorescence spectrometer with the flame photometric method. The final result of the measurement of minor elements is presented in oxides formula, and the concentration of trace elements are expressed in ppm.

3.3.8 Atterberg limits

The plastic and liquid limits were measured according to Portuguese norms. The plastic limit was determined from cracked pieces of the rolls of fine fraction of clay which were formed by hand at 3 mm of diameter. The liquid limit was obtained by the Casagrande cup method. Each test was performed four times and samples with different water content were dried at 105°C for 24 hours. The difference between the liquid limit, which is defined as the humidity of the sample for 25 counts, and plastic limit gave the plasticity index. It also gave an idea about the mineral composition of the fine fraction of clay.

3.3.9 Cooling time

The cooling time is defined as the period of time in which the sample decreased in temperature from 65°C to 28°C. For these measurements, 100g of dried sample were placed in the oven for 12 hours. After that, by using a Dual Thermometer LT Lutron TM-906A, the temperature was controlled every 30 seconds. The position of wire in the sample had to be more than 1cm below the surface of sample, which was very important. The final result of the experiment is presented as diagram of cooling time.

3.3.10 Swelling test

The swelling test was prepared according to Portuguese norm for soil consistency. 80 g of fine fraction was dried in the oven and placed in oedometer, which measured the vertical change of sample caused by swelling effect. Sample was firmed and compacted; excess of clay was removed by a spatula. Oedometer consisted of two metal rings with different heights, the thicker ring is filled with clay. Only the measurement of free swelling was performed. The swelling test with load wasn't performed. In the experiment, distilled water was used and pure filter with normalized porosity. The change of volume was measure by gauge.

3.3.11 Abrasiveness

Measurement of abrasiveness has been done by the Einlehner Abrasion Tester. The final result is obtained by the difference between the initial mass and the final mass of bronze mesh. This element is destroyed during measurement by rotation of small element covered by PCV and immersed in clay suspension. The suspension was prepared from 50g of sample and 500ml of distilled water. It was stirred several minutes and dispersed by ultrasound optionally. Experiment was been done for 7250 numbers of rotation in constant speed. Therefore, according to the formula from protocol, normalization for 174000 rotations has to be done. Index of abrasiveness was calculated from formula:

$$\mathrm{IA} = \frac{\mathrm{Wi} - \mathrm{Wf}}{(305 \times 10^{-6})}$$

Where:

Wi- initial mass of mesh

Wf- final mass of mesh

Numbers of denominator represent mesh area

3.4 Results

3.4.1 Granulometry

The content of <63µm fraction in Mirandela (Mi) sample is almost 69%. This value was calculated after sieving the raw sample into portions of coarse fraction and fine fraction. The more detailed data concerning the fine fraction was obtained from Sedigraph 5100.

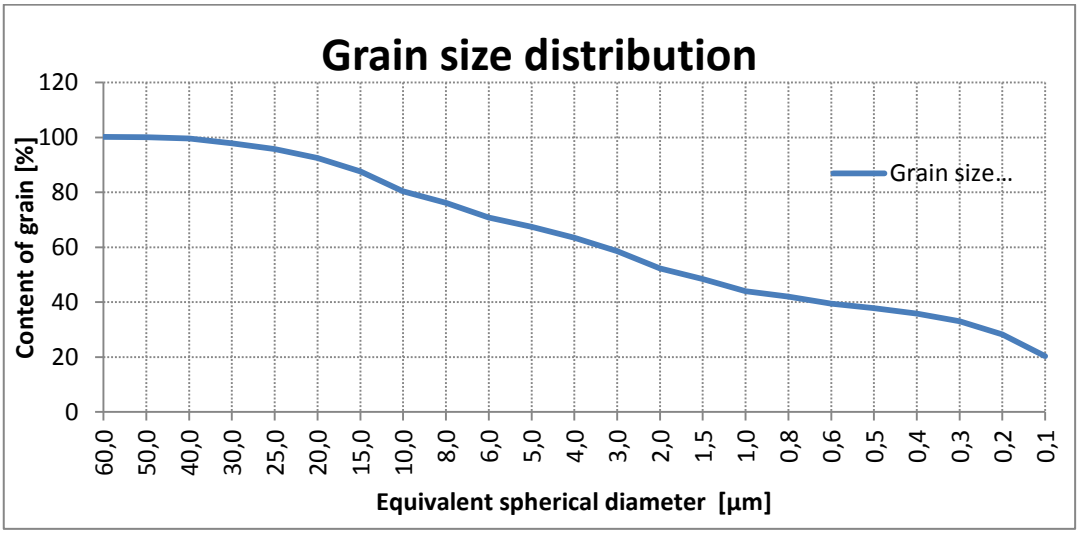

Figure 5 Grain size distribution diagram

In the fine fraction, 44% of grain with diameter ≤ 1µm is present. The high content of the smallest grain (colloidal) is connected with plastic properties of sample (Migas 2008). 52. 3% of fine fraction can be classified like clay fraction (diameter ≤ 2µm). Rest of grains are in silt fraction. Median diameter of grain 1, 7µm indicated also that content of clay fraction is high. Modal diameter of grain indicated that grains with diameter 8, 17µm are the common ones in the sample.

3.4.2 pH measurement

The value of pH 7, 53 for Mirandela (Mi) sample was obtained at a temperature of 24,8°C. Slightly basic pH is typical for other portuguese Cainozoic clays.

3.4.3 Cation Exchange Capacity

CEC gave information about the total amount of cations that were adsorbed. Adsorption can take place on external surface (basal surface) of clay, edges and in the interlayer space. A very low value, which was obtained for Mirandela (Mi) sample suggests that adsorption was not possible in the interlayer space. In other words, 4,45meq/100g value is the result of adsorption by edges or basal surface. Morel (1996) prepared some tables with CEC values of clays. Range between 5-15 meq/100g was ascribed to kaolinite. In the other publication, lower values of CEC were presented. Ma and Eggelton (1999) studied CEC of several kaolinite samples from Australia and New Zealand. The differences between CEC values were connected with the purity of materials and grain size. In kaolinite, the CEC value depends on pH because edge and basal adsorption that are present here are determined by the amount of negative charges on the external surfaces. When pH is alkaline, more negative charges on the basal surface is created (Ma and Eggelton 1999). In the case of illite, the same mechanism of adsorption is dominant (but adsorption by interlayer space is possible). Morel (1996) presented range between 10-40 meq/100g as CEC values for illite. For smaller particles of the same materials, CEC should have higher value than for larger ones because more edge surfaces will be present in small particles.

3.4.4 X-Ray Fluorescence

Fe_2O_3	TIO_2	CaO	K_2O	Cl	SO_3	P_2O_5	SiO_2	Al_2O_3	MgO	Na_2O	LOI	
6,29	0,94	0,13	3,59	0,03	0,03	0,09	54,89	25,62	1,5	0,35	6,32	%

Figure 6 Major elements proportion in Mirandela (Mi) sample

In the Mirandela (Mi) sample, a low content of Na and Ca was detected in comparison to iron oxide value. Usually Na and Ca that can be connected with major minerals like feldspars or carbonates are present in higher abundances. A significant concentration of Fe in the sample is an indicator of the presence of some iron minerals like goethite or hematite and clays with high Fe content-some illite. Silica content is connected with quartz, feldspars, and phyllosilicates. A rather high amount of K suggests the presence of potassium feldspar and some illite. Content of trace elements in the sample is also interesting. A significant concentration of metals like Cr, Ni, and Pb is observed. Also elements like Y, U, and Th are present in Mirandela (Mi) sample. A high content of barium was also detected. The table below presents the chemical composition and content of trace elements in Mirandela (Mi) sample.

Proportion of trace elements in the sample Mirandela in ppm									
Sc	**V**	**Cr**	**Mn**	**Co**	**Ni**	**Cu**	**Zn**	**Ga**	**As**
10,1	103,6	87,6	267,8	15,3	56,7	41	155,5	25,4	44,4
Br	**Rb**	**Sr**	**Y**	**Zr**	**Nb**	**Sn**	**I**	**Cs**	**Ba**
4,1	187,8	46,2	51,1	394,6	22,6	7,5	9,2	13,8	775,9
La	**Ce**	**Nd**	**Sm**	**Hf**	**W**	**Tl**	**Pb**	**Th**	**U**
61,3	125,9	53,9	7,5	7	4,4	2,6	50,6	23,4	5,2

Figure 7 Trace elements composition in the sample

3.4.5 X-Ray Diffraction

From random powder diffractogram, the mineral composition of the fine fraction was interpreted. The mineral composition of the sample is presented in the table below. The main minerals in the <63µm fraction belong to the phyllosilicate group (4,45Å 19,94θ) and were described in more detail from oriented powder section. Moreover, a significant amount of quartz (3,34Å 26,67θ) was detected. Minerals belonging to the feldspar group (3,21-3,18Å 27,78-27,98θ) are also present. This group is represented mostly by potassium feldspar which is consistent with chemical analysis. Some not well crystalline minerals, like opal (4,03Å 22,08θ) was found. In addition, anatase (3,48Å 25,52θ) and several iron minerals such as goethite (4,16Å 21,33θ), hematite (1,59Å 57,67θ) and siderite (2,78Å 32,11θ) have representation in the sample.

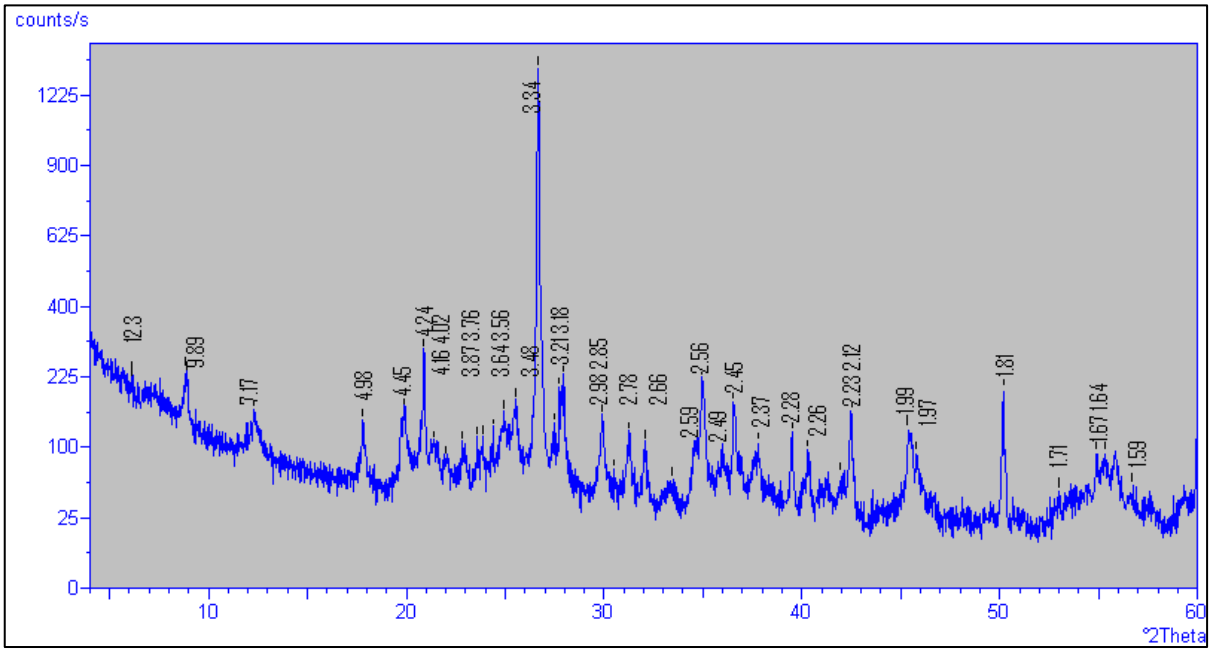

Figure 8 Randomly orientated powder spectra of Mirandela (Mi) sample

The members of phyllosilicates group were identified and described from the oriented diffractograms. Kaolinite was identified on the naturally oriented diffractogram by d-spacing 7,34Å (12,03θ) of symmetrical peak. On the glycolated spectrum, kaolinite peak is moving slightly on 7,30Å (12,10θ). After heating to 500°C, peak from kaolinite has no significant intensity on the spectra- intensity is on 2 % level. Illite was identified on the naturally oriented diffractogram by 001 peak (10,32Å 8,56θ) and 002 peak (5,07Å 17,46θ). After sample saturation by glycol, peak of illite was moving slightly to 10,22Å (8,64θ). During heating process process, illite is stable (10,24Å 8,63θ). Spectra indicated also the presence of mixture layer clay minerals in the Mirandela (Mi) sample. Two peaks from the naturally orientated spectra 001 value (21,02Å 4,19θ) and 003 value (6,00Å 14,75θ) indicate mixture between illite and smectite. After saturation by glycol, 001 peak is moving up to 19,33Å (4,56θ). Smectite is unstable in high temperature; therefore the peak from mixture layer mineral is absent on the heated spectra.

After quantification of phyllosilicates, a group presentation of the mineralogical composition of the Mirandela (Mi) sample is possible:

Mineral composition of Mirandela(Mi) sample in %									
kaolinite	illite	illite-smectite	quartz	feldspars	anatase	hematite	goethite	opal	siderite
37	30	<1	20	5	4	<1	<2	<2	1

Figure 9 Table with mineral composition of the sample

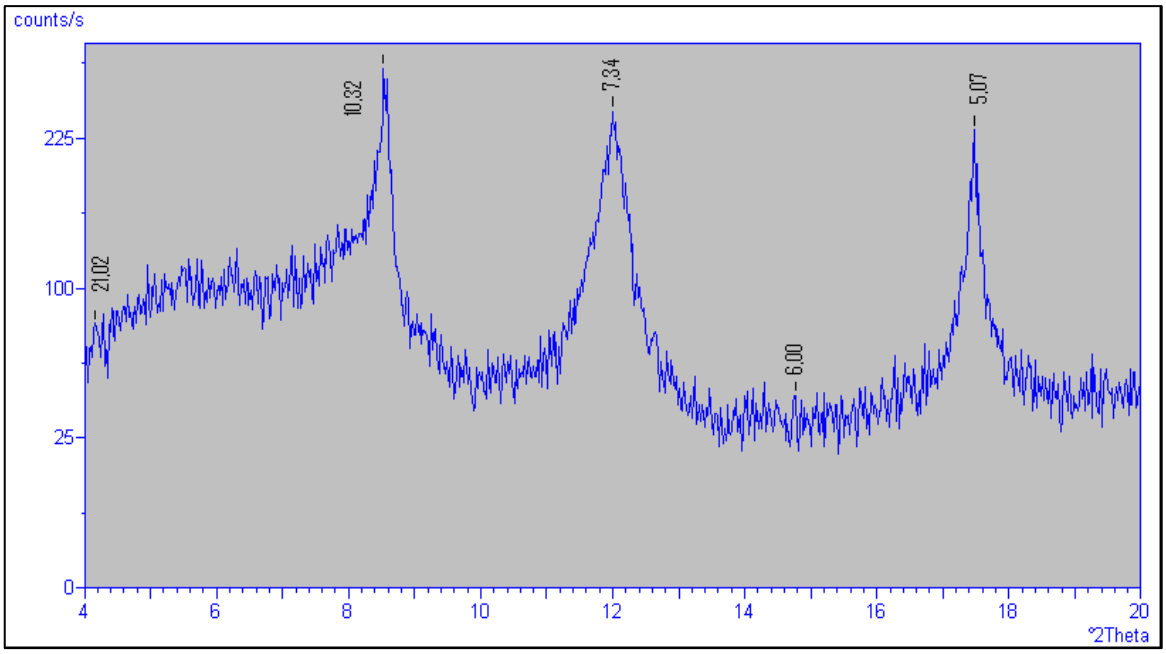

Figure 10 Natural oriented powder spectra of Mirandela (Mi) sample

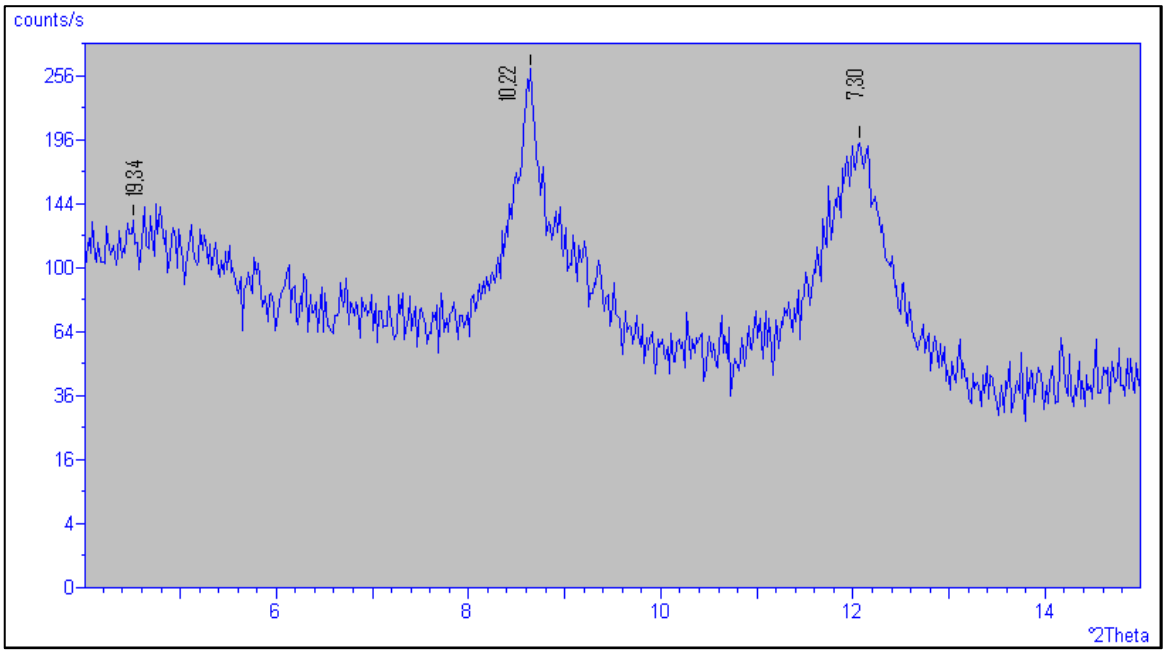

Figure 11 Glycolated powder spectra of sample

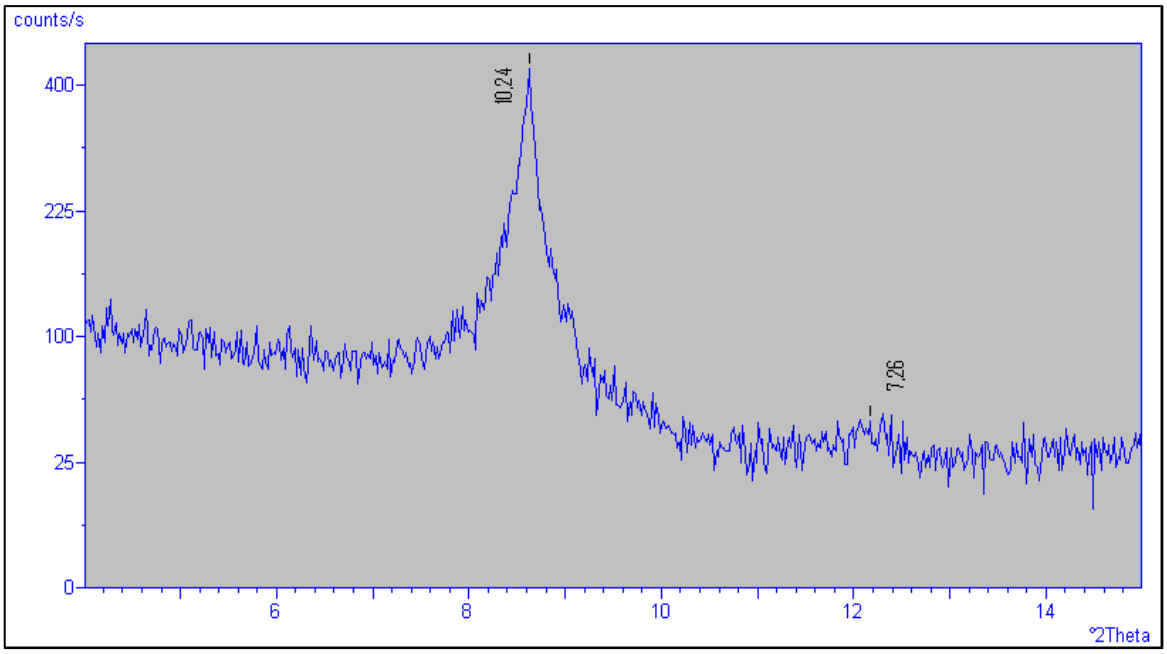

Figure 12 Powder spectra of sample after heating at 500°C

3.4.6 Specific Surface Area

Mirandela (Mi) sample has a brown, reddish colour. Therefore, application of methylene blue method for determination of SSA is not an ideal solution. Obtained value 2.66 m²/g is very low and can be connected with difficulties during examination of water colour after centrifugation. According to Morel (1996), the total SSA for kaolinite should be in the range between 10 and 30 m²/g.

3.4.7 Atterberg limits

Plasticity limit of Mirandela (Mi) sample was determined four times. Average value of humidity for plastic behaviour equals 21%. Liquid limit was also repeated four times and after diagram, the humidity of liquid vs. number of counts was prepared. Average value of humidity for liquid limit is 48%. Consequently, plasticity index has a value of 27. These data enable for classification of Mirandela (MI) sample by using Casagrande chart. The C letter on the diagram is equal to inorganic clay and L, I, H, V, E are contractions from plasticity state (low, intermediate, high, very high, and

extremely high). According to the diagram, plasticity of sample is intermediate (liquid limit between 35 and 50). A-line separates inorganic clay from inorganic silt and organic soil (Bain 1971). Mirandela (Mi) sample is located on the diagram in clay area in the range of value which can be characterized for illite slightly above A-line.

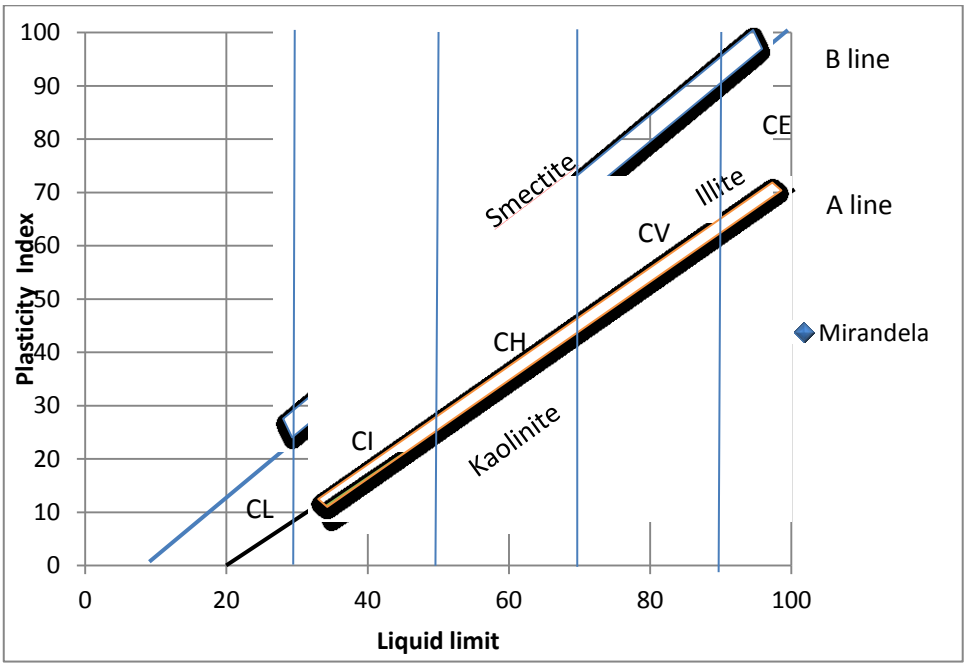

Figure 13 Casagrande chart for determination of plastic behavior and classification of sample

3.4.8 Swelling test

The swelling test for Mirandela (Mi) sample lasted more than two days. After this time, the sample increased in height to 1,36 mm. The final result of this experiment can be described by a swelling potential ε_g equal to 9%. For pure kaolinite, swelling potential has a zero value, as opposed to bentonite, where swelling potential has a high value. Low value of swelling is determined by the high content of kaolinite in the sample. Swelling value for Mirandela (Mi) sample is consistent with CEC value that is also very small and directly connected with the swelling properties of materials. On the

diagram below, the swelling of Mirandela (Mi) sample is presented as a function of time.

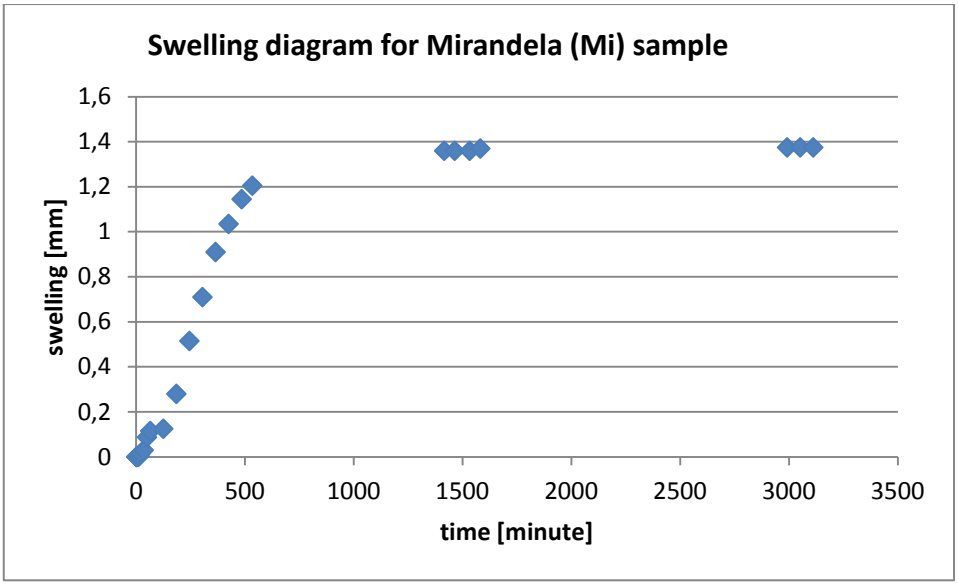

Figure 14 Diagram of swelling for Mirandela(Mi) sample

3.4.9 Cooling time

Mirandela (Mi) sample cooled down from 65°C to 28°C in 52 min. A long time of cooling is directly connected with the chemical composition of the sample. High amount of Fe in goethite and also in clay minerals is responsible for good thermal properties of material. Diagram of cooling over time is presented below:

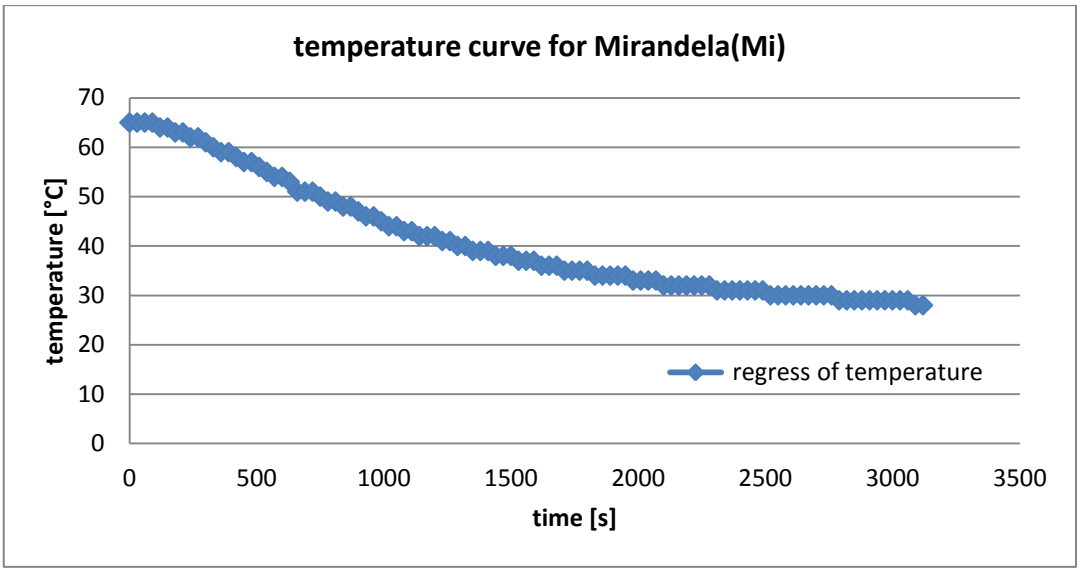

Figure 15 Cooling curve for Mirandela (Mi) sample

3.4.10 Abrasiveness

Result of abrasiveness test for the Mirandela (Mi) sample was obtained for 7250 rotation. Index of abrasiveness is 975 g/m². This high value is connected with the mineralogical composition of the sample. Amount of quartz and anatase in sample is responsible for high value of abrasiveness of the Mirandela (Mi) sample.

3.5 Discussion

Geological materials used for topical application on the skin should be characterized by several properties. Fakhfakh *et al.,* (2005) Carrterro and Lagaly (2007), and Veniale *et al.,* (2007) suggested that samples should be characterized by high SSA and CEC, adequate swelling capacity, plasticity properties, non-toxic chemical composition, cooling index, colloidal behaviour and appropriate grain size.

Veniale *et al.,* (2007) and Rabelo *et al.,* (2011) announced that natural samples which can be used in topical applications have to contain at least 70-80% of clay fraction particles. Quintela *et al.,* (2010) presented data for a Portuguese sample, which had a high content of clay fraction- up to 70%. Mirandela (Mi) sample contains 52% of clay fraction. In comparison with the data mentioned above, this content is too low for topical applications. However, Veniale *et al.,* (2007) sums up that the sample from the Spanish Thermal Centre contained 57-70% of the particles between 2μm-20μm and was successfully applied. Therefore, Mirandela (Mi) sample, which is characterized by a high content of clay and slit, is also an acceptable material.

The mineral composition of the Mirandela (Mi) sample is similar to some samples which were studied by Rebelo *et al.,* (2010). The high content of kaolinite and illite in the Mirandela (Mi) sample determines an application for this material as an exfoliant (Carretero and Pozo 2007). Moreover, a high content of quartz and anatase in the sample counts out other application

The chemical composition of the Mirandela (Mi) sample presents also some similarity to the rest of Portuguese clays described by Rebelo *et al.,* (2011). As for major elements, a high content of silica, aluminium, and variable content of iron oxide is consistent with the chemical composition of Mirandela (Mi) sample. Low content of sodium is also a common property of Mirandela (Mi) sample and materials described by

Rebelo *et al.,* (2011). Trace elements detected in the Mirandela (Mi) sample belong to the fourth class of toxicity (EMEA 2007). In first class A, Pb, Tl, were detected; according to European direction (nr 85/391/CEE, nr 86/179/CEE), these elements have to be absent in cosmetic products, including peloids (Summa and Tateo 1998). Secondly, class 1C of elements which were detected in the sample are elements which have to be limited in cosmetics products like V, Cr, Ni due to significant safety concerns (EMEA 2007). The third group of trace elements detected in the sample belongs to class 1 of metals (Cu, Mn) with low safety concerns. In class 3, Zn was detected as a metal with minimal safety concerns. However, Gomes and Silva (2007) made a note that the elements may be present at toxic or deficient levels in the environment but may not pose a direct risk to health. The best example is content of Cr in mineral, which is not dangerous for health because this element can be adsorbed in bioactive form like vitamin B12 (EMEA 1998). In the case of Cr, the oxidation states of the element determine the toxicity (Gomes and Silva 2007). In other words, the best way for the determination of toxicity is by checking the bioavailability of the elements. The amount or fraction of the element, which is actually available for uptake, is dependent on the concentration of element in the source, particle size and specific physical and chemical properties (Gomes and Silva 2007).

Cation exchange capacity for Mirandela (Mi) sample is consistent with values proposed by Ma and Eggelton (1999). The lower value of CEC depends on the mineralogical composition of sample and grain size distribution; a sample with a big content of sand fraction can influence the CEC (Fakhfakh *et al.,* 2005). High value of CEC is one of the factors which characterizes clays used in spa centres for topical applications. The low CEC determines the application of Mirandela (Mi) sample as an

exfoliant because during the peeling process, removal of the old epidermis can be done without exchanging cations between skin and mud.

Specific Surface Area value for Mirandela (Mi) sample is different from the rest of Portuguese kaolinite sample described by Rebelo *et al.,* (2011). These samples have similar mineral compositions; thus, mistakes during detection are possible. Specific surface area is connected with particle size and influences the plastic properties of sample; therefore, value should be obtained once again in BET method.

Value of pH for Mirandela (Mi) sample is close to neutral value. Moreover, for exfoliation, the substance's pH should be different than skin's acidic pH which varies between 4,5 and 6,5 and depends on many individual factors, for example, the level of hormones or sugar in the blood. In previous literature, it was mentioned that basic pH of skin increases growth of many bacteria (ex *Staphylococcus aureuson*) on the skin, however Schmid-Wendtner and Korting (2006) suggest that also acidic pH substances, including peloids, can provoke growth of many types of different bacteria. To sum up, they suggest to avoid using, for a prolonged period of time, basic soap and acidic syndent because it changes pH of skin and flora of bacteria. Regarding mud bath procedures, cosmetics with skin pH are recommended, (for example, skin lotions with fruit acids should not be used).

Plastic properties of Mirandela (Mi) sample are better than for kaolinite clay sample described by Rebelo *et al.,* (2011). High content of clay minerals and high content of particles lower than 1μm (Migas 2008), which are responsible for good plastic properties, allow the sample to be used in the spa centre (Veniale *et al.,* 2007). Low value of swelling, which is connected with the mineral composition of Mirandela (Mi) sample, is not a disadvantage because this type of material with high kaolinite

content is characterized by good rheological properties which are dependent on particle morphology and surface charge, and allow for its use as a good emulsifying material (ET AL., Carretero and Pozo 2007).

The abrasiveness value for Mirandela (Mi) sample is higher than the 870g/m² value (for 7250 rotation) recommended for topical application by Gomes (2002). The result is the presence of a significant amount of quartz, anatase, and feldspars grains, which can provoke discomfort during application (Rebelo *et al.,* 2010).

Cooling properties of Mirandela (Mi) sample are very good to compare with other Portuguese sample described by Rebelo *et al.,* (2011). High amount of iron in the sample is the reason for a longer cooling time. Fakhfakh *et al.,* (2005) proposed 25'-30' minutes, as a minimal time for cooling that is consistent with time of spa procedure. However, samples with longer times of cooling can be used also as mud compresses which treat rheumatoid arthritis (Codish *et al.,* 2005).

3.6 Conclusions

Mirandela (Mi) sample presents acceptable properties to be used as a peeling and mud compress. Grain size distribution, content of clay in raw sample, cooling time, plasticity, mineral clay composition, and pH do not need any improvements. However, abrasiveness has to be decreased by the separation of quartz and anatase from sample. Moreover, bioavailability and geoavailability of potential toxic trace elements has to be determined. Low value of CEC can be acceptable for above application.

4 Modified kaolinite- introduction

4.1 Introduction

Intercalation reaction consists in the direct or indirect introduction of organic molecules into minerals' crystal structure. In this process, new hydrogen bonds between organic and inorganic molecules are created. The intercalation process is initialized by change of OH group orientation due to the presence of organic molecules adsorbed on the edges of mineral (Lagaly et al., 2006). In the next stage, organic molecules are introduced to the interlayer space of minerals. Consequently, elastic deformation of the interlayer space takes place. The first described layered material with an expanded interlayer spacing due to intercalation by Hofmann and Frenzel in 1930, was a graphite with sulfuric and nitric acid (Ray and Okamoto, 2003). In 1933, Hofman et al. showed that montmorillonite could be intercalated by water molecules which affects the basal spacing.

In comparison with swelling clays, minerals from the kaolinite group were regarded as non- reactive compounds in which the intercalation process did not occur. The situation was completely changed when the first paper describing the successful intercalation of potassium acetate was published by Wada (1961). This was confirmed by an increase of the kaolinite basal spacing to 1.4 nm. Based on Lagaly *et al.,* (2006), molecules able to intercalate directly into kaolinite are divided into three groups:

1. Molecules which are able to create hydrogen bonding. These compounds are characterized by the presence of two functional groups where one is an acceptor of the proton and the second plays the role of the donor like hydrazine, formamide and urea (Olejnik *et al.,* 1971).
2. Compounds characterized by a high dipole moment, like DMSO
3. Potassium, rubidium, cesium and ammonium salts of short fatty acids

A kaolinite-DMSO complex is the most important and frequently used precursor (Olejnik *et al.,* 1968) for modification. This type of complex is used as a starting material for the introduction into kaolinite of other types of molecules which cannot be introduced directly. A good example is the production of mineral-polymer complexes.

In the reaction of grafting, covalent bonding is created between organic molecules and silanol groups and Al-O group of kaolinite. Al-O groups are reactive in the interlayer space of kaolinite, in contrast to the smectite group, where only silanol groups react with organic molecules. A grafting reaction is usually preceded by the intercalation of DMSO or N-formamide molecules. An example was obtained by Tunney and Detelllier (1994) by the reaction of kaolinite with organic liquids such as ethylene glycol or 1,2-propanediol. The same authors described, for the first time, the reaction of methanol with kaolinite in high temperature conditions (1996). Later publications involved the interlamellar grafting reactions of kaolinite with amino alcohols, (Tunney and Detellier 1996), diols (Gardolinski and Lagaly 2005; Murakami *et al.,* 2004), and imides (Elbokl and Detellier 2008).

Due to the structural properties of kaolinite such as the lack of a layer charge and the inability to swell, a direct intercalation of polymers was not possible so far. Therefore, polymerization of the monomer in the kaolinite structure is a method for the introduction of polymers into the kaolinite structure (Elbokl and Detellier 2009; Sun *et al.,* 2010)

Intercalation of two prospective monomers of nylon-6 in the structure of kaolinite was obtained through the preintercalates, such as DMSO and methanol.

Introduction of ε-caprolactam in the structure of kaolinite was reported by Kuroda *et al.,* 1999 and 6-aminohexanoic acid by Matsumura *et al.,* 2001.

4.2 Techniques of characterization

4.2.1 XRD measurements

X-ray diffraction patterns were obtained using a Philips PW 3710 instrument equipped with Ni-filtered Cu-Kα radiation (λ= 0.15405 nm). The measurements of the sample were made under the operating condition 45 kV and 40 mA with step size 0.020 and time/step 0.75 s.

The compounds were investigated under two different preparation techniques. Spectra of powdered non-oriented samples were obtained from samples prepared by overnight air-drying and gentle crushing in the mortar. Then, the fine grained powder was compacted in the sample holder for obtaining flat and smooth mineral surfaces. The second method of XRD sample preparation used for the investigation of modified kaolinite samples consisted of the deposition of the slurry of a sample onto the glass slide and drying at room temperature. This method of preparation allows for the orientation of particles from the investigated compound in the glass slide.

The powdered spectra of the kaolinite organic intercalation compound were scanned in the full range from 2° until 15°. The method and type of samples for preparation of the oriented sample impose scanning from 3°-4° to eliminate low angle uncertainties associated with transition between glass and metal in the sampler.

4.2.2 Thermal Analysis

Thermal investigation of kaolinite intercalation compounds includes differential thermal analyses (DTA) and thermal gravimetric analyses (TGA) which were recorded using SDT 2960 Simultaneous DSC-TGA instrument under N2 flow (100mL min-1) with a heating rate of 10°C min-1. Approximately from 12 to 20 mg of overnight dried ,finely ground powder sample is used for the thermal analyses.

4.2.3 IR Analysis

Infrared spectra were recorded by using a Thermo Nicolet Nexus 670 FTIR spectrometer under dry air with 128 scans at resolution of 4 cm^{-1}. The spectra for kaolinite-sarcosine intercalation compound were collected by using KBr pellets. The rest of precursors were investigated by using attenuated total reflectance (ATR) module which allows one to measure samples in powder state without preparation of pellets with the same number of scans. Between measurements, KBr crystal from ATR module was cleaned by using isopropanol.

4.2.4 NMR characterization

The ^{29}Si and ^{13}C NMR CP/MAS solid state spectra were collected using Bruker Avance III 200 NMR spectrometer.

4.2.5 SEM characterization

SEM images were obtained on a JEOL JSM-7500F FESEM microscope. Secondary Electron Images were obtained with accelerating voltage 2.00 kV and magnification from 9000 to 20 000 times. The samples were coated by carbon film.

4.3 Experimental procedures

4.3.1 Purification

60 g of kaolinite kGa-1 was mixed with 4l of deionized water in the beaker. The mixture was stirred by a magnetic stirrer for 30 minutes. The aim of this procedure is the dispersion of kaolinite aggregates in the water. Purification procedures were based on Stokes' law, where speed of sedimentation depends on the density of minerals, diameter of particles and viscosity of the medium. This formula makes it possible to calculate the time in which the particles of a given size drop at a defined height.

After 21 hours, 30.75 cm from the height of supernatant was gently removed by mouth pipetting. The process is repeated several times with the remaining residue with the addition of deionized water to recover as many fine particles as possible.

Adjusting the pH of the supernatant up to 6 M with 0.1M solution of HCl resulted in the flocculation of suspended clay particles. The excess of water on the top of the flocculated clay is removed by mouth pipetting. The fine fraction of kaolinite is washed with deionized water and centrifuged several times until the removal of chloride ions is confirmed by silver nitrate test.

Purified kaolinite was dried in the oven at 80°C overnight, then crushed and stored for future modification.

4.3.2 Intercalation of DMSO into kaolinite

Several methods of obtaining kaolinite-DMSO intercalated precursors have been developed during the last 50 years (Olejnik *et al.,* 1968). In our case, 10g of purified kaolinite were added to a mixture of 60ml of DMSO and 5ml of water. Then, the suspension was magnetically stirred and heated up to 80°C in the oil bath for 10 days. For the next 5 days, the suspension was stirred continuously without heating. A small percentage addition of water during the process is beneficial for intercalation of DMSO

in the kaolinite structure. However, an excess of water can provoke deintercalation of DMSO. The suspension of kaolinite DMSO was filtrated by using vacuum pump and washed with isopropanol twice. Prepared material was dried overnight in an oven at 60°C and stored for future use.

4.3.3 Preparation of kaolinite methanol intercalated compound

For the preparation of methanol intercalation compound which was reported previously by Komori *et al.,* 2000, DMSO-kaolinite was used as a starting material. 8g of DMSO- kaolinite precursor was mixed with 200 ml of methanol and stirred for 7 days. The solution was replaced by fresh methanol every day. After the reaction of grafting was completed, the wet product was centrifuged to separate kaolinite from the suspension and air dried.

4.3.4 Preparation of caprolactam kaolinite intercalation compound

The successful preparation of a caprolactam-kaolinite intercalated compound was previously reported by Kuroda, 1999. Caprolactam was not intercalated directly to DMSO-kaolinite and this will be discussed in the next chapter. The next reaction is based on methoxy kaolinite, which is an intermediate precursor for introducing caprolactam molecules between kaolinite interlayer spaces.

2 g of air dried kaolinite with grafted methoxy groups in the interlayer space was mixed with a solution made from 6g of caprolactam and 80ml of methanol. Suspension was placed in the beaker and stirred for 2 days. That amount of time is sufficient for intercalation of caprolactam in kaolinite structure and this was confirmed by d-spacing 13.7Å obtained from XRD. That value is similar with 13.1Å obtained by Kuroda, 1999.

When the process is completed, the wet sample was centrifuged and the precursor with an excess of caprolactam on the external surface of kaolinite plates was obtained. After that, the sample was air dried and stored for future use. Several trials for removing the

excess of caprolactam by washing of the precursor were made. Unfortunately, washing with water, ethanol or isopropanol is not accomplished because, during that process, deintercalation of caprolactam from the interlayer space of kaolinite took place. Therefore, caprolactam- kaolinite precursor was used with slight excess of external caprolactam in the sample.

4.3.5 Preparation of aminohexanoic acid (AHA) kaolinite from methoxy kaolinite as the intermediate step

Intercalation of AHA in the structure of kaolinite was previously reported by Matsumura *et al.,* (2001). They used methanol kaolinite as the preintercalated precursor. 12g of AHA was dissolved in 50ml of a mixed solvent of water with methanol in ratio of (3:1). Because aminohexanoic acid is less soluble in alcohol than in water, a mixed solvent was applied for increasing the concentration of acid in the suspension. Then, 4 g of air dried methoxy kaolinite was added to the solution of acid. Obtained suspension was stirred for 3 days without replacing the solvent for fresh. After that, the obtained precursor was centrifuged and washed with ethanol twice to eliminate excess of acid on the external surface of kaolinite platelets.

4.3.6 Preparation of sarcosine intercalation compound from methoxy kaolinite as the intermediate step

Sarcosine was intercalated successfully into the structure of kaolinite for the first time by using methanol kaolinite as the intermediate step. Wet form of methanol kaolinite precursor was used for preparation of sarcosine kaolinite. 6 g of sarcosine was dissolved in 10ml of water and added to the suspension of methoxy kaolinite (ca. 1g) in 50ml of methanol. The obtained mixture was stirred for 2 days without replacing solvent by fresh one. Then, the precursor was centrifuged and washed twice with

ethanol for the removal of the excess of external sarcosine on the platelets of kaolinite. Intercalation was confirmed by XRD test made on orientated slide.

4.4 Resulting and Discussion

4.4.1 DMSO kaolinite precursor

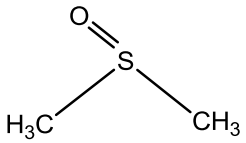

Figure 16 DMSO structure

4.4.1.1 XRD results

Intercalation of DMSO molecules directly into the interlayer space of kaolinite was reported by Olejnik *et al.,* 1968. In the diffractogram, a shift to lower angle of the 001 reflection in comparison with pure kaolinite (0.72 nm) at 1.10 nm is observed. The value is similar to that reported previously (Letaief and Detellier 2009, Tunney and Detellier 1996, Letaief and Detellier 2007, Gardolinski et al., 1999, Letaief and Detellier 2011, Letaief *et al.,* 2008). Also, higher order reflections with d=0.56nm and d=0.37 nm are confirmation of the introduction of DMSO molecules (Matusik *et al.,* 2011). The increase of the interlayer space is due to the separation of the layers, which is related to the keying of one of the DMSO methyl groups in the siloxane rings of the tetrahedral sheets (Letaief and Detellier 2011). The intercalation ratio (IR) of DMSO is based on the respective intensities of the 001 reflection of kaolinite and kaolinite-DMSO. Almost 96% of kaolinite is characterised by introduced DMSO molecules.

Intercalation ratio is calculated from the formula, which is presented below:

$$IR = \frac{I_{DMSO}}{I_{TOT}} \times 100\%$$

Where

IR- intercalation ratio

I_{DMSO}- Intensity of 001 DMSO kaolinite reflection

I_{TOT}- Intensities of 001 reflection from pure kaolinite and DMSO kaolinite which are present in the same sample

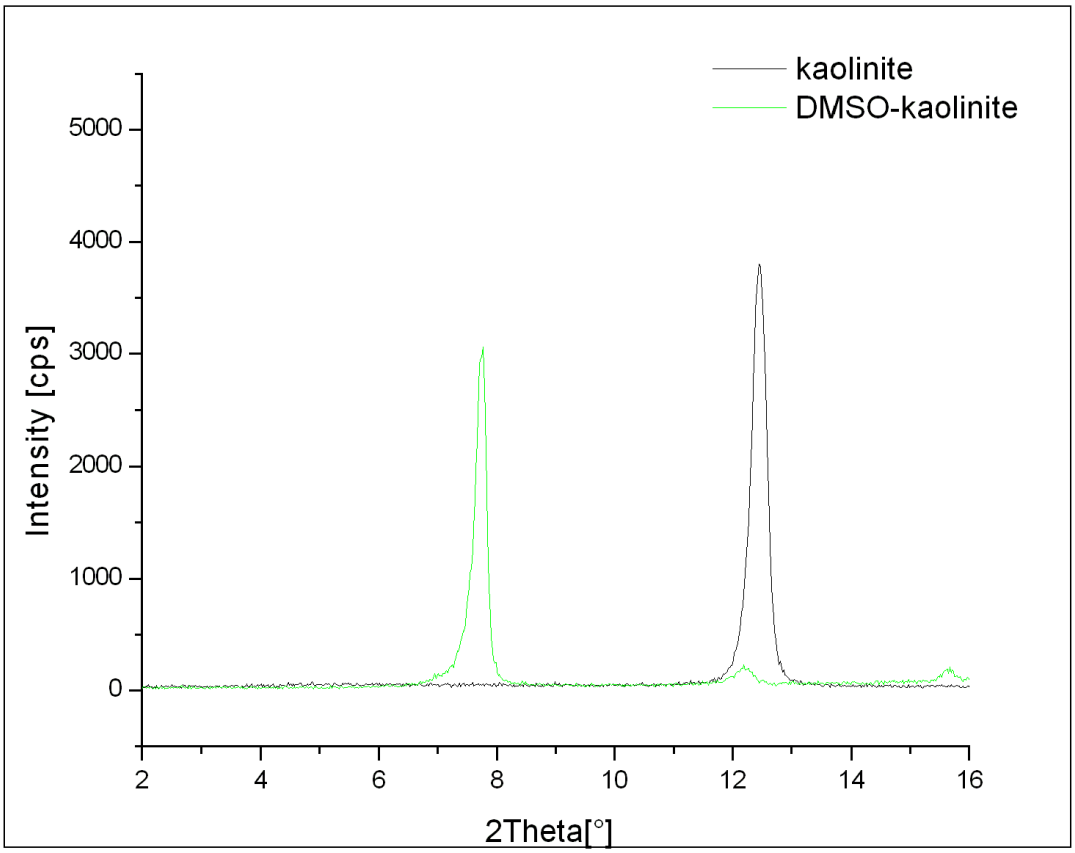

Figure 17 XRD difractogram of pure kaolinite and DMSO-kaolinite

4.4.1.2 Thermal Analysis

The thermal behavior of DMSO-kaolinite is characterized by 27% total mass loss. The total mass loss of pure kaolinite of 14% is caused by the removal of external water and dehydroxylation of the mineral. For pure kaolinite and DMSO-kaolinite, the first mass loss around 43°C corresponded with the removal of externally adsorbed water on the kaolinite platelets. The second mass loss in DMSO-kaolinite diagram with maximum at 181°C is attributed with the removal and decomposition of DMSO (15% with first mass loss) which is consistent with results presented by Letaief and Detellier (2011).This mass loss is assigned to the endothermic peak on the DTA. The third mass loss for DMSO-kaolinite is assigned to the dehydroxylation of kaolinite layers (12%)

with a maximum at 514°C and an endothermic peak on the DTA curve. The dehydroxylation process is also observed in the case of the pure kaolinite sample with maximum at 514°C.Exothermic peak on the DTA curve with maximum at 1000°C is attributed with the transformation of the heated kaolinite to mullite and recrystallization. Once DMSO molecules are removed from the kaolinite structure, the thermal behavior of the sample is identical to that of pure kaolinite and this is attested by the third mass loss and recrystallization above 1000°C.

When the total mass loss observed during thermal treatment of DMSO kaolinite is known, it is possible to calculate the total amount of DMSO loaded on 1 unit structure of kaolinite using the following formula:

$$Total\ amount\ of\ DMSO\ per\ 1\ unit\ structure\ of\ kaolinite = \frac{n_{DMSO}}{n_{KAOLINITE}}$$

Where

$$n_{DMSO} = \frac{m_{DMSO}}{M_{DMSO}}$$

$$n_{KAOLINITE} = \frac{m_{KAOLINITE}}{M_{KAOLINITE}}$$

It corresponds to 0.75mol of DMSO per 1 structural kaolinite unit which is in agreement with value proposed by Letaief and Detellier (2011).

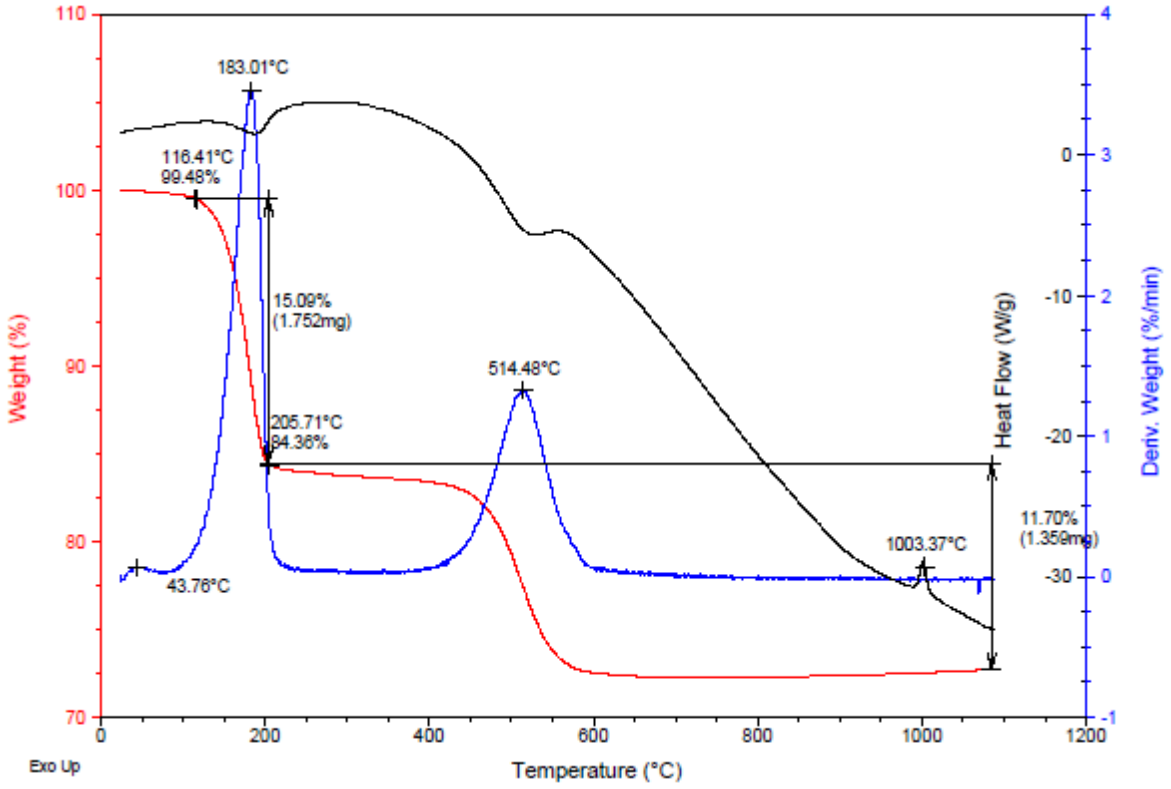

Figure 18 TGA results for DMSO-kaolinite ; DTG blue line, TG red line, DTA black line

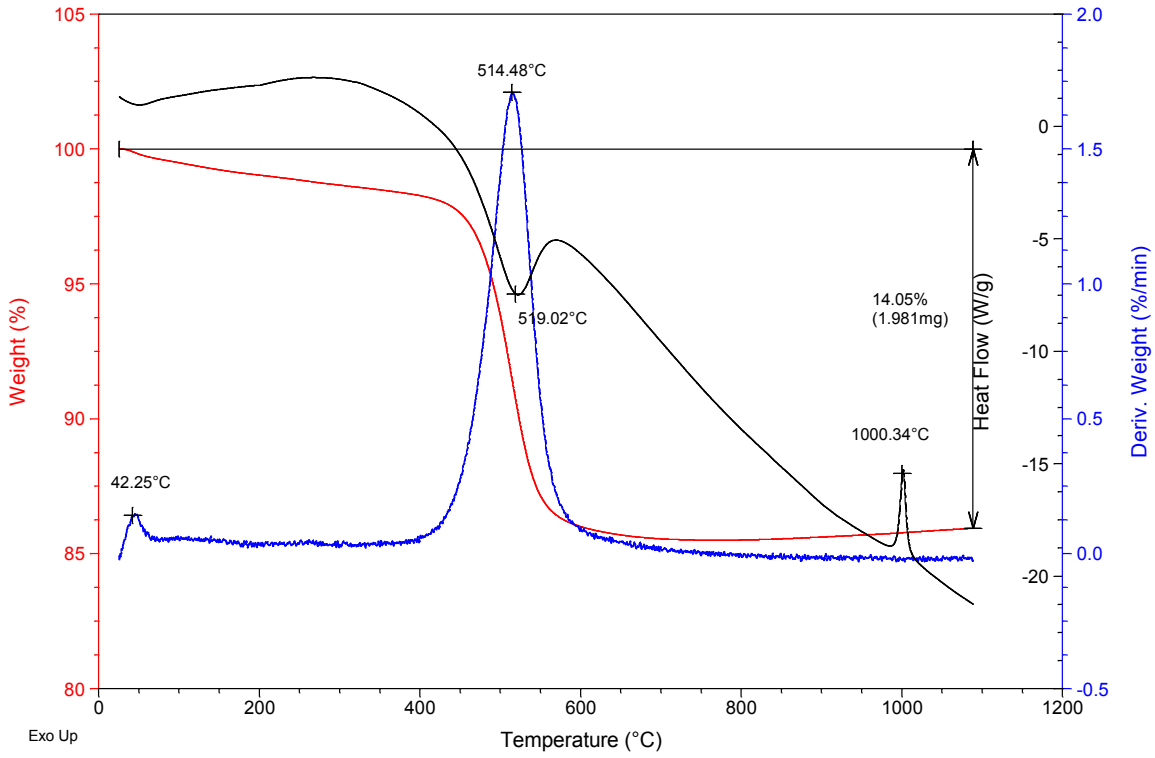

Figure 19 TGA results for pure kaolinite; TG red line, DTG blue line, DTA black line

4.4.1.3 IR study of DMSO-kaolinite

After intercalation of DMSO molecules in the interlayer space of kaolinite, characteristic changes in the OH stretching region were observed. The peaks at 3670 cm^{-1} and 3653 cm^{-1} disappeared completely, while new peaks appeared at 3503 cm^{-1}, 3539 cm^{-1} and 3663 cm^{-1} (Letaief and Detellier 2009). Those bands are ascribed to the perturbed inner surface hydroxyl groups stretching vibration which are bonded to the DMSO molecules (Olejnik *et al.,* 1968). The band at 3695 cm^{-1} is ascribed to the inner hydroxyl surface stretching vibration of pure kaolinite which is present in some quantity in the DMSO kaolinite sample. The band at 3620 cm^{-1} (Frost 1997) is attributed to non perturbed inner hydroxyl stretching vibration because this OH group is not affected by intercalation. Two weak and broad signals around 3000 cm^{-1} may be ascribed to the methyl groups of DMSO (Matusik *et al.,* 2012). In the stretching region of Si-O, occurrence of bands at 1097 cm^{-1}, 1038 cm^{-1} and 1018 cm^{-1} is noticed. Last two bands are shifted to the higher wave numbers in comparison with pure kaolinite where bands are located at 1112 cm^{-1} and 1032 cm^{-1}. In the low frequency region, bands related to the Al-OH deformation vibration occurred at 958 cm^{-1}, 905 cm^{-1}, 686 cm^{-1}, and 605 cm^{-1}. The signal at 905 cm^{-1} is shifted to the lower wave numbers compared to pure kaolinite, which may be attributed with reduced hydrogen bonding of Al-OH (Sato 1999). Band at 552 $cm^{-1}$is attributed with Al-O deformation (Yariv *et al.,* 2000).

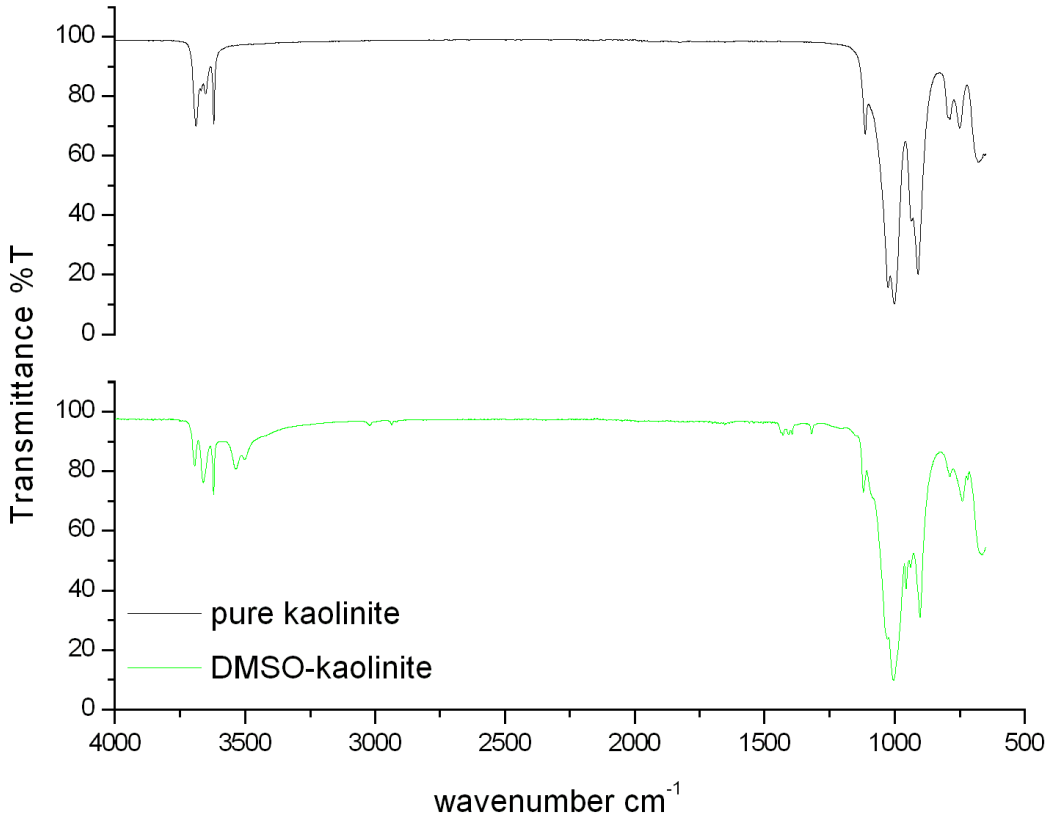

Figure 20 FT-IR spectra of pure kaolinite and DMSO-kaolinite

4.4.1.4 NMR study of DMSO- kaolinite

The ^{29}Si CP/MAS NMR of DMSO-kaolinite is characterized by three signals at -90.89 p.p.m, -91.55 p.p.m, and the most intense at – 92.69 p.p.m. The lower intensity signals are attributed to relation between silicon and oxygen in pure kaolinite, and this is attested by the chemical shift for pure mineral of -91.19 p.p.m (Mackenzie and Smith 2002). New signals shifted to the lower frequencies is related to the keying of one of the DMSO methyl groups in the siloxane rings of the tetrahedral sheets (Raupach *et al.,* 1987; Hayashi *et al.,* 1992; Letaief *et al.,* 2008). Appearance of new signals confirms the intercalation of DMSO molecules to the kaolinite interlayer.

Two signals are present on the ^{13}C CP/MAS NMR of DMSO- kaolinite spectra. Two equally intense carbon methyl signals at 44.06 p.p.m and 42.97 p.p.m are also reported by Letaief *et al.,* (2008), Letaief and Detellier (2009); Letaief and Detellier (2011) and are consistent with the theory of asymmetric localization of DMSO molecules in the kaolinite interlayer space (Hayashi 1997; Bergaya *et al.,* 2006). According to that theory, the asymmetric localization of DMSO molecules may be related to the wobbling motion of one of the DMSO methyl groups keyed into the ditrigonal holes. Keyed methyl groups are released from ditrigonal holes above 320K and that makes DMSO anisotropic rotation enabled (Bergaya *et al.,* 2006).

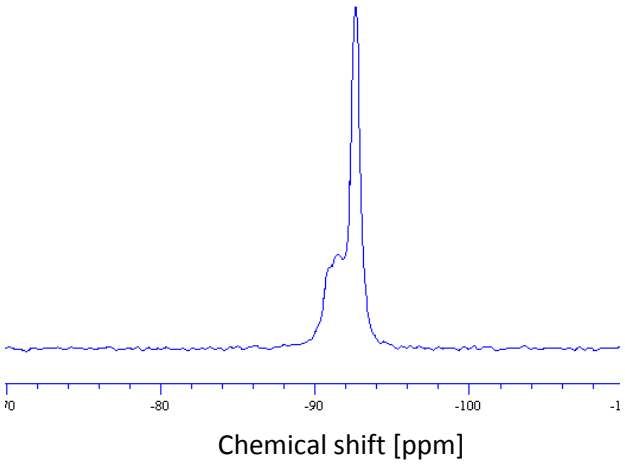

Figure 21 ^{29}Si CPMAS NMR spectra of DMSO-kaolinite

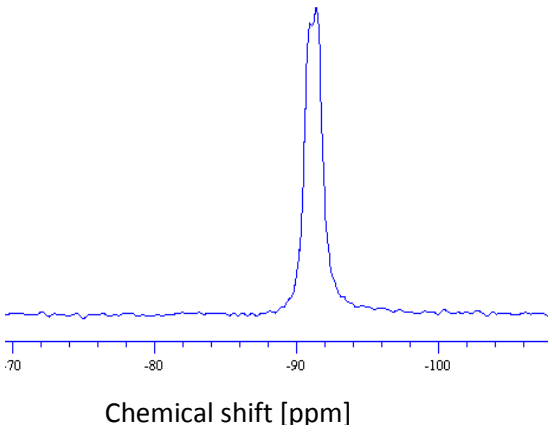

Figure 22 ^{29}Si CPMAS NMR spectra of kaolinite

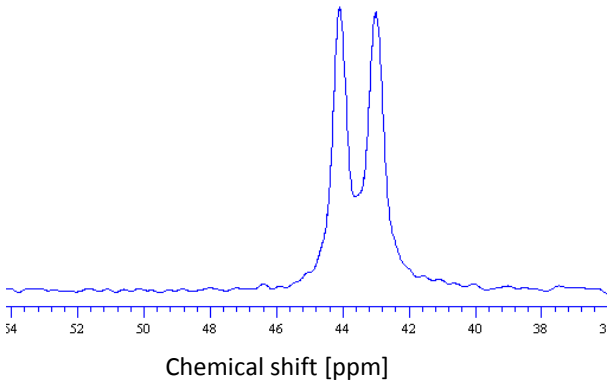

Figure 23 ^{13}C CPMAS NMR spectra of DMSO-kaolinite

4.4.2 Kaolinite-methanol precursor

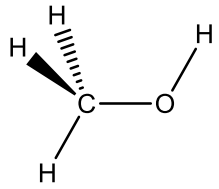

Figure 24 Methanol structure

4.4.2.1 X-ray diffraction

After reaction with methanol, kaolinite is characterized by a new basal spacing of 0.84 nm. The 001 peak is located at 10.56 2θ. The value corresponds with functionalization of kaolinite interlayer space by methanol molecules (Tunney and Detellier 1996). Secondary broad peak 002 from intercalated methanol is located at 21.52 2θ, with d= 0.41 nm. Intercalation ratio for methanol kaolinite is approximately 90% which is consistent with the value obtained by Matusik (2010) and was calculated from the formula presented before for DMSO introduced to the kaolinite structure. Residual untreated pure kaolinite is present in the sample which is attributed to the 001 peak at 12.92 2θ and a basal spacing of 0.72 nm. Secondary peak from pure kaolinite is located at 24.62 2θ with d= 0.36 nm. Absence of peaks related to the DMSO indicated

removal of the molecules from the interlayer space of kaolinite by low temperature methanol treatment.

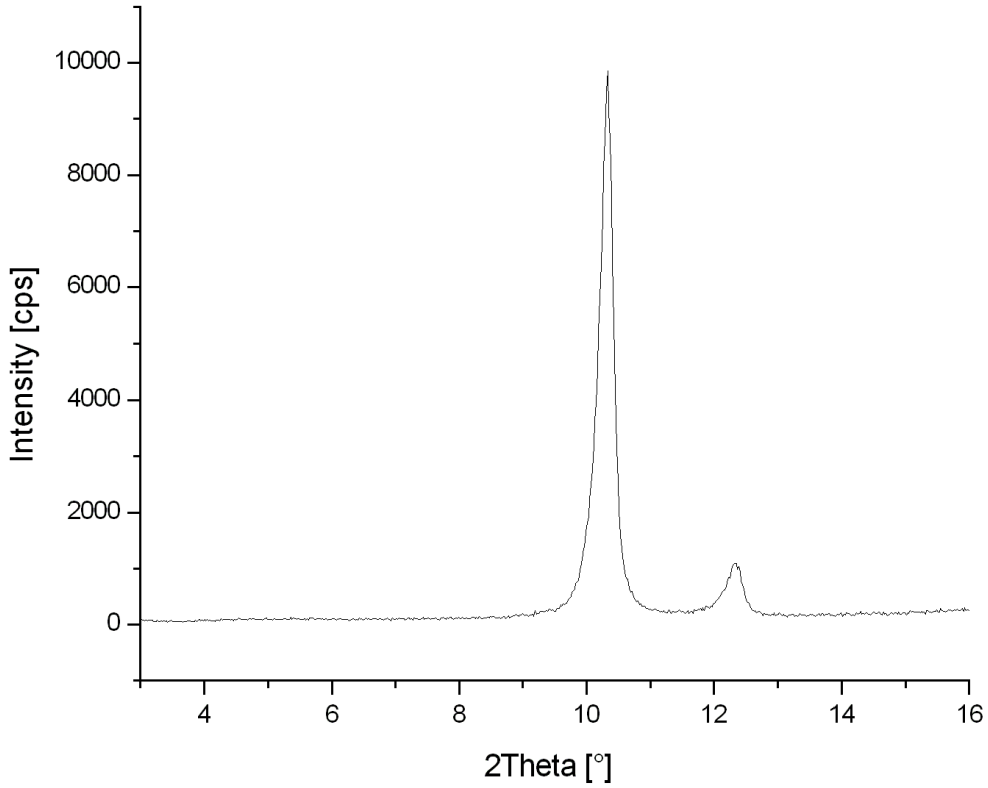

Figure 25 Diffractogram of kaolinite-methanol compound

4.4.2.2 Thermal Analysis of kaolinite methanol precursor

The thermal stability of organokaolinite material obtained by introduction of methanol to the kaolinite structure was quite remarkable. The material did not decompose until above 350°C. Previous mass loss (3.6%) on the TG is associated with removing moisture from the sample as well as externally adsorbed methanol molecules. Second mass loss (13.2%) is related to the decomposition of methanol kaolinite characterized by endothermic peak on DTA at 500°C, which is lower than the dehydroxylation temperature of pure kaolinite (Tunney and Detellier 1996). Lower temperature of dehydroxylation is an attestation of the grafting of methanol molecules in the interlayer space of kaolinite (Letaief and Detellier 2011). Exothermic peak on the

DTA curve at 1005°C is ascribed to a reorganization of the crystalline structure of metakaolinite to mullite which is not associated with mass loss. The total mass loss for kaolinite methanol is 16.8%. From the formula presented before for the kaolinite DMSO precursor, the approximate loading of methanol per 1 kaolinite unit was determined to be 0.51 mol of methanol.

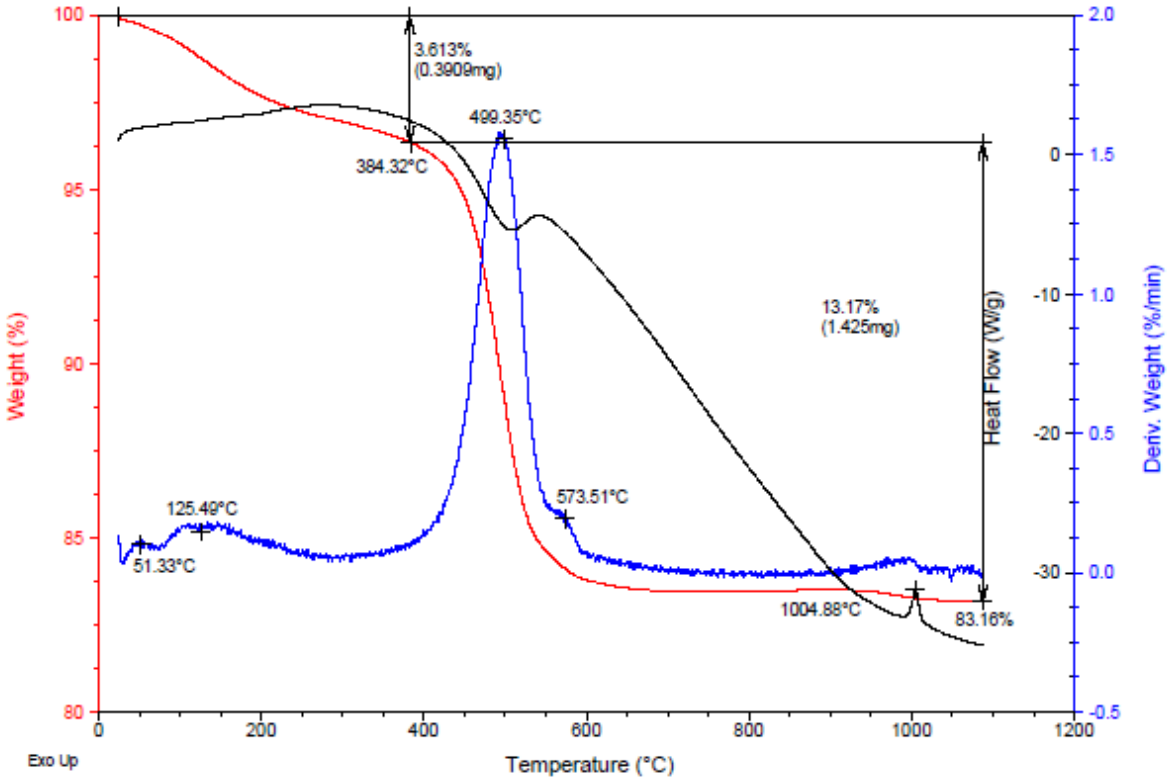

Figure 26 TGA analysis of kaolinite-methanol compound; TG red line, DTA black line, DTG blue line

4.4.2.3 IR study of methanol kaolinite

The major difference between IR spectra of pure kaolinite and methanol-kaolinite is emphasized in the region of OH stretching. The appearance of a band at 3640 cm^{-1} shifted in comparison with 3646 cm^{-1} (Tunney and Deathlier 1996) to the lower wave number is characteristic of methanol – kaolinite. This band is assigned to the OH stretching motion of weakly perturbed surface Al-OH groups. The band at 3691 cm^{-1} is ascribed to one of the stretching modes of the surface hydroxyl groups of

kaolinite. The unshifted band at 3620 cm^{-1} is attributed with inner hydroxyl stretching vibration (Johnson *et al.,* 2008). Broad weak intense band at 3537 cm^{-1} may be ascribed to the externally adsorbed water which is suggested by Tunney and Detellier (1996). Group of broad bands in the region 3300- 2800 cm^{-1} is definitely attributed to methanol. The OH stretching bands from alcohol molecules is visualized by band at 3265 cm^{-1}, whereas bands at 2969 cm^{-1} and 2839 cm^{-1} are assigned to the C-H stretching mode of methanol. Tunney and Detellier (1996), based on publication of Greenler (1962), proposed ascribing those vibration bands to the methoxide group which is evidence of the grafting reaction in the kaolinite interlayer space. Also the bands at 1203 cm^{-1} and 1123 cm^{-1} are attributed to the C-O stretching deformation in methanol molecule. In the region of the spectra assigned to the lattice Si-O, vibration bands at 1038 cm^{-1} and 1004 cm^{-1} are present. Those bands are shifted in comparison with pure kaolinite which was reported by Tunney and Detellier (1996), Johnson *et al.,* (1984). Although low intensity bands related to the Al-OH deformation at 940 cm^{-1} are present, band ascribed to the Al-OH in-plane bending vibration of the inner hydroxyl of kaolinite is shifted from 915 cm^{-1} to 905 cm^{-1}, in contrast to previous publications. New kaolinite bands at 797 cm^{-1} and 744 cm^{-1} appeared. All of the modifications of the bands related to the Si-O and Al-OH vibrations are related to the perturbation of the kaolinite structure due to grafting of the methanol molecule.

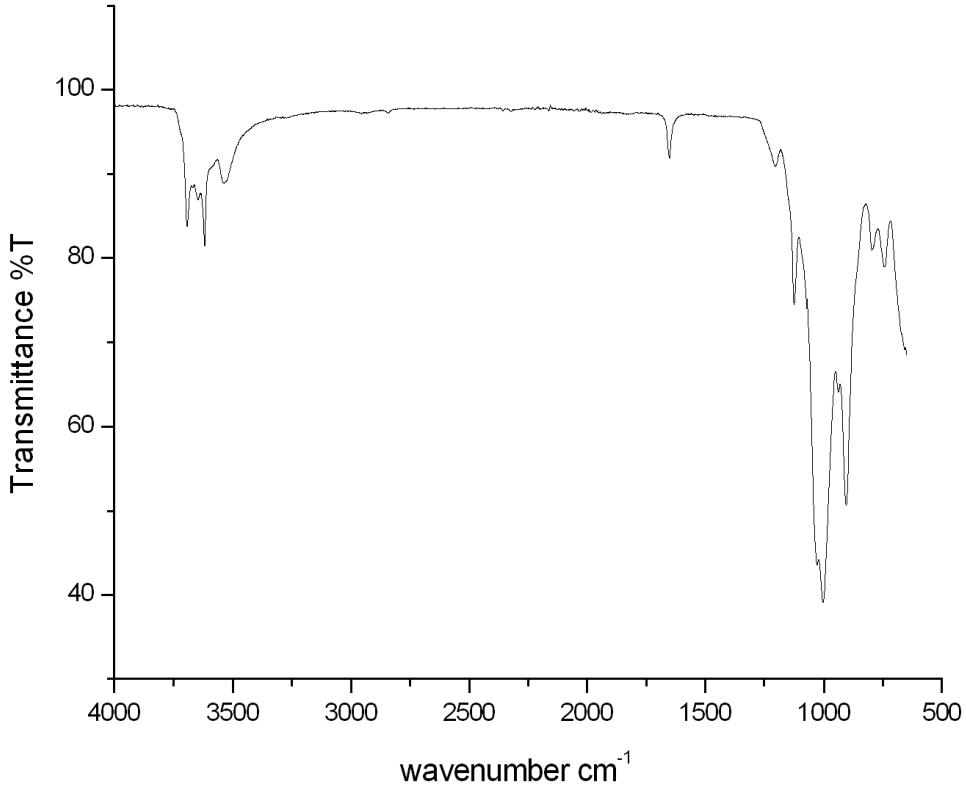

Figure 27 IR spectrum of kaolinite-methanol compound

4.4.2.4 NMR study of methanol- kaolinite

The ^{29}Si CP/MAS NMR spectrum of methanol- kaolinite precursor is characterized by one signal at - 91.67 p.p.m which is shifted in comparison to pure kaolinite NMR spectrum. Appearance of one signal instead of two for methanol-kaolinite is related to the intercalation of molecules in the interlayer space of kaolinite (Bergaya *et al.,* 2006).

Only one resonance is visible on the ^{13}C CP/MAS NMR spectra. A signal at 50.82 p.p.m is slightly shifted downfield in comparison with liquid methanol from 50.41 p.p.m to 48.50 p.p.m (Gottlieb *et al.,* 1997). Appearance of signal at 50.82 p.p.m is connected with functionalization of kaolinite by adding CH_3 group from methanol, and is consistent with Tunney and Detellier (1996) results. Simultaneously, the lack of

resonances assigned to DMSO is a confirmation of the preparation of the methanol-kaolinite precursor.

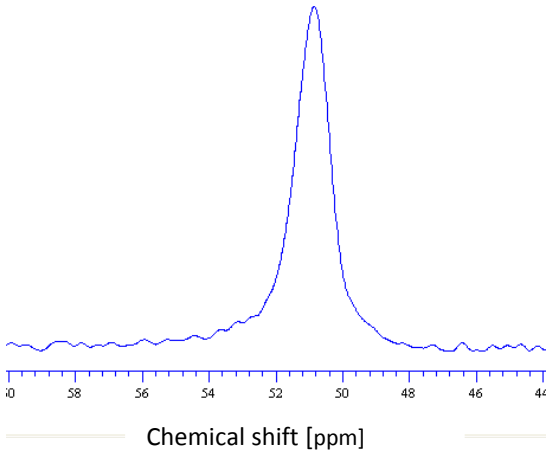

Figure 28 ^{13}C NMR spectra of methanol-kaolinite

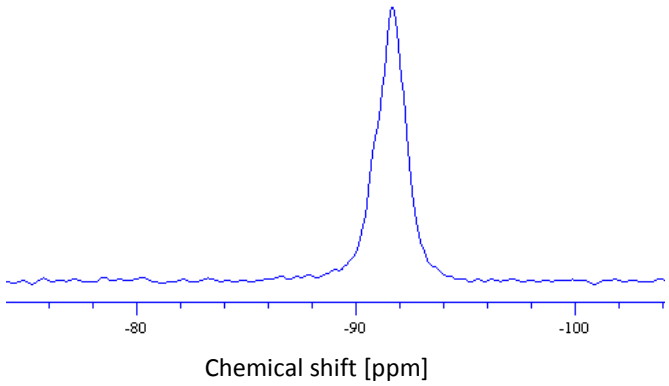

Figure 29 ^{29}Si NMR spectra of methanol-kaolinite

4.4.3 Kaolinite-ε-caprolactam

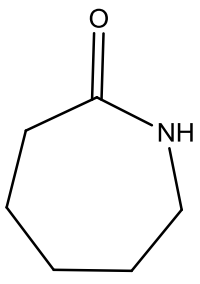

Figure 30 Structure of ε-caprolactam

4.4.3.1 XRD study of kaolinite-ε-caprolactam

Komori *et al.,* (1999) successfully achieved the intercalation of ε-caprolactam in kaolinite. The basal spacing of kaolinite ε-caprolactam compound is 1.37 nm (2θ 6.45°) which is similar to the values of 1.31 nm obtained by Komori *et al.,* (1999). In the diffractogram, a secondary reflection 0.67 nm from the intercalation compound is visible at 2θ 13.24°. Peak representing pure, unmodified kaolinite is observed at 2θ 12.12° and is represented by d spacing 0.73 nm. Some residual ε-caprolactam is present in the sample despite washing procedures. A reflection from an excess of organics (0.62 nm) is located at 14.45° 2θ. Based on the Gardolinski and Lagaly (2005) publication and interlayer distance of the product (0.65 nm), ε-caprolactam molecules are intercalated parallel to the inner surface of kaolinite in monolayer agreement.

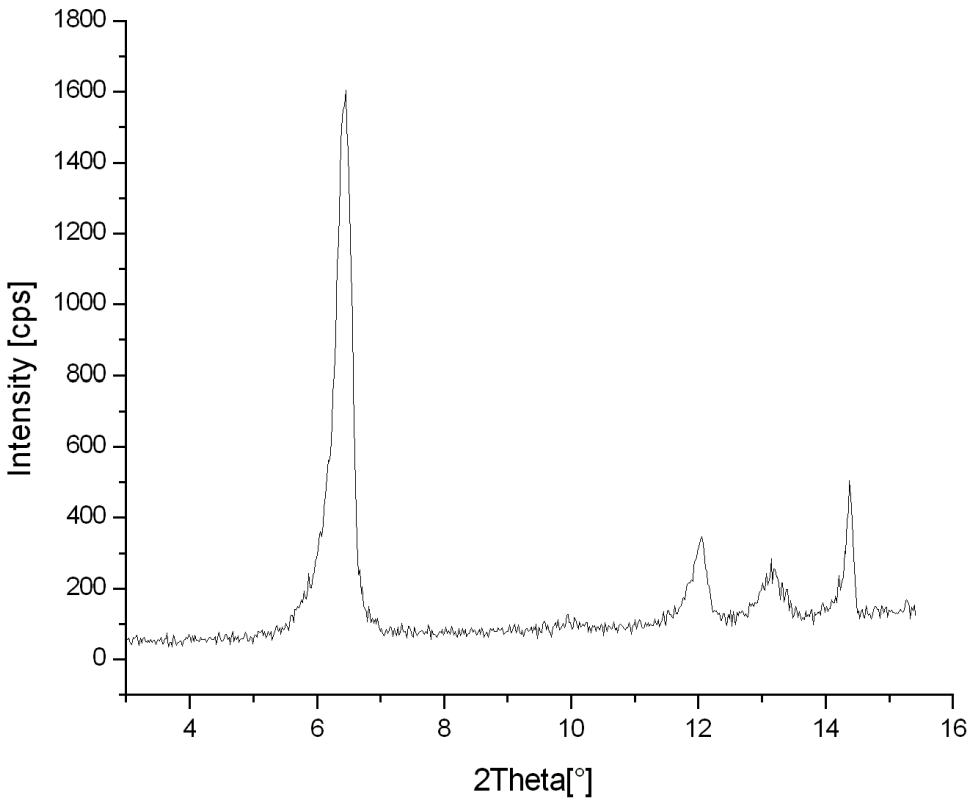

Figure 31 XRD of kaolinite-ε- caprolactam

4.4.3.2 Thermal study of kaolinite- ε-caprolactam

The thermal study of kaolinite-ε- caprolactam was made at 250°C, which is the temperature of the ring opening polymerization of ε- caprolactam (Fang *et al.,* 2002). For comparison, the thermal study of pure caprolactam under the same conditions were prepared. Two peaks on the DTG at 172°C and 201°C are related to the decomposition of organic matter on the external surface of kaolinite and also in the interlayer space. The significant role in the process of ring-opening polymerization of ε-caprolactam is played by water (Giori and Hayes 1970). However, the water adsorbed externally by kaolinite is removed (42°C) below temperature of melting of ε-caprolactam (69°C) which makes it impossible for opening of the ring and in situ polymerization. Consequently, ε-caprolactam is decomposed and volatilised from the kaolinite structure (Komori et al., 1999), which is also attested by the thermal behaviour of ε-caprolactam. The mass loss related to the decomposition of organic matter is around 61% and signifies that an excess of caprolactam on the external surface of kaolinite is present even after washing. For this study, one major conclusion was made: caprolactam is removed from the structure of kaolinite before polycondensation.

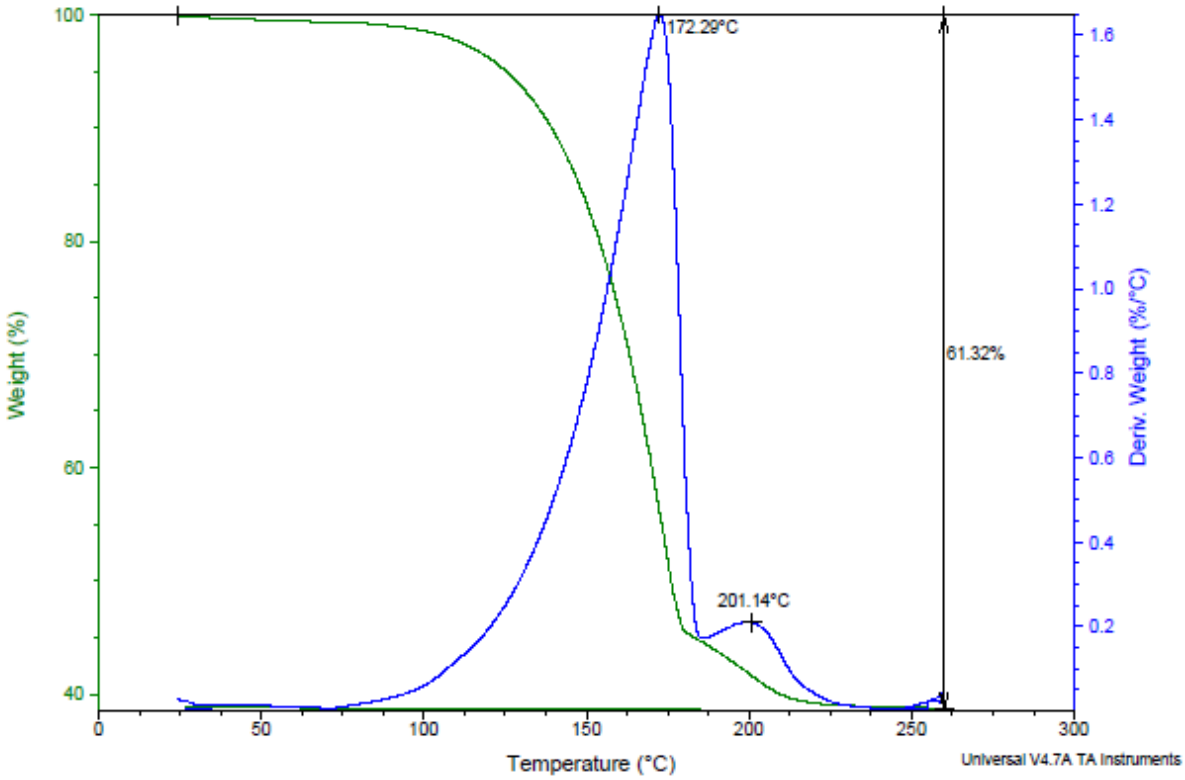

Figure 32 TGA results of kaolinite-ε- caprolactam compound, TG green line, DTG blue line

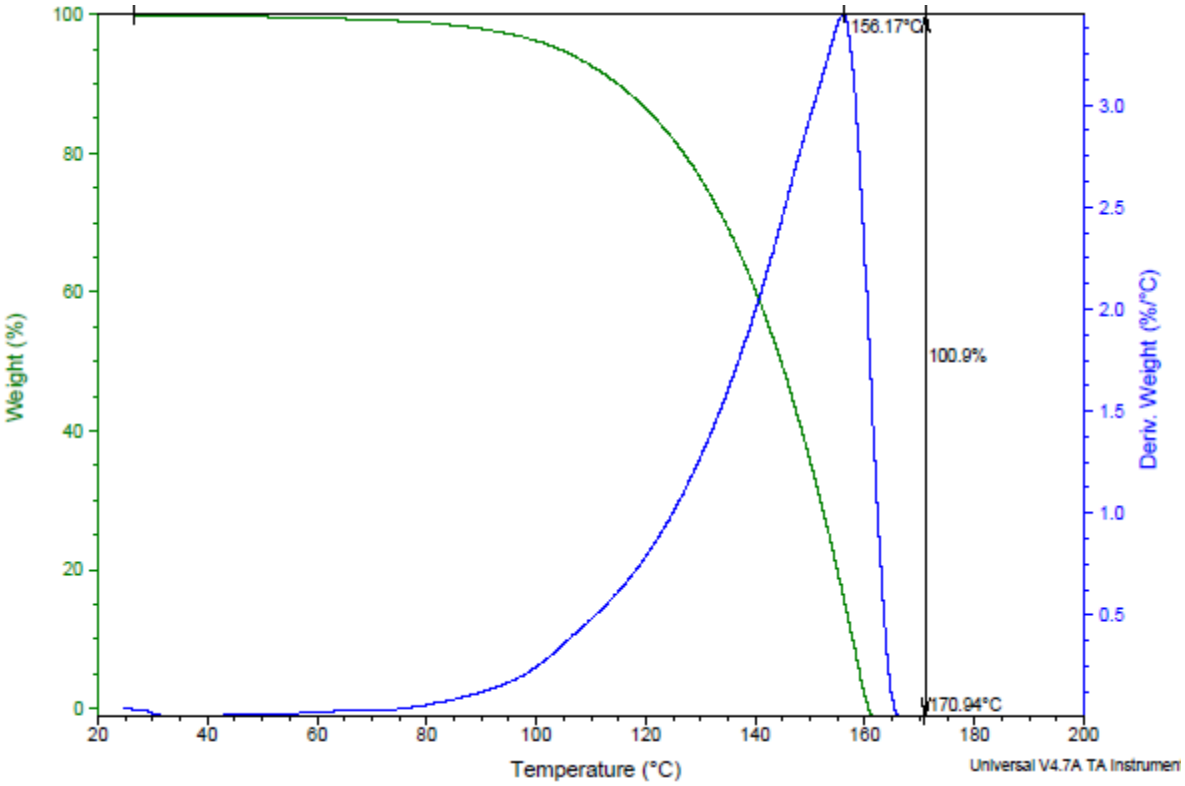

Figure 33 TGA results of ε- caprolactam; TG green line, DTG blue line

4.4.3.3 IR study of kaolinite-ε- caprolactam

In the region associated with kaolinite OH stretching, vibration band ascribed to the inner surface OH is shifted slightly to 3618 cm^{-1}, in comparison to the pure kaolinite. OH groups represented by this band do not participate in the bond creation with intercalated molecules (Brigatti *et al.,* 2006). Surface hydroxyl groups are represented by band at 3694 cm^{-1}, while interlayer hydroxyl stretching modes are represented by a broad peak 3640 cm^{-1} that has shifted in comparison to the pure kaolinite and may be an attestation of the perturbation of surface of Al-OH due to the intercalation of organic molecules. The band at 3291 cm^{-1} is ascribed to the stretching vibration of NH group in lactams (Flego and Dalloro 2003). The signal at 3070 cm^{-1} may be attributed to the secondary amide (Flego and Dallaro 2003). The stretching band from methylene groups (CH_2) is located at 3197 cm^{-1}. The bands of C- H, are placed at 2926 cm^{-1} and 2854 cm^{-1} (Mayo et al., 2004). Carbonyl group vibration is represented by band at 1652 cm^{-1}. In the range 1500-1400 cm^{-1}, deformation band from CH_2 in cyclic compounds are located which are represented in ε-caprolactam by band at 1484 cm^{-1} and 1416 cm^{-1} and may be overlapped with C-C stretching in the ring. The band at 1346 cm^{-1} is also ascribed to the interaction between carbons in the cyclic molecules.

The perpendicular Si-O stretching bands in the intercalated compound are shifted from 1104 cm^{-1} to 1123 cm^{-1} and from 1032 cm^{-1} to the 1026 cm^{-1}. In the low frequency region, the band at 910 cm^{-1} is ascribed to the Al-OH bending vibration. Contrary to 6-aminohexanoic acid, the appearance of an additional band from Al-OH around 900 cm^{-1} related to reduced hydrogen Al-OH bonding is not noticed. An additional band attributed with Al-OH is at 799 cm^{-1}.

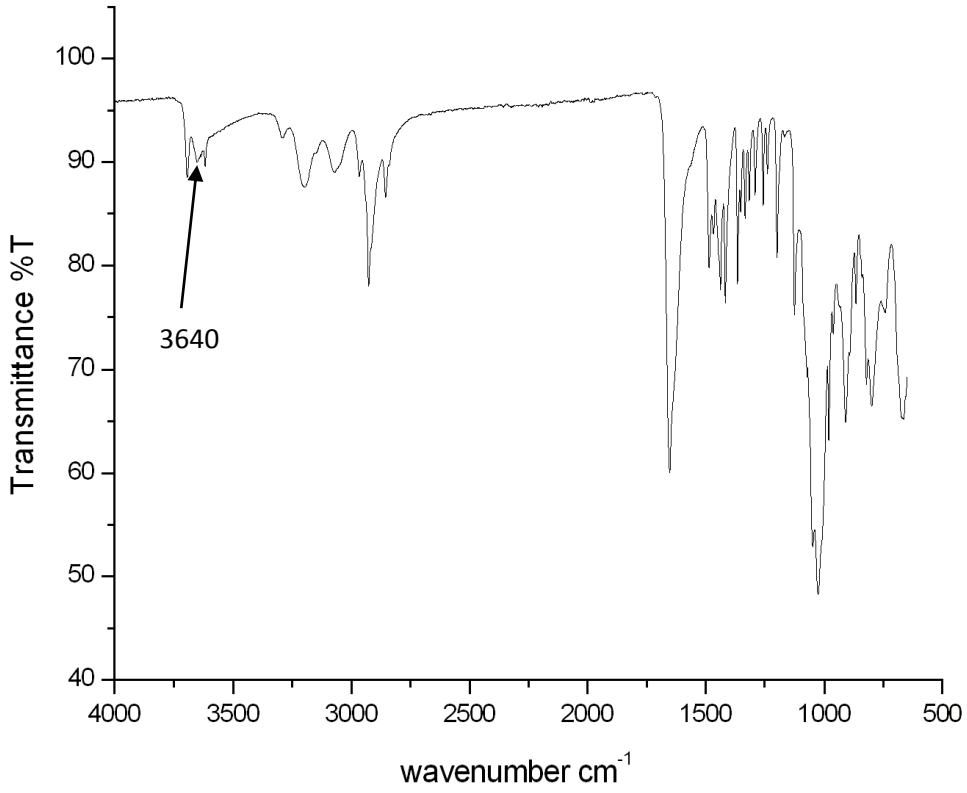

Figure 34 IR spectra of kaolinite-ε-caprolactam

4.4.3.4 NMR study of ε-caprolactam-kaolinite

A ^{29}Si CP/MAS NMR spectra of ε-caprolactam- kaolinite is characterized by 3 signals at frequencies of -91.01 p.p.m, -91.50 p.p.m, both of which are more intense than the third signal at – 92.74 p.p.m. The two first resonances are related to the character of Si atoms in the structure of pure kaolinite. The third signal has a low intensity and its shift to the lower frequencies is related to changes made in the structure of kaolinite due to the intercalation of ε-caprolactam. With comparison to the kaolinite at – 91.50 p.p.m, signal is shifted 1.2 p.p.m which may be related to the perturbation of the silicate surface, but without major significant structural changes, which was observed for methanol-kaolinite complex (Tunney and Detellier 1996). The silicon atoms occupied the same tetrahedral sites.

The ^{13}C CP/MAS NMR spectra of ε-caprolactam- kaolinite is characterized by splitting of the signal at 182.40 p.p.m and 180.73 p.p.m, which are related to two kinds of carbonyl groups. Similar results were obtained by Kuroda *et al.,* (1999) for poly-vinylpyrrolidone (PVP) intercalated in the kaolinite interlayer space. A low intensity signal at 49.77 p.p.m is related to CH_3 group from methanol preintercalated in the kaolinite structure. Signal at 41.2 9 p.p.m may be related to carbon from methylene group (CH_2) which is connected to NH in the structure of caprolactam. Chemical shift at 36.80 p.p.m is attributed to carbon from methylene group bonded to carbonyl group. Two signals at 30.4 6 p.p.m and 25.17 p.p.m are connected to carbons from methylene group bonded each other (Spectral Data Base for Organic Compounds).

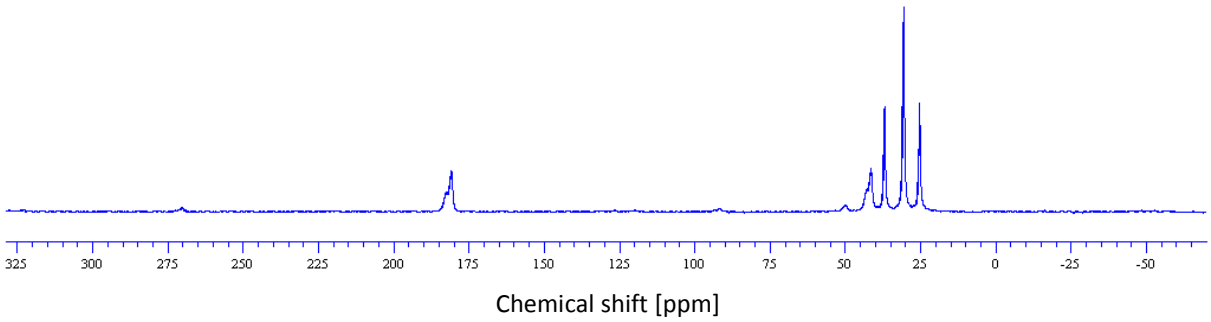

Figure 35 ^{13}C CPMAS NMR spectra of kaolinite-ε-caprolactam

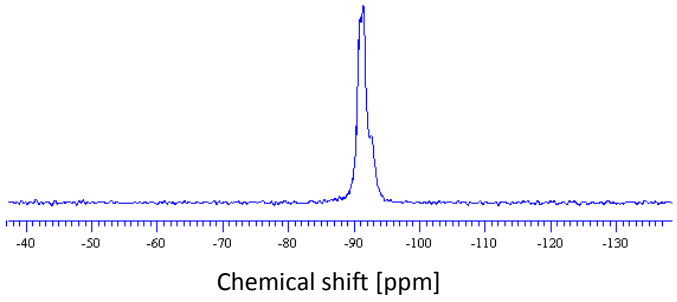

Figure 36 ^{29}Si CPMAS NMR spectra of kaolinite-ε-caprolactam

4.4.4 AHA-kaolinite precursor

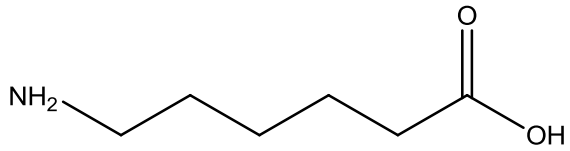

Figure 37 6-aminohexanoic acid structure

4.4.4.1 X-Ray Diffraction

AHA intercalated into kaolinite is characterised by a basal spacing of 1.47 nm. (2θ 6;1°) Matsumura *et al.,* 2001 reported smaller basal spacing for AHA intercalated into kaolinite of 1.23 nm. A second reflection on the diffractogram (1.02 nm 2θ 8.4°) is ascribed to the methanol-kaolinite intercalated compound. The peak with the highest intensity at 2θ 10.55° is ascribed to the AHA adsorbed on the surface of kaolinite (0.84 nm) and (0.86 nm) to the unreacted phase (dried kaolinite- methanol compound) (Matsumura *et al.,* 2001). The basal spacing obtained experimentally for AHA-kaolinite corresponds with data published by Sato (1999) for δ-aminovaleric acid (1.44 nm). The interlayer thickness of 6-aminohexanoic acid intercalates Δ is calculated for the following formula:

$$\Delta=[d_{(001)}\text{-}0.72\ \text{nm}]$$

Where:

$d_{(001)}$- basal spacing of the kaolinite- 6-aminohexanoic acid compound

Interlayer thickness of AHA molecules in the interlayer space of kaolinite is 0.75 nm. The molecular size of AHA is ca 0.42×0.51×1.00nm. Based on the values presented above, AHA molecules are intercalated in a monolayer agreement within the kaolinite interlayer space (Gardolinski and Lagaly 2005). Although the AHA molecules are intercalated in a monolayer agreement, they are tilted from a planar orientation (Gardolinski and Lagaly 2005).

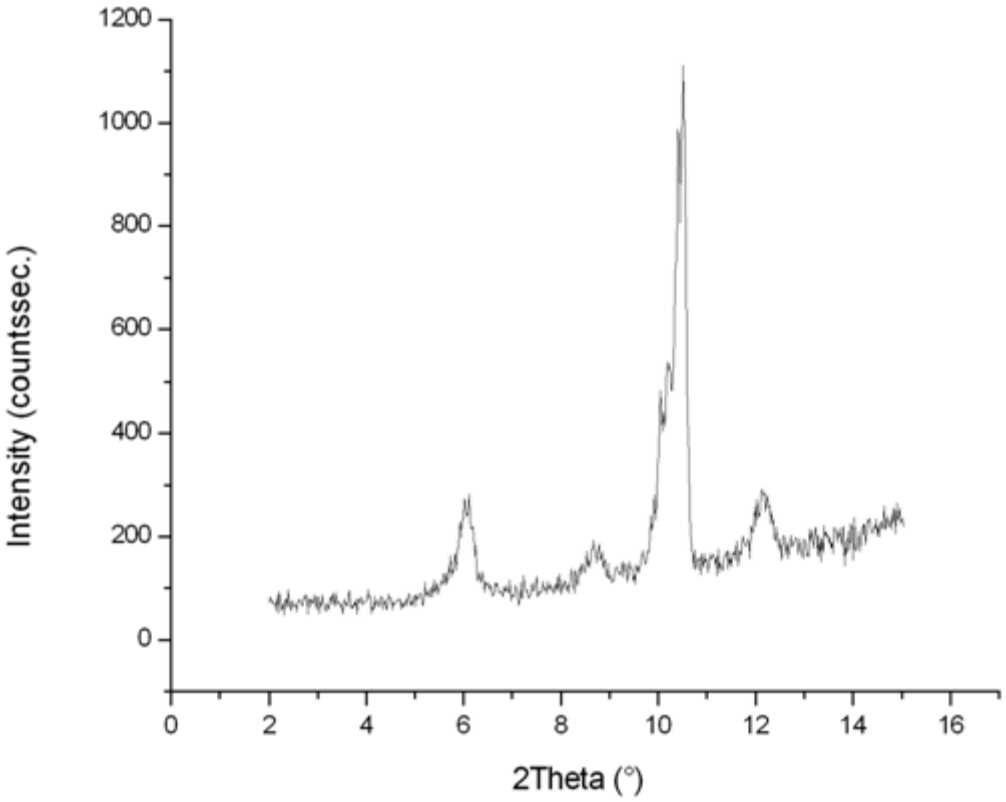

Figure 38 XRD results for AHA-kaolinite precursor

4.4.4.2 Thermal analysis of AHA- kaolinite.

The graph of the thermal analysis of AHA- kaolinite sample is provided. TG of AHA- kaolinite is characterized by 4 mass losses. The first mass loss is ascribed to the evaporation of external water from the surface of kaolinite during the heating, which is represented by an endothermic peak in the DTA. That process has the highest intensity at 54°C, which is shown on the DTG. The second mass loss is attributed with polycondensation reaction and the partial volatilization of acid. The process started at around 150°C and finished at around 250°C, with maximum at 198°C on the DTG. The third mass loss is also related to the polymerization of acid, and the volatilization and decomposition of acid which was not polymerized. This third stage started at around 250°C, with a maximum at 298°C visible on the DTG, and finished at around 350°C. Appearance of 2 peaks related to the decomposition of organic matter may be related

with reaction during polymerization of nylon 6. The lower temperature of condensation of AHA between the kaolinite interlayer indicates the peculiar environment of AHA molecules between the layers of kaolinite (Matsumura *et al.,* 2001). The mass loss between 150°C and 350°C (around 12mass %) is lower than reported by Matsumura et al., (2001). The fourth mass loss is related to the decomposition of nylon-6 and the dehydroxylation of kaolinite. On the DTG, a broad shoulder is visible around 400°C which is indicative of 2 peaks overlapping in the area 390°C- 500°C. Nylon 6 is probably decomposing at the temperature around 390°- 430°C as was reported previously by Sato *et al.,* (2006). Moreover, decreasing of the dehydroxylation temperature of kaolinite is related to the interaction between organic molecules and clay layer (Gardolinski 2005). Total loss mass and molecular weights of kaolinite and AHA were used for estimating the total amount of AHA loaded on 1 unit of structure of kaolinite. It corresponds to 0.63 mol of AHA per unit structure of kaolinite. Additionally, the percentage amount of organic material loaded to the clay was calculated to be 24%.

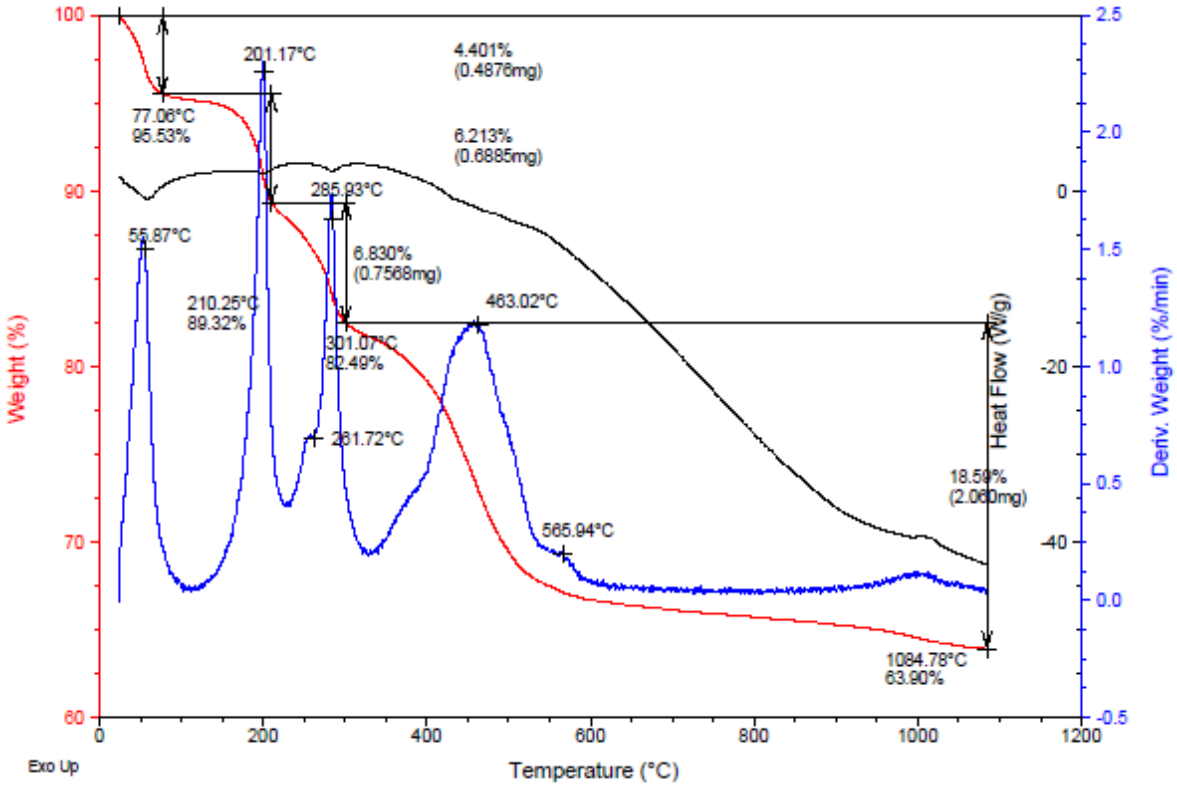

Figure 39 TGA results of AHA-kaolinite; TG red line, DTA black line, DTG blue line

4.4.4.3 IR study of 6- aminohexanoic- kaolinite precursor

On the IR spectrum of AHA-kaolinite, changes in the OH-stretching region are visible. Through the intercalation reaction, the outer OH groups are perturbed due to bonding with guest species. This is expressed by new bands appearing at lower wave numbers. The inner OH groups represented on the spectra by stretching vibration band at 3620 cm^{-1} are not affected (Theng 1974). Intensity of the band at 3694 cm^{-1} does not decrease significantly which is what Matsumura *et al.,* (2001) observed, and Sato (1999) for kaolinite-amino acid intercalates. Bands at 3652 cm^{-1} are not present on the spectrum of AHA kaolinite; however, a new band around 3640 cm^{-1}appears. This band is attributed to the hydrogen bonded inner-surface hydroxyls. Broad band at 3556 cm^{-1} might be attributed with OH stretching vibration of intercalated water, as was reported for β-alanine (Sato 1999, Mayo *et al.,* 2004). The broad strong absorption band, which

appears at 3276 cm^{-1} may be assigned to the asymmetric stretching vibration of NH_3^+ (Rotter and Ishida 1992).

In the low frequency region of the AHA kaolinite spectra, the bands owing to the Al-OH deformation vibration are shifted. The band appearing in kaolinite at 938 cm^{-1} is present at 941 cm^{-1}. In addition, the band at 915 cm^{-1} is replaced by an additional band at 906 cm^{-1}. The same behaviour was reported by Sato (1999) for β-alanine. It may suggest reduced hydrogen bonding of Al-OH. Moreover, the band at 79 cm^{-1} is reduced, with comparison to the kaolinite spectra. The perpendicular Si-O stretching band at 1104 cm^{-1} is at the same position as that for pure kaolinite; however, 1032 cm^{-1} is shifted to 1028 cm^{-1} for AHA-kaolinite. In- plane stretching of Si-O occurs at 1005 cm^{-1}. This observation is consistent with data for β-alanine published by Sato (1999).

In the region $2000-1100\ cm^{-1}$, bands associated with intercalated 6-aminohexanoic acid appeared. The band at 1620 cm^{-1} may be attributed with NH_3^+ asymmetric deformation vibration, while the band at 1503 cm^{-1} represents the symmetric deformation of NH_3^+. The band at 1270 cm^{-1} is associated with rocking of NH_3^+ and is not a distinctive group frequencies (Mayo *et al.,* 2004). By comparison to Satoès' (1999) studies of β-alanine, the band at 1547 cm^{-1} is associated with asymmetric COO^- stretching vibration of 6-aminohexanoic acid intercalated in kaolinite in zwitterionic form. Symmetric stretching vibration of COO^- is represented by band at 1403 cm^{-1} (Mayo *et al.,* 2004). The bands 1462 cm^{-1}, 1342 cm^{-1}, and 1317 cm^{-1} are respectively attributed with CH_2 scissor, wagging deformations and twisting (Sato, 1999; Mayo *et al.,* 2004). Symmetric and antisymmetric stretching of methylene groups are represented by two bands at 2865 and 2938 cm^{-1} (Mayo *et al.,* 2004).

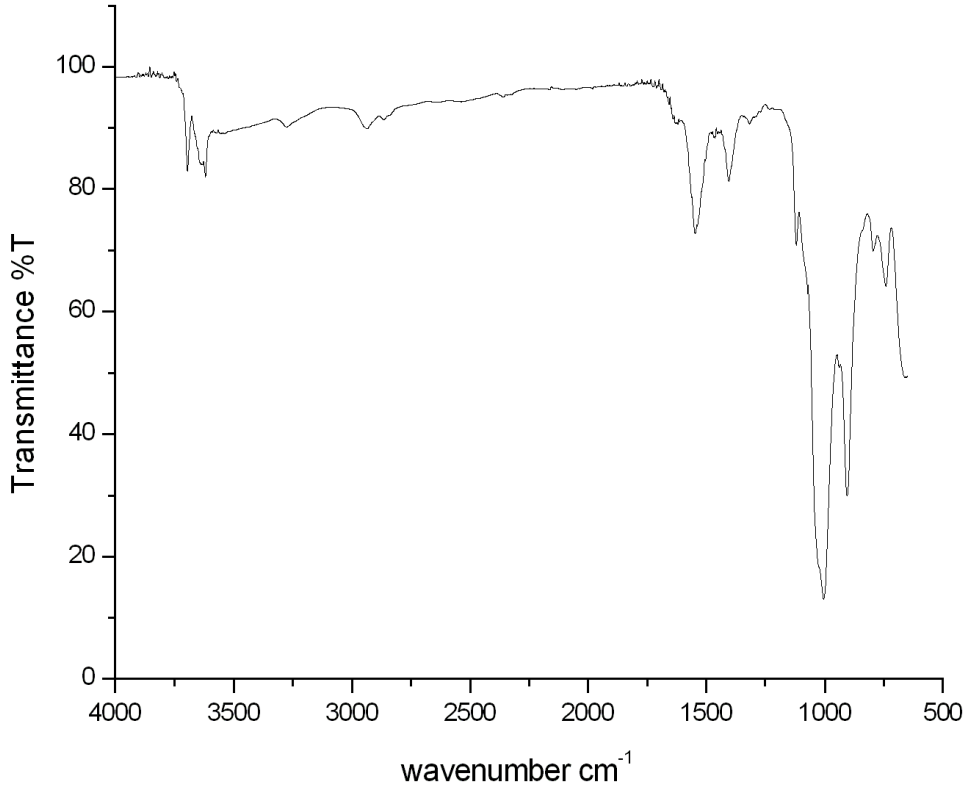

Figure 40 IR spectra of AHA- kaolinite compound

4.4.4.4 NMR study of AHA-kaolinite

On the ^{29}Si CP/MAS NMR spectra of AHA-kaolinite, one signal at – 91.57 p.p.m is present which is consistent with values presented by Matsumura *et al.,* (2001). A 0.17 p.p.m shift to the lower frequencies, in comparison to the signal at -91.4 p.p.m (Matsumura et al., 2001) does not affect the coordination of Si in the kaolinite crystalline structure.

The ^{13}C CP/MAS NMR spectra of AHA-kaolinite is characterized by resonance at 181.17 p.p.m which is attributed to the carbonyl group. The chemical shift of this signal is lower than reported by Matsumara *et al.,* (2001) for AHA molecule, 182.4 p.p.m, which may be related to the interaction of AHA molecules in the kaolinite structure. The signal at 49.84 p.p.m is ascribed to the methyl group (CH3). However, this signal is

shifted downfield in comparison to liquid methanol 48.50 p.p.m (Gottlieb *et al.,* 1997). The chemical shift at 39.31 p.p.m is related to methylene group bonded with carbonyl group and has the same value as for AHA (Matsumura *et al.,* 2001). Splitting of this signal may be related to the methylene group bonded to NH3 group which is represented on the spectra of pure AHA obtained by Matsumura *et at.* (2001) at 40.6 p.p.m. Three signals at 31.02 p.p.m; 28.31 p.p.m; 19.31 p.p.m are assigned to methylene groups. The resonance at 28.31 p.p.m is shifted by 1.4 p.p.m in comparison with pure AHA (Matsumura *et al.,* 2001) which may be due to the change of geometry of AHA molecules intercalated to the kaolinite interlayer space.

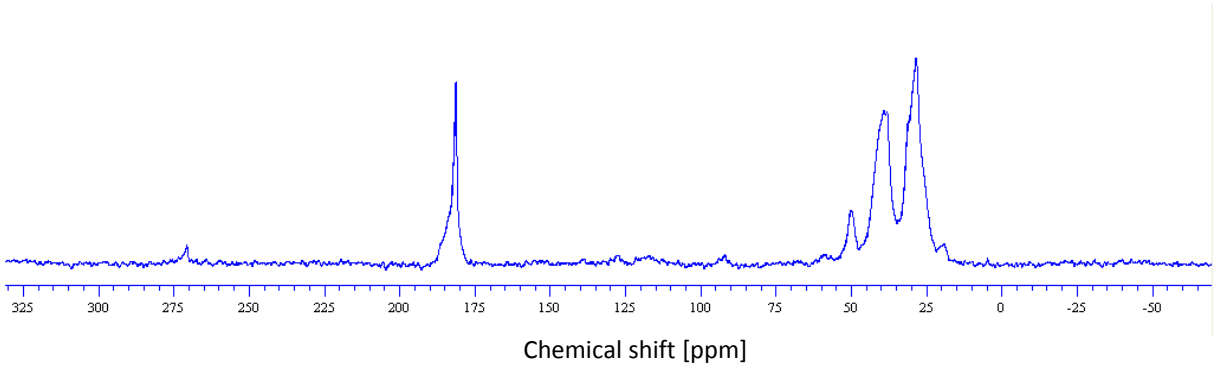

Figure 41 ^{13}C CPMAS NMR spectra of AHA-kaolinite

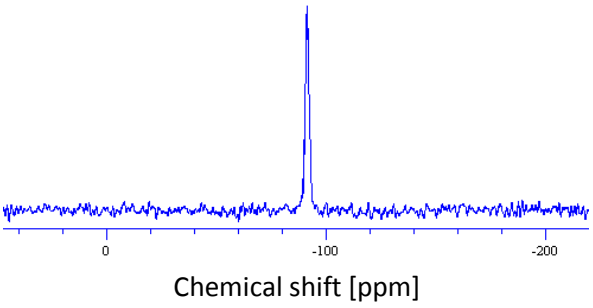

Figure 42 ^{29}Si CPMAS NMR spectre of AHA-kaolinite

4.4.5. Kaolinite-sarcosine precursor

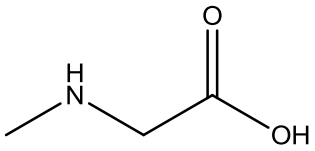

Figure 43 Sarcosine structure

4.4.5.1 XRD study of kaolinite-sarcosine precursor

The XRD study of kaolinite –sarcosine compound was made, as well as that of a pure sarcosine sample; this was done to assign peaks to sarcosine. On the diffractogram of pure sarcosine, the first reflection is present at 15.10° 2θ with a basal spacing of 0.59 nm. Also, reflections located at higher angles (16.71° 2θ; 17.26° 2θ; 20.29° 2θ) are respectively represented by d-spacings of 0.53 nm, 0.52 nm and the most intense at 0.44 nm. After introduction of sarcosine into the kaolinite structure, a new peak with basal spacing of 1.28 nm appeared at 6.92° 2θ. This value may be comparable with γ-aminobutyric acid presented by Sato (1999). Secondary reflections from the intercalate is visualized by a peak at 14.63° 2θ with d-spacing of 0.61 nm. On the diffractogram of kaolinite-sarcosine, a broad peak with a maximum around 0.72 nm represents pure kaolinite. Shifting of residual sarcosine peaks to lower angles in the spectra of the intercalation compound is noted. The first peak from the external excess of sarcosine in the intercalation compound appears at 15.06° 2θ, while the next one appears at 16.39° 2θ and the third one at 17.05° 2θ, with basal spacing 0.59 nm, 0.54 nm and 0.52 nm respectively. The interlayer thickness of sarcosine intercalate Δ is calculated by the following formula:

$$\Delta=[d_{(001)}\text{-}0.72\ \text{nm}]$$

Where:

$d_{(001)}$- basal spacing of the kaolinite- sarcosine compound

The value of interlayer thickness of kaolinite-sarcosine is 0.56 nm which is similar to the values obtained for γ-aminobutyric acid (Sato 1999) and 6-aminohexanoic acid (Matsumura *et al.,* 2001). Based on the calculation made by Mosad and Natarajan (1989), the approximate molecular size of sarcosine molecule was determined (ca. 3.38× 3.46× 6.74Å). Thus, sarcosine molecules are intercalated in a monolayer agreement between the kaolinite interlayer space (Gardolinski and Lagaly 2005). Although the sarcosine molecules are intercalated in a monolayer agreement, they may be tilted from the planar orientation. (Gardolinski and Lagaly 2005).

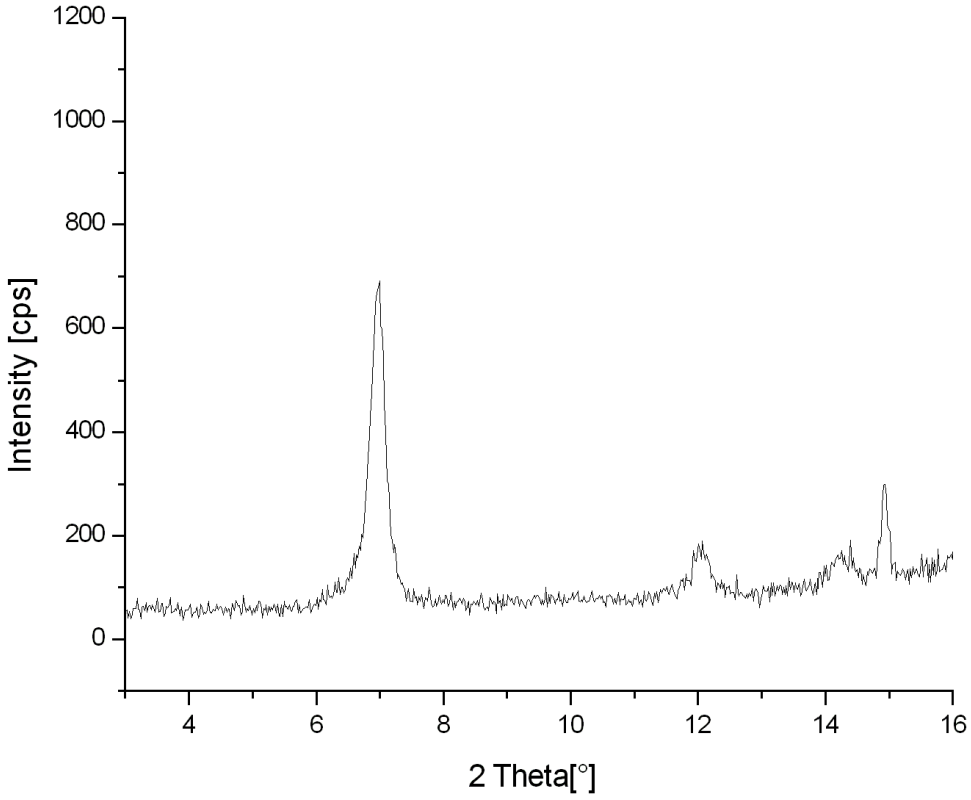

Figure 44 XRD results for kaolinite-sarcosine

4.4.5.2 Thermal analysis of kaolinite- sarcosine precursor

The thermal behavior of the kaolinite-sarcosine precursor is described, as well as that of the pure sarcosine sample. In the DTA curve of sarcosine, an endothermic peak with minimal value at 223°C represents melting of glycine derivative with a melting point of 208°C (Alfa Aeasar). For the kaolinite sarcosine precursor, the maximum of the melting process occurred at 214°C, which is represented by an endothermic peak. Sato (1999) observed an exothermic peak for kaolinite-glycine intercalate in this temperature range, although the presence of endothermic peak was ascribed to the melting of pure glycine. In the DTA curve of sarcosine, the endothermic peak with a minimum at 260°C is associated with the decomposition of organics. For the kaolinite-sarcosine precursor, the decomposition of organics is associated to two stages, which is visible on DTA and TG as two separate mass losses. The first mass loss for the kaolinite-sarcosine compound is related to the removal of externally adsorbed water (removed at temperatures below 100°C and signalized by a DTG peak at 43°C) and the decomposition of sarcosine which is externally keyed to kaolinite. The endothermic peak on the DTA at 242°C is related to the decomposition of an excess of sarcosine, which corresponds also with a mass loss of 56%. The second mass loss (5.3%) on the TG curve of the kaolinite-sarcosine precursor is attributed to the decomposition of sarcosine from the interlayer space of kaolinite. Removal of organics intercalated into the kaolinite structure is confirmed by the appearance of an endothermic peak on the DTA in the range of 250°C to 320°C, with minimum at 287°C. The temperature of dehydroxylation of kaolinite-sarcosine is shifted to lower values in comparison to pure kaolinite which may be a confirmation of the intercalation of sarcosine molecules into the kaolinite structure (Letaief and Detellier 2011). The maximum of the exothermic decomposition peak on DTG at 473°C for kaolinite-sarcosine is located in the same range as for glycine and β-alanine (Sato 1999). The third mass loss (6.8%) is ascribed to

the dehydroxylation. Above 1000°C, the exothermic peak on the DTA curve represents reorganization of the crystal structure of clay without mass loss.

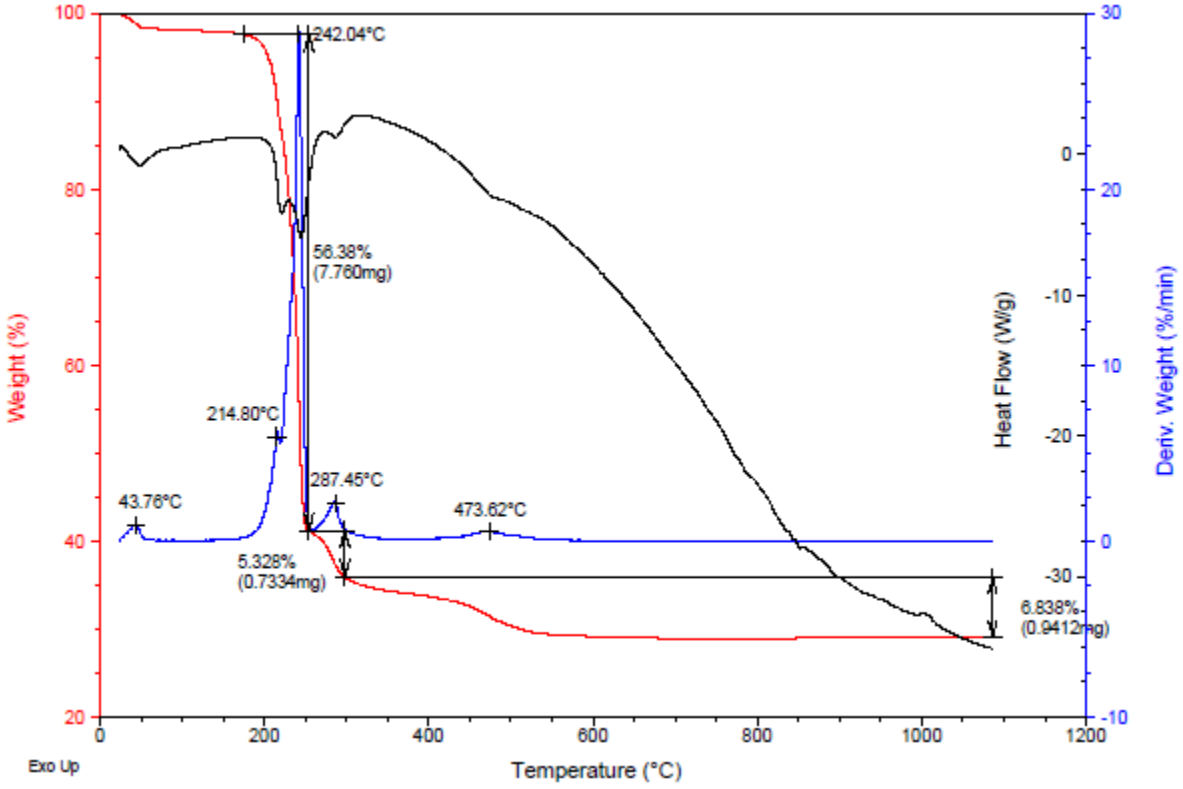

Figure 45 TGA results for sarcosine-kaolinite; TG red line, DTG blue line, DTA black line

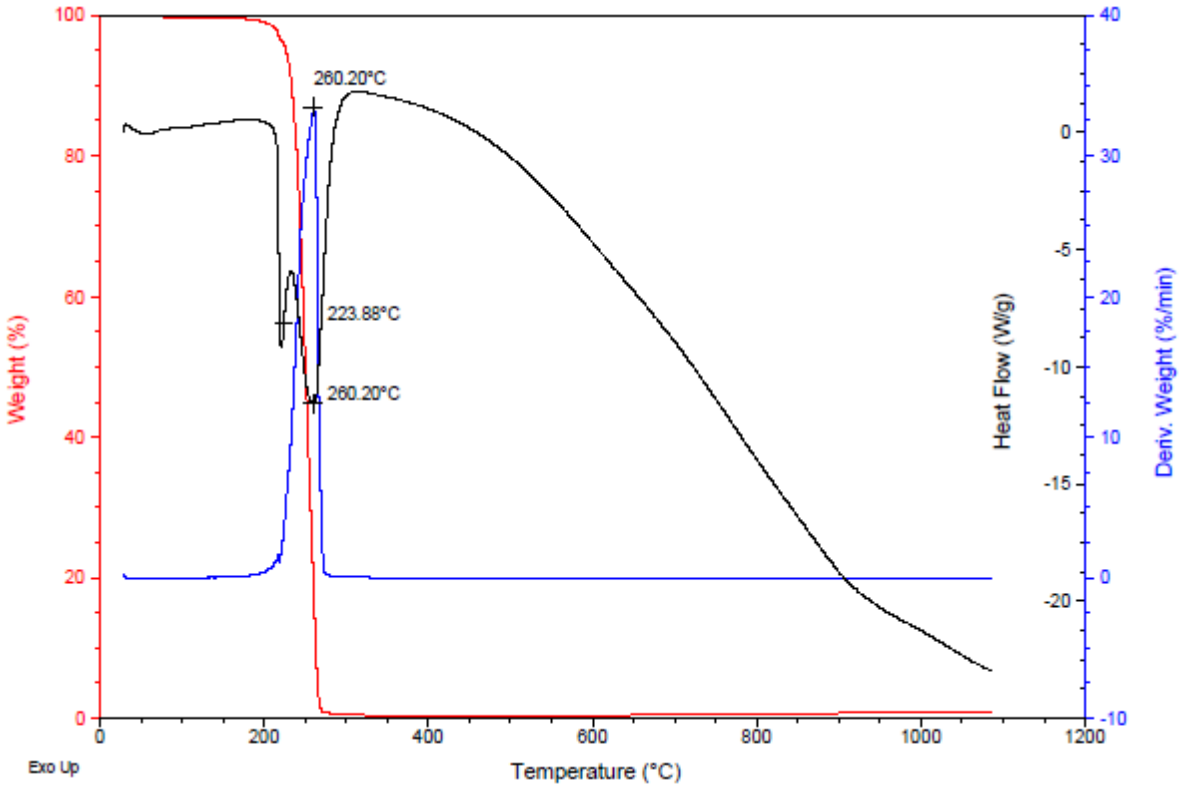

Figure 46 TGA results for sarcosine; TG red line, DTA black line, DTG blue line

4.4.5.3 IR study of sarcosine kaolinite

A sarcosine derivative of glycine is intercalated in the kaolinite structure mainly in zwitterionic form (Gomez- Zavagila and Fausto 2003). In the range of spectra related to the kaolinite OH stretching vibration, four bands are present. The band at 3620 cm^{-1} ascribed to the inner OH group stretching vibration is not affected by guest sarcosine molecules. This band is superimposed over 3629 cm^{-1} which may be the result of hydrogen bonding between inner hydroxyl groups and sarcosine molecules. The band with similar characteristic was described by Sato (1999) in the glycine kaolinite precursor. The inner surface OH-stretching band at 3695 cm^{-1} is slightly shifted in comparison to that of pure kaolinite. Two bands with low intensity at 3645 cm^{-1} and 3664 cm^{-1} may be ascribed to the stretching vibration of inner surface OH groups which are perturbed due to the introduction of sarcosine molecules in the interlayer space of **kaolinite. Similar changes were reported for glycine and β-alanine by Sato (1999).**

Two bands at 3475 cm^{-1} and 3407 cm^{-1} may be related to the OH stretching vibrations of strongly and weakly bonded H_2O as has been observed in the case of amino acids (Sato 1999, Gomez Zavagila and Fausto 2003). However, strong intensity of these bands suggests that they should be assigned to the NH stretch vibration (Fischer *et al.,* 2001). Also the bands located at 3185 cm^{-1} and 3006 cm^{-1} may be ascribed to the intermolecular hydrogen bonding $COO^{-}\ldots NH_3^{+}$ (Uvdal *et al.,* 1990). In the range between 3000 cm^{-1} and 2700 cm^{-1}, bands ascribed to the methyl group stretching vibration are located. The signal from carbonyl group is attributed to the bands at 1643 cm^{-1} which is shifted in comparison with pure sarcosine (1645 cm^{-1}) (Gomez-Zavagila and Fausto 2003). Sato (1999) assigned the band at 1627 cm^{-1} in glycine to the asymmetric deformation of NH_3^{+} which can be connected with the band at 1625 cm^{-1} in the sarcosine kaolinite system. The asymmetric stretching vibration of COO^{-} is represented by the band at 1586 cm^{-1} which is consistent with the studies of Sato (1999). The band at 1488 cm^{-1} may be assigned then to the symmetric NH_3^{+} deformation vibrations. At 1409 cm^{-1}, the band ascribed as COO^{-} symmetric stretching vibration is localized (Sato 1999). Twisting vibration of methyl group is represented by bands at 1093 cm^{-1} and 1045 cm^{-1}. Vibrations related to the methylene group (CH_2) are ascribed to the bands at 1309 cm^{-1} and 931 cm^{-1} which superimpose with that of the Al-OH deformation vibration of the kaolinite structure, shifted to lower wave numbers in comparison with pure kaolinite. Torsion of C-O bonding is visualized by band at 968 cm^{-1} shifted in comparison to pure sarcosine (Gomez-Zavagila and Fausto 2003). Sato (1999) suggests that bands in the range of 1600 cm^{-1} to 1400 cm^{-1} are assigned to the organic molecules adsorbed on the external surface of kaolinite particles.

In the lower wave number region from 1100 cm^{-1} to 600 cm^{-1}, bands related to the kaolinite structure are located. The perpendicular Si-O stretching bands at 1104 cm^{-1} and 1032 cm^{-1} for kaolinite are slightly shifted in the intercalate to 1097 cm^{-1}, 1045 cm^{-1}, and 1031 cm^{-1}. The splitting of the Si-O perpendicular vibration may be a result of the crystalline structure or crystal orientation because of intercalation and separation of the lamellae (Olejnik *et al.,* 1971) due to intercalation of sarcosine molecule. The bands related to the Al-OH deformation vibration at 931 cm^{-1} are shifted to lower wave numbers in comparison to pure kaolinite; moreover, a new band at 903 cm^{-1} appeared which was also observed by Sato (1999) for β-alanine. This band may be related to the reduced hydrogen bonding Al-OH. Also, bands at 794 cm^{-1} and 746 cm^{-1} are assigned to Al-OH.

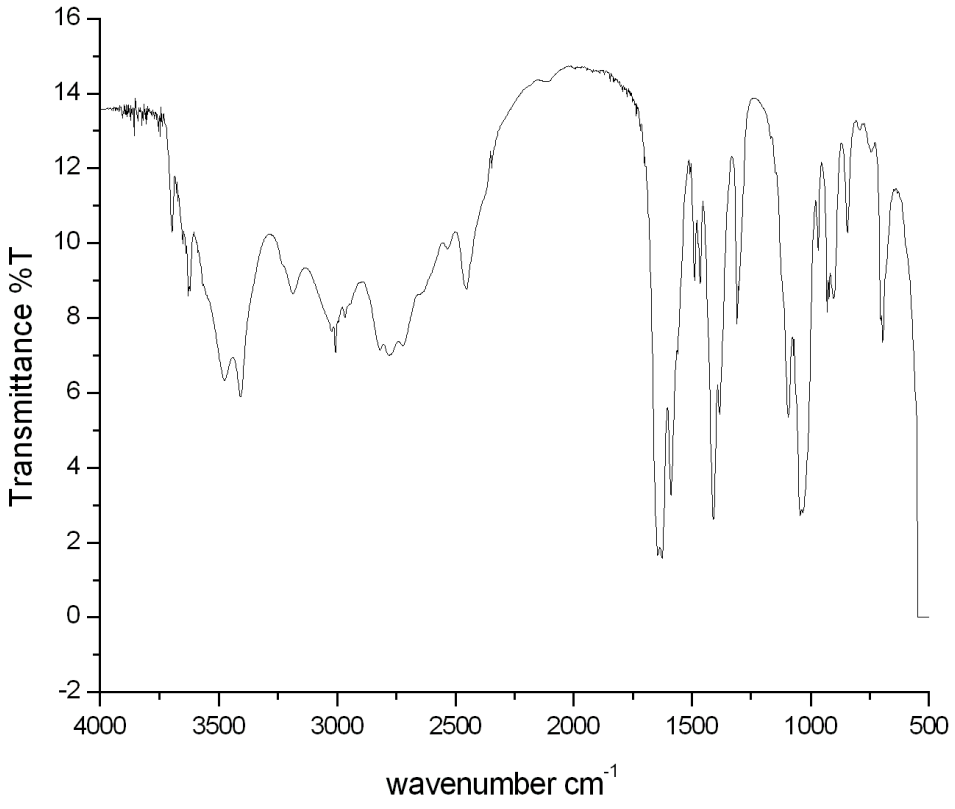

Figure 47 IR spectra of sarcosine-kaolinite

4.4.5.4 NMR Study of Sarcosine-kaolinite

In the ^{29}Si CP/MAS NMR spectrum, two signals are visible at – 91.32 p.p.m and at – 92.74 p.p.m which are attributed to sarcosine intercalated in the kaolinite interlayer. These results are in accordance with the ^{29}Si chemical shift observed for other organokaolinite intercalates (Tunney and Detellier 1996).

The ^{13}C CPMAS NMR spectrum of sarcosine-kaolinite is characterized by chemical shift at 172.51 p.p.m, which is attributed to carbon from the carbonyl group bonded to OH group. This signal is shifted to lower frequencies in comparison to sarcosine signal of 173 p.p.m (Ilszczyn *et al.,* 2003). Two signals, which may be attributed to methylene group bonded to carbonyl group, are present at 51.25 p.p.m and 50.58 p.p.m. Resonance attributed to the methyl group of sarcosine is located at 35.45 p.p.m (Ilszczyn *et al.,* 2003). Therefore, three signals on sarcosine-kaolinite spectra may be interpreted as carbon methyl group (CH_3) at 36.33 p.p.m, 32.04 p.p.m, and 31.27 p.p.m. Splitting of signals may be attributed with the asymmetric localization of sarcosine molecules in the kaolinite interlayer space.

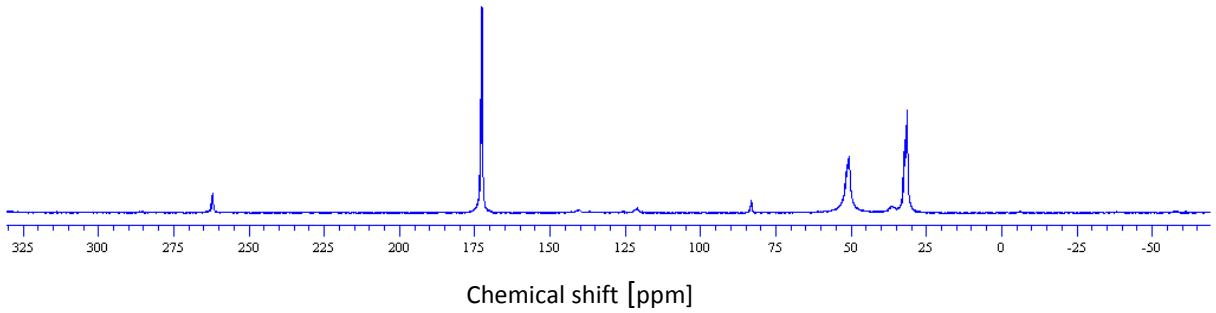

Figure 48 ^{13}C CPMAS NMR spectra of sarcosine-kaolinite

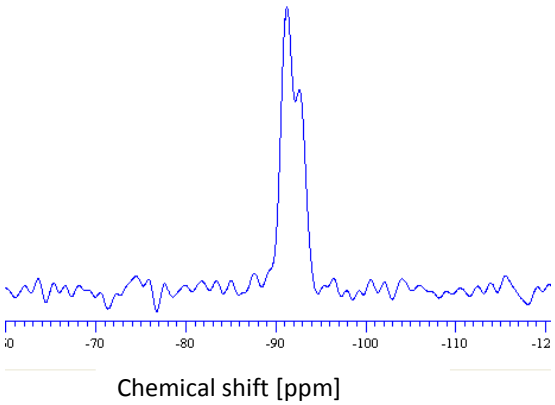

Figure 49 ^{29}Si CPMAS NMR spectra of sarcosine –kaolinite

4.5 Conclusions

Organo-kaolinite compounds were synthesized and confirmed by the techniques of XRD, NMR, TGA and FTIR. Increasing of the basal spacing of kaolinite treated by organic compounds is the indication that introduction of molecules in the interlayer space of the mineral. During experimental procedures, the direct intercalation of ε-caprolactam, 6 –aminohexanoic acid and sarcosine into pure kaolinite and also directly from DMSO-kaolinite did not take place. Therefore, compounds listed above were introduced into kaolinite through a methanol-kaolinite precursor.

5 Kaolinite-nylon 6 composite

5.1 Introduction

A composite is defined as a solid material, which results from the combination of simpler materials represented by continuous phase materials such as polymers or ceramics, and a dispersed phase such as glass fibres or clay minerals (Ruiz-Hitzky and Van Meerbeek 2006). Composites with dispersed phase particles, which have at least one dimension in the nanometre range are called nanocomposites. Clay minerals are characterised by two dimensions in the range of nanometres; therefore, those minerals are prospective fillers for the preparation of nanocomposites. The first step for nanocomposite production is intercalation, which is defined as a reversible introduction of molecules, ions, or atoms between the clay layers. On the other hand, exfoliation takes place when layered filler particles are segregated into individual layers in the nanocomposite material matrix. During delamination process, splitting of the individual layers into single-phase layered material takes place.

On the diagram presented below, the difference between intercalation and exfoliation/ delamination is presented.

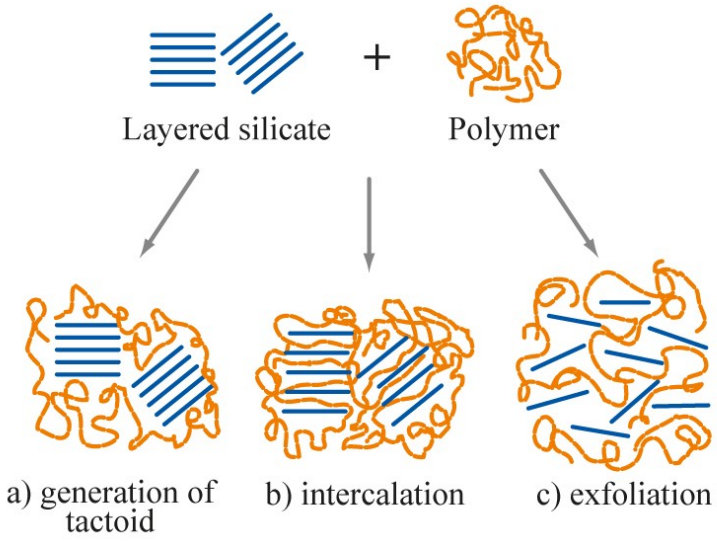

Figure 50 Differences between intercalation and exfoliation (after Pinnavaia and Beall 2000)

In the last 20 years, much interest has been paid to polymer- clay nanocomposites, because those materials are often characterised by unique properties, which are differ from the components taken separately (Turhan *et al.,* 2010; Sun *et al.,* 2010).

The concept of nylon- clay nanocomposite was developed for the first time in 1976 by Fujiwara and Sakamoto, who reported the preparation of a nylon 6 –clay nanocomposite in two steps. In the first step, they intercalated protonated aminocarboxylic acid by an exchange with sodium ions from montmorillonite interlayer. Intercalation of caprolactam in the interlayer space and polymerisation of the complex in situ was the second step of the procedure. The obtained component was characterised by a large basal distance of 69.8Å. Later, Usuki *et al.,* (1992) improved and commercialized a technology of nylon 6- clay nanocomposite. The nylon 6 – clay nanocomposite had various improved properties over pure nylon 6, such as high strength, high distortion temperature, low permeability, and high modulus (Liu *et al.,* 1998; Ysue *et al.,* 2000 and Sato *et al.,* 2006). From the economic point of view, the two-step method is not efficient because of the high cost of production; therefore, Yasue *et al., (*2000) successfully improved the production process by intercalation of ε-caprolactam directly into the structure of specific layered silicate swellable synthetic mica. Although most of the papers are based on the technique developed in Toyota Central Research and Development Laboratory (Usuki *et al.,* 1992, Kawasumi 2003), an extensive study on the interaction between polymer and silicates in nylon 6- clay nanomaterial was made by Sato *et al.,* 2006. All of the successful results in field of nylon 6- clay nanocomposite were obtained using two kinds of fillers, synthetic swellable mica and montmorillonite from Wyoming repository.

Excellent properties of nylon 6-clay nanocomposite made with montmorillonite filler are one of the reasons for an investigation of kaolinite and nylon 6 in plastic materials (Fornesa *et .al.,* 2002). Unal *et al.,* (2003) showed that the tensile strength and modulus of elasticity of nylon 6 increased with a higher ratio of the filler in the material, but the impact strength and maximal elongation decreased with an increased content of clay. The homogenous properties of composites are dependent on a good dispersion of the fillers in polymer, which is obtained by intercalation of monomers between clay layers and polymerisation.

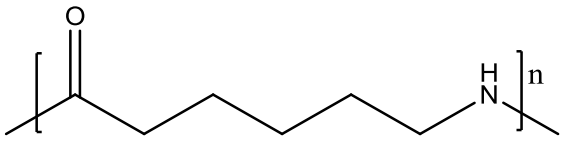

Figure 51 Nylon -6 structure

The trials on the production of nylon-6 kaolinite nanocomposite were started by Komori *et al.,* (1999). The main proposal of this work was the intercalation of nylon monomer - ε-caprolactam into kaolinite through methanol-kaolinite precursor and in-situ polymerization of obtained precursor. Intercalation of monomer was confirmed by a basal spacing attributed to ε-caprolactam. Polymerisation of the nylon monomer was unsuccessful. In 2001, Matsumara *et al.,* (2001) intercalated 6-aminohexanoic acid in the kaolinite interlayer through kaolinite-methanol and performed a polymerization in situ. However, delamination of kaolinite plates was not observed. In both cases, the polymerization procedure was performed under nitrogen conditions in the tube furnace.

5.1.1 Mechanism for polymerization of nylon

Nylon 6 is created through a polycondensation with creation of water which does not increase with the reaction progress. Therefore, it is not necessary to remove water from the system. The first stage of the polymerization of nylon-6 is the hydrolysis of ε-caprolactam according to reaction:

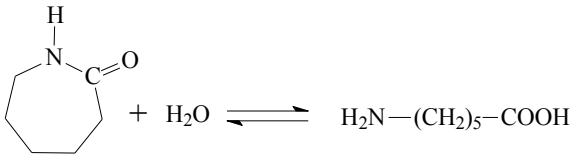

The polycondensation process occurred in the temperature range between 250-270°C in a nitrogen atmosphere which prevents side reactions and by-products of the process (Cho and Paul 2001; Kristofic *et al.,* 2005). In order to decrease the initiation time of the hydrolysis of ε-caprolactam, a small amount of 6-aminocaproic acid may be added (Nahal Tunzun 2008).

The next step of polymerization is an addition of caprolactam molecules to the created polycaprolactam:

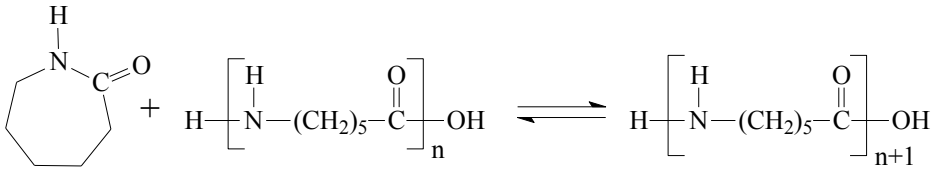

Due to the presence of the carboxylic and the amine group endings on nylon-6, an accelerated susceptibility to hydrolysis is ascribed. Thus, a substance which reacts with those groups to improve nylon-6 is necessary. For the same reason, regulators of the molar mass of polymer molecules are added during the process.

The final step for polymerization of nylon-6 is the condensation of polycaprolactam molecules with varied length:

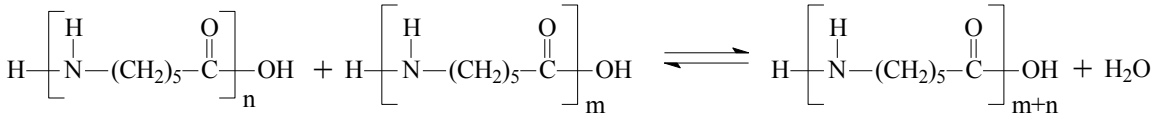

Presence of monomers and oligomers in the nylon-6 have a negative impact on the properties of the material, therefore these molecules have to be removed by washing of polymer in hot water (85°C).

Procedures of polymerization of precursors

Simple polymerization of kaolinite precursors by polycondensation was chosen as the simplest method of nylon production. Therefore, high temperature experimental conditions were required. Two different equipment which provide high temperature and an oxygen-free atmosphere were used for production of kaolinite nylon nano-composites. Thermo Scientific Lindberg Blue Tube Furnace which provided a nitrogen atmosphere and Shel Lab Vacuum Oven were used in the set of experiments described below.

5.1.2 Polymerization of kaolinite precursors in tube furnace

1) 150 mg of AHA kaolinite with an excess of acid on the external surfaces of kaolinite platelets was distributed homogeneously in the ceramic sample holders. Then, the sample holders were introduced gently into the glassy tube with nitrogen atmosphere. A single set point heating program up to 250°C was applied for two hours. After completion, the sample cooled down progressively in the nitrogen atmosphere.
2) 150mg of AHA kaolinite, without an excess of acid on the external surfaces of kaolinite platelets was introduced into the tube furnaces for 2h at 250°C. The same type of sample holders and program was used as for AHA kaolinite with an excess of acid on the external surfaces of kaolinite. Both preparations were washed by ethanol twice.

5.1.3 Polymerization of AHA kaolinite precursors in the vacuum oven

A set of samples were polymerized in the vacuum oven. Every time 50mg of AHA kaolinite sample was introduced in the ceramic cups to the oven, the air from that space was removed by using a vacuum pump. For comparison purposes, 70mg of pure aminohexanoic acid was also polymerized in the vacuum oven.

For all samples, the same experimental setup of pressure was applied: 84kPa. Two time durations for the experimental procedures were chosen. The first set of samples was heated at the defined temperature for 2h and was then cooled down progressively with ventilation of the vacuum oven. The second set of the samples was heated in the vacuum oven overnight and cooled down by the same procedure, as described above.

AHA kaolinite precursors were heated under four temperature conditions from 100°C, 150°C and 180°C up to 240°C.

All of the conditions for the set of samples polymerized in the tube furnace and vacuum oven are presented below in the table:

Name of sample	Temperature of reaction [°C]	Time of heating [h]	Atmosphere	Amount of sample [mg]
KAHA 100°C 2h	100	2	Vacuum	50
KAHA 150°C 2h	150	2	Vacuum	50
KAHA 150°C 17h	150	17	Vacuum	50
KAHA 180°C 2h	180	2	Vacuum	50
KAHA 180°C 18h	180	18	Vacuum	50
KAHA 240°C 2h	240	2	Vacuum	50
AHA 150°C 17h	150	17	Vacuum	70
KAHA 250°C ex	250	2	Nitrogen	150
KAHA 250°C	250	2	Nitrogen	150

5.1.4 Polymerization of standard in TGA

15 mg of KAHA precursor was heated in the TGA in a nitrogen atmosphere up to 300°C isothermally at a ramp of 50°C per minute. That sample was used as an internal standard for the comparison between samples prepared in tube furnace and vacuum oven.

5.4 Results and Discussion

5.4.1 X-Ray Diffraction

AHA intercalated in kaolinite is characterised by a basal spacing of 1.47 nm. Influence of the heat treatment on the AHA kaolinite precursor is manifested by the appearance of a new peak on the diffractogram. The values of the basal spacing are related to the temperature of heating and time of process. Matsumura *et al.,* (2001) reported a basal spacing of 1.16 nm for polymerised AHA kaolinite under nitrogen flow in a tube furnace. Sample KAHA250°C2H was polymerised under the conditions consistent with paper cited above; however, the obtained basal spacing is slightly lower: 1.14 nm. The sample produced in the TG instrument as a standard is characterised by a basal spacing of 1.15 nm. On the spectra of a precursor (KAHA240°C2H) polymerised in a vacuum oven at the temperature of 240°C for 2h, the presence of a peak with basal spacing of 1.16 nm is visible. Nevertheless, those values are higher than for the methanol-kaolinite precursor, 0.86 nm (Tunney and Detellier 1996), DMSO-kaolinite, 1.10 nm (Letaief and Detellier 2009), and glycine intercalated in hydrated kaolinite, 1.03 nm (Sato 1999). The intensity of the peaks related to nylon- 6 in the structure of kaolinite, as compared with the intensity of kaolinite peaks is also dependent on the conditions of polycondensation. The samples made in a vacuum condition are characterised by more intense peaks related to the intercalated polymers than the standard sample produced in TG and in tube furnace. Higher intensity of nylon 6-kaolinite, with comparison to kaolinite, is evidence of the better efficiency of the process of polymerisation in kaolinite's interlayer space. In other words, a higher percentage amount of nylon 6 kaolinite is present in the samples produced under vacuum conditions than in the sample produced under nitrogen flow. Influence of temperature of polymerisation process of nylon 6 in the kaolinite interlayer is shown by results obtained for the series of four samples heated under the vacuum condition for 2h.

The highest value for basal spacing is presented by a sample heated to 100°C for 2h (KAHA100°C 2H), 11.8 nm, which is the same as for a shorter amino acid, β-alanine, intercalated in kaolinite (Sato 1999). Probably, when the sample is heated up to 100°C, the majority of the molecules which are present in the interlayer space of the mineral are AHA and concurrently the initial nylon 6 molecules are created; therefore, the basal spacing of KAHA100°C 2H is larger than that of the sample heated up to higher temperatures. When the temperature of polymerisation was increased to 150°C and 180°C, the basal spacing of nylon 6-kaolinite in the heated samples decreased respectively from 1.12 nm (KAHA150°C2H) to 1.11 nm (KAHA 180°C2H). For the sample heated up 240°C, the basal spacing increased up to 1.16 nm. Also, during the heat treatment, the basal spacing of kaolinite decreased from 7.23Å for KAHA100°C2H to 7.16Å for KAHA240°C2H. On the KAHA250°C2H diffractogram, a hump in the range 2θ (4-6°) is visible. It is connected with technique of XRD measurement. The broadening comes from vaseline, which was used for preparing the powder spectra of the heated samples. The intensity of the broadening that appeared in each spectrum depends on the amount of vaseline used for sample preparation. The excess of vaseline versus powder is represented by visible hump or broadening in the range mentioned above.

Two series of measurements were done for investigating the effect of the duration of heating time on XRD results. In the first series, samples heated to 150°C for 2H and overnight were compared. The inconsistency in the basal spacing of the sample treated overnight (KAHA150C°17H), 1.11 nm, with KAHA150°C2H, 1.12 nm, is negligible and connected with kinetics. For samples heated up 180°C for 2h and overnight, the same range of discrepancies was observed, but the basal spacing of the

sample treated overnight (KAHA180°C18H), 1.12 nm, was slightly bigger than for KAHA180°C 2H ,1.11 nm.

The average interlayer thickness Δ (Δ=d(001)- 0.72 nm) of nylon 6-kaolinite is 0.42 nm, which is consistent with the values presented by Matsumura *et al.,* (2001).The values indicate that the polymer thickness in the interlayer space of kaolinite is that of a single chain of nylon 6.

After investigation of the higher angle spectra of KAHA 150°C 17H and AHA150°C17H, the crystalline structure of nylon 6 polymerised in the vacuum oven was determined. Spectra of pure amino acid after heat treatment is characterised by two peaks, 0.43 nm and 0.37 nm, which are attributed to α-form of nylon 6 with planar zigzag structure, whereas nylon 6 polymerised between the interlayer spaces of kaolinite is γ- form of a helix structure which is attested by only one peak with a basal spacing of 0.44 nm (Okada *et al.,* 1989; Malta *et al.,* 1979).

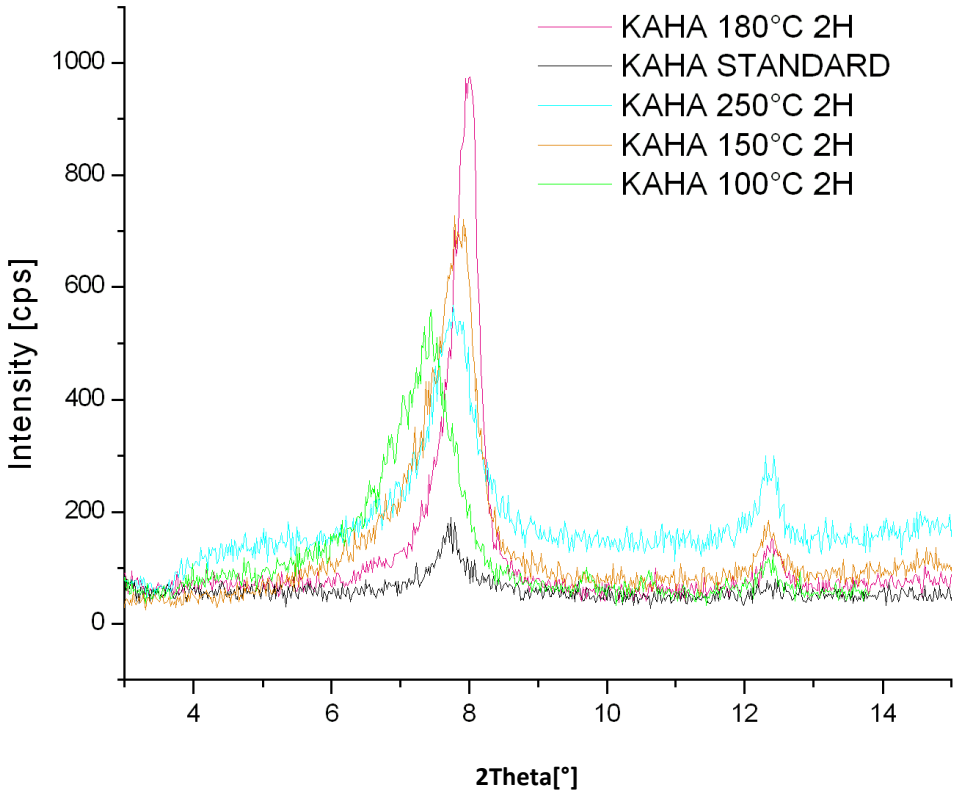

Figure 52 XRD patterns of the heated kaolinite-AHA samples

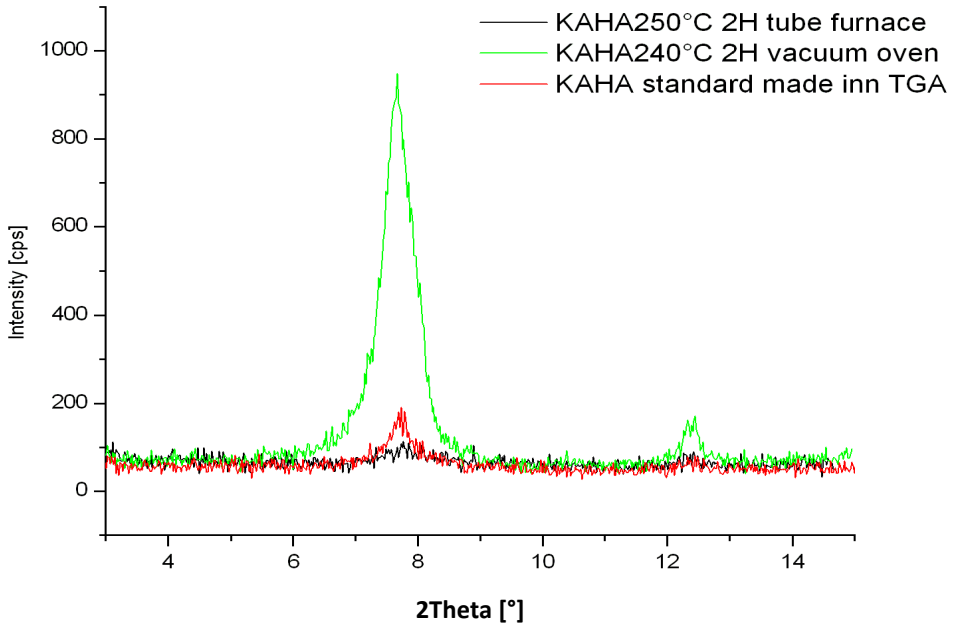

Figure 53 Comparison of the XRD patterns of samples heated in the vacuum oven and tube furnace

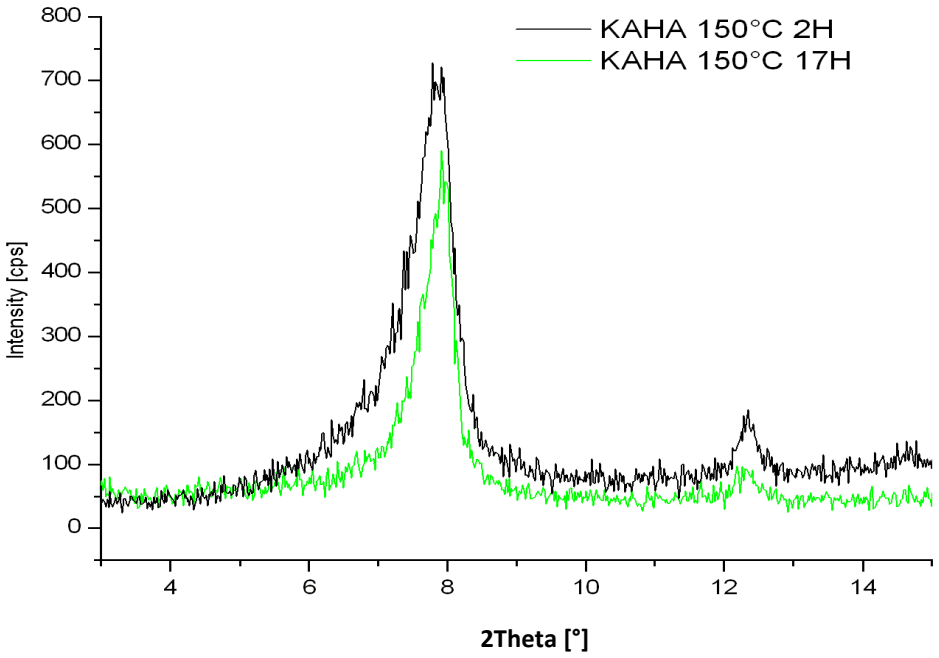

Figure 54 Comparison of the XRD patterns of the samples heated under varying time durations

5.4.2 IR study of nylon 6-kaolinite composite made in various conditions

On the IR spectra of AHA-kaolinite precursors heat treated under various conditions, some changes in comparison to AHA-kaolinite in the regions associated with OH stretching regions are visible. The inner OH group represented by stretching vibration band at 3620 cm^{-1} is not perturbed by the possible polymerization of monomer in the structure of kaolinite. Small shift of those bands in the spectra of KAHA150°C2H, KAHA250° and KAHA250°Cex are caused by shift of the whole bands in that spectra to the lower wave number. The bands attributed with OH stretching of inner-surface hydroxyl groups 3694 cm^{-1}(Madejova and Komadel 2001) are shifted to the lower wave number of 3692 cm^{-1} for KAHA250°C and KAHA150°C2H; 3693 cm^{-1} for KAHA180°C18H and KAHA250°Cex. Intensity of this band increases slightly with the temperature of polymerization for samples heated under vacuum at temperatures of 100°C, 150°C, 180°C and 240°C. Spectra of samples heated under nitrogen flow are characterized by a more intense band at 3694 cm^{-1} than 3620 cm^{-1}. Also, broad band at 3640 cm^{-1} appeared in AHA-kaolinite precursor is more defined in the spectra of samples polymerized under higher temperature than KAHA100°C 2H. For samples heated under the temperature conditions of 150°C and 180°C, bands related to the intercalated guest species are more intense than the rest of OH stretching vibration related to kaolinite. In the temperature of 240°C and 250°C, the intensity of the bands at 3640 cm^{-1} are comparable to inner stretching hydroxyl group band. In the spectra of sample KAHA250°C, band at 3640 cm^{-1} is replaced by 3633 cm^{-1} which is also visible in the spectra of KAHA250°Cex.

On the spectra of samples heated at 150°C and 180°C, the band near 3730 cm^{-1} appears. What is also peculiar for samples heated overnight (KAHA150°C17H and

KAHA180°C18H), is that the intensity of this band is higher than for KAHA180°C2H and KAHA150°C2H. It may be attributed to the formation of a silanol group formed during the dehydroxylation process; that high temperature hydroxyl band was observed for halloysite and dickite by Frost and Vassallo (1996). However, the dehydroxylation of halloysite is characterized by steps, in contrast to kaolinite.

On the spectra of KAHA180°C2H, KAHA180°C18H, KAHA240°C2H and KAHA250°C, broad bands around 3400 cm^{-1} are present, which could be associated with vibration of NH from non bonded amide groups which are separated due to the thermal treatment (Do *et al.,* 1987). The band at 3292 cm^{-1} on KAHA250°Cex is associated with stretching vibration of N-H with H trans bonded to the C=O in nylon 6 (Do *et al.,* 1987). The broad, low intense band around 3270 cm^{-1} visible on all of the sample spectra, with the exception of KAHA250°Cex, may be attributed to the asymmetric stretching vibration of NH_3^+ (Rotter and Ishida 1992). The broadening near to 3080 cm^{-1} is present on the whole series of spectra, apart from KAHA250°Cex where a band which may be attributed with H bonded stretching vibration of N-H in amino acid (Mayo *et al.,* 2004) manifested.

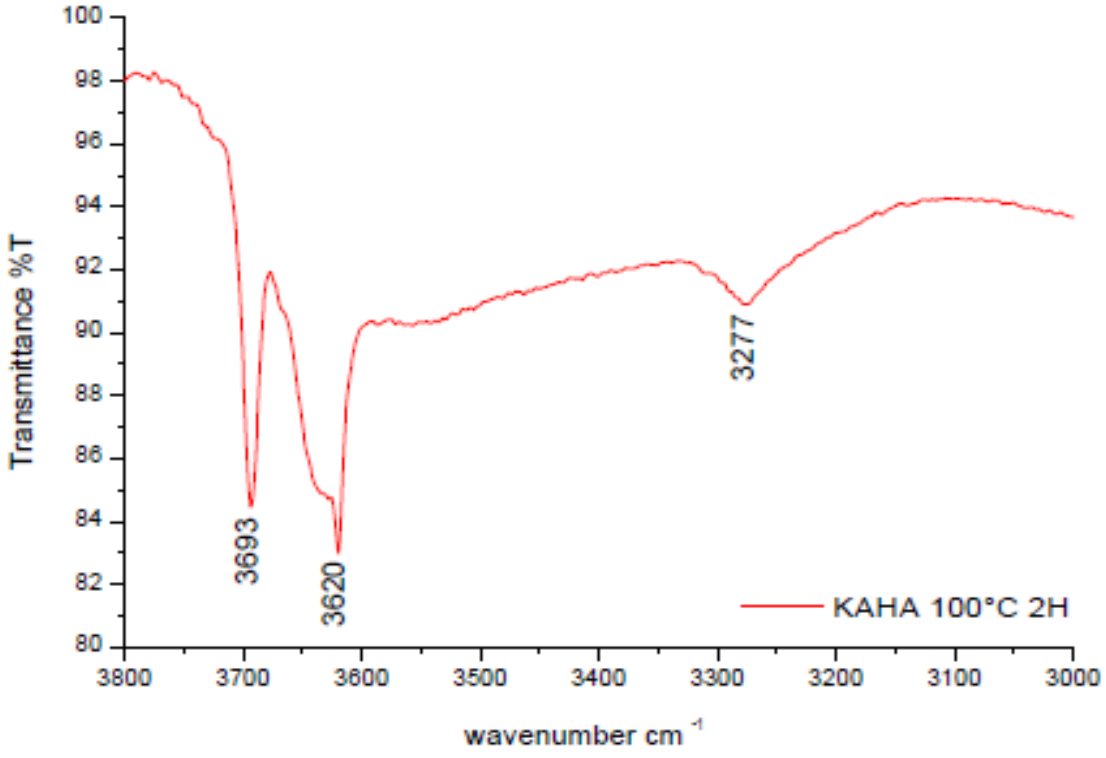

Figure 55 IR spectra of KAHA 100°C 2H in the range of 3800-3000 cm^{-1}

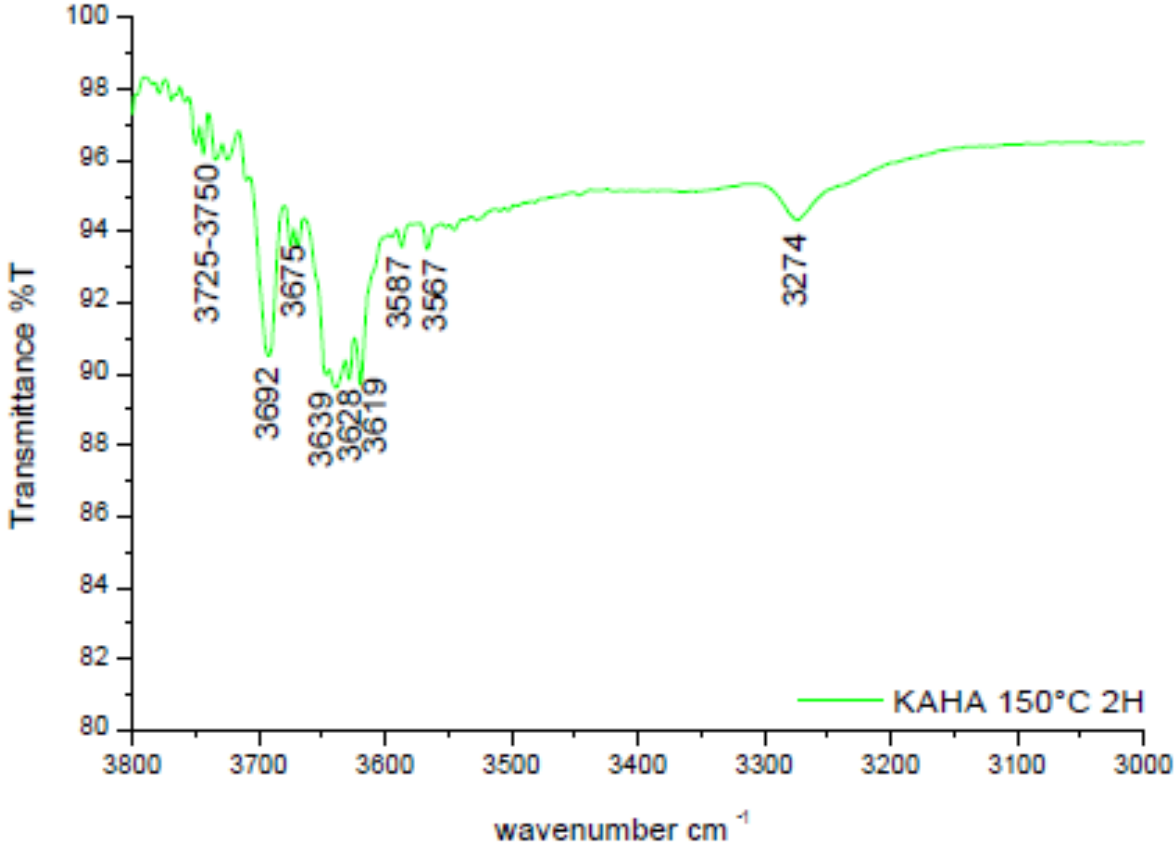

Figure 56 IR spectra of KAHA 150°C 2H in the range of 3800-3000 cm^{-1}

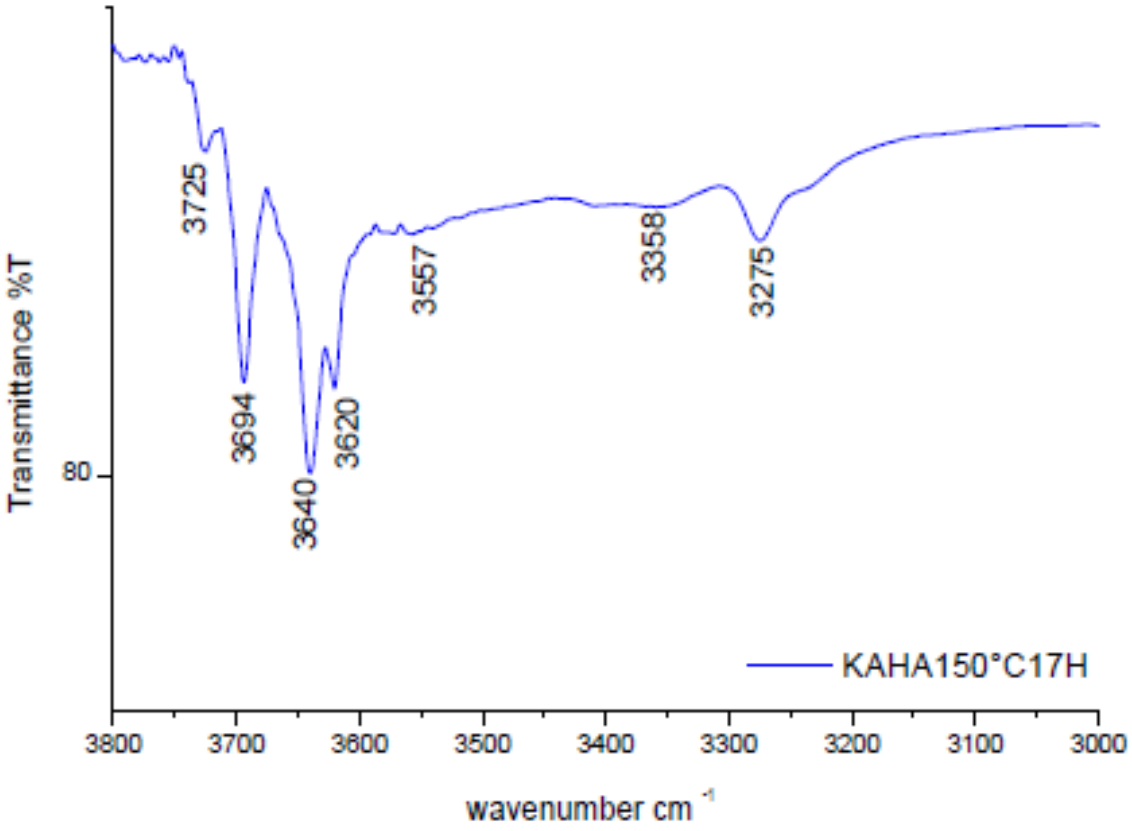

Figure 57 IR spectra of KAHA 150°C 17H in the range of 3800-3000 cm^{-1}

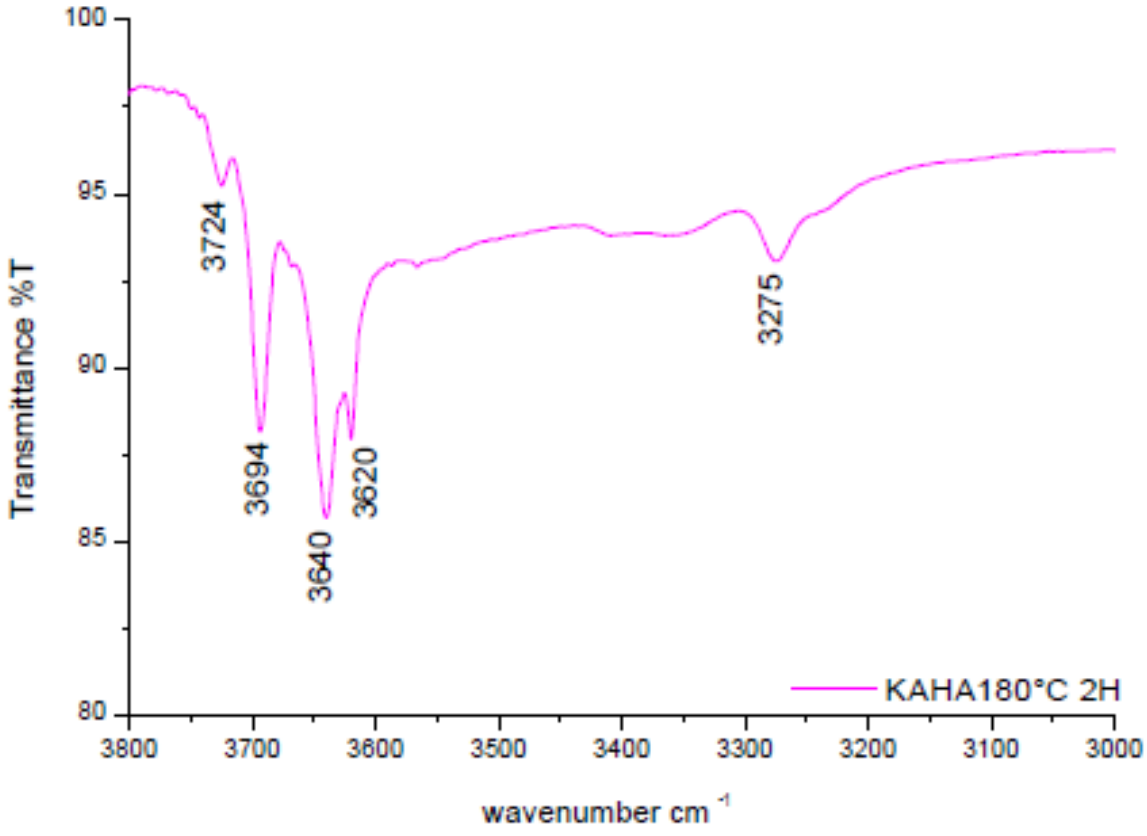

Figure 58 IR study of KAHA180°C 2H in the range of 3800-3000 cm^{-1}

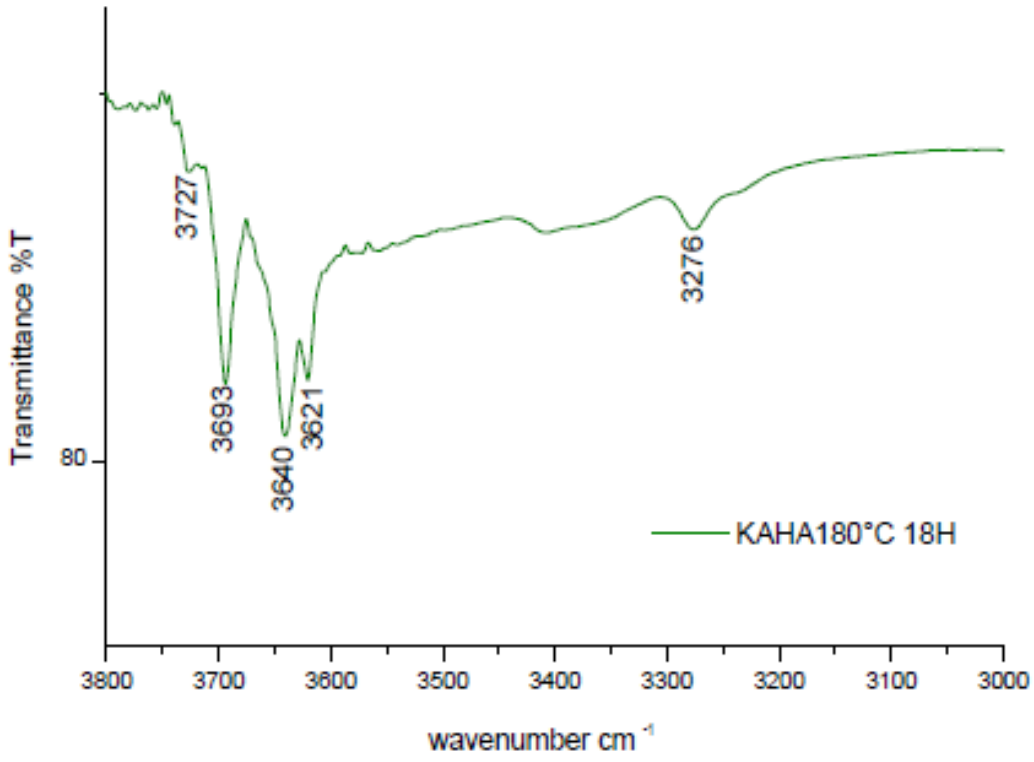

Figure 59 IR spectra of KAHA 180°C 18H in the range of 3800-3000 cm^{-1}

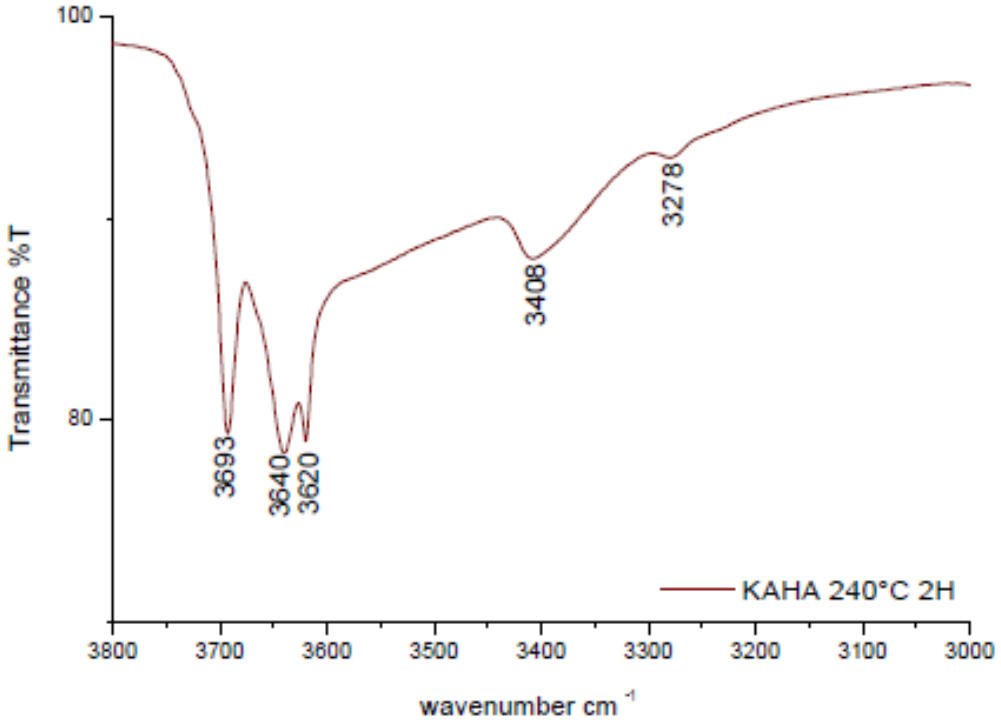

Figure 60 IR spectra of KAHA240°C 2H in the range of 3800-3000 cm^{-1}

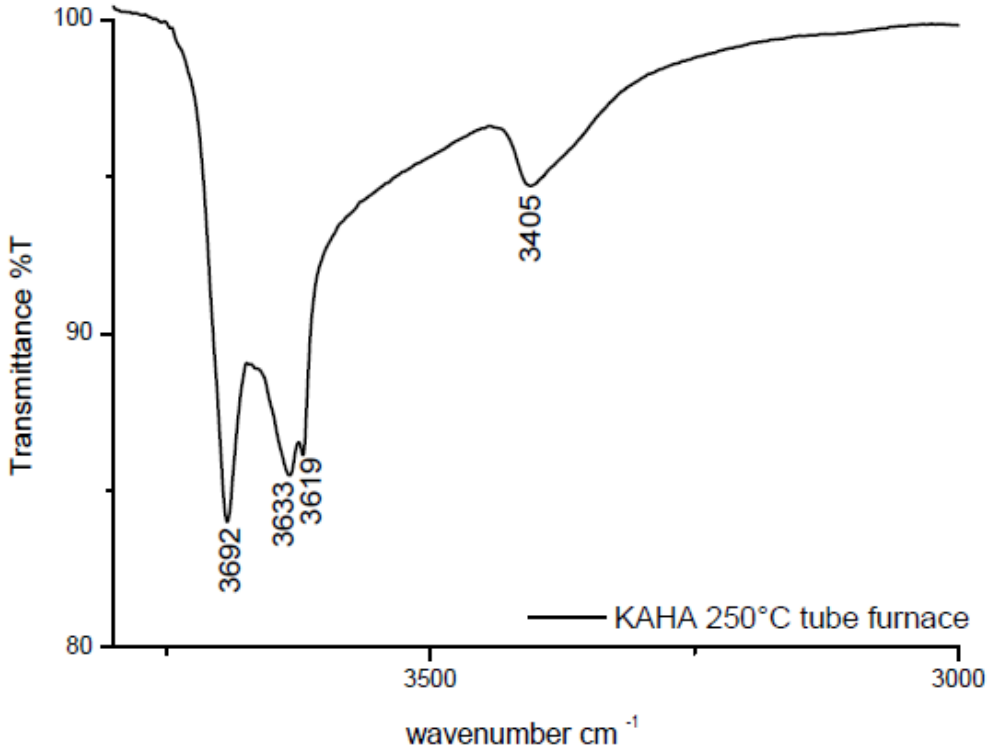

Figure 61 IR spectra of KAHA250°C tube furnace i the range of 3800-3000 cm^{-1}

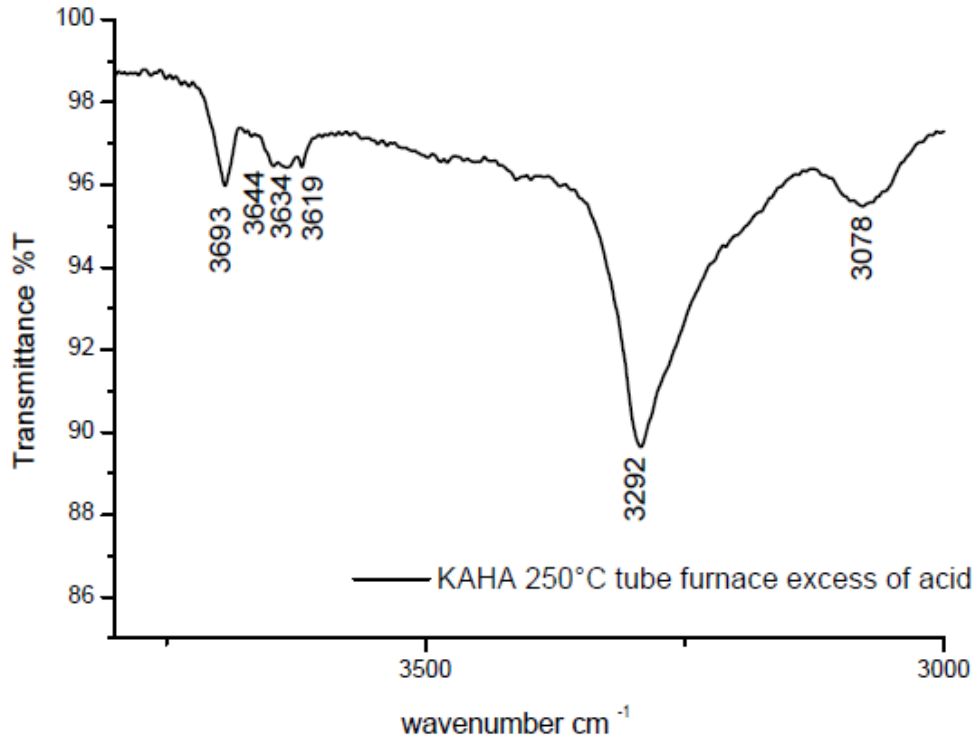

Figure 62 IR study of KAHA250°Cex with excess of the acid in the range of 3800-3000 cm^{-1}

In the region between 2000 and 1100 cm^{-1}, a band around 1620-1630 cm^{-1} is present for all the spectra. That band may be attributed with asymmetric NH_3^+ deformation vibration when it is located near to 1620 cm^{-1}, like for the sample KAHA100°C2H. In case of samples heated to 150°C and 180°C, the shift of bands to higher wave numbers is observed at, respectively, 1623 cm^{-1} for KAHA150°C2H, KAHA180°2H and 1627 cm^{-1} for KAHA180°C18H. For samples heated at 250°C, the band is shifted to 1630 cm^{-1} and 1633 cm^{-1}. Intensity of this band increases with temperature and it is interpreted as an amide I band (Matsumura *et al.,* 2001). Rotter and Ishida (1992) connected this band to α-crystalline form of nylon. Additionally, a broad band around 1650 cm^{-1} is present on the spectra of samples treated at temperatures of 150°C, 180°C and 240°C which may be attributed to amide I vibration in γ-crystalline form of the mesomorphous type of nylon- 6 (Rotter and Ishida 1992). In the spectra of KAHA250°C, a band at 1551 cm^{-1} is present, which is associated with amide II (Matsumura *et al.,* 2001). In the sample with an external excess of monomer, KAHA250°Cex, amide II band is located at 1538 cm^{-1} (Do *et al.,* 1989). For the sample heated under vacuum conditions, the band assigned to the COO^- asymmetric stretching vibration is moved from 1545 cm^{-1} for KAHA100°C2H, KAHA150°C 17H, KAHA180°C2H to 1547 cm^{-1} for KAHA240°C 2H and it may be overlapped with amide II band (Rotter and Ishida 1992; Do *et al.,* 1989). It may suggest that polymerization of monomer is partial and the progress depends on temperature of treatment. This assumption may be attested by XRD results, where for the KAHA100°C2H sample, the basal spacing of the obtained product is larger than for samples heated at higher temperatures. CH_2 scissors deformation are assigned to the bands at 1465 cm^{-1},1432 cm^{-1},1453 cm^{-1} for samples heated under vacuum condition

and 1443 cm^{-1} and 1434 cm^{-1} for KAHA250°C and KAHA250°Cex. The band at 1404 cm^{-1} is attributed to the symmetric stretching vibration of COO^- (Mayo *et .al.,* 2004). Decreasing of the intensity of this band for samples heated at higher temperatures may be connected with polymerization of bigger portions of the monomer in comparison to the lower temperature experiments. On the spectra of KAHA100°C2H, this band is characterized by an intensity similar to 1545 cm^{-1}, while for KAHA180°2H, the band at 1404 cm^{-1} is significantly less intense. In the spectrum of samples heated under vacuum conditions, an appearance of band at 1340 cm^{-1} for KAHA100°C2H and KAHA150°C2H; at 1341 cm^{-1} for KAHA150°C17H and KAHA180°C2H, at 1342 cm^{-1} for KAHA180°C18H and KAHA 240°C2H is noticed. The band may be attributed with CH_2 wagging deformation (Sato 1999). Appearance of a band at 1372 cm^{-1} for KAHA250°Cex which is shifted to 1376 cm^{-1} for KAHA250°C and 1382 cm^{-1} for KAHA240°C2H, is assigned to amide III vibration and CH_2 wagging deformation (Rotter and Ishida 1992). Also, the band at 1296 cm^{-1} is present on the spectra of all samples prepared under vacuum conditions and shifted to 1289 cm^{-1} for KAHA250°C, and this is associated with CH_2 wagging deformation and probably amide III for higher temperature treatment. At 1238 cm^{-1}, 1234 cm^{-1} and 1231 cm^{-1} bands related to the CH_2 wagging deformations are located (Rotter and Ishida 1992).

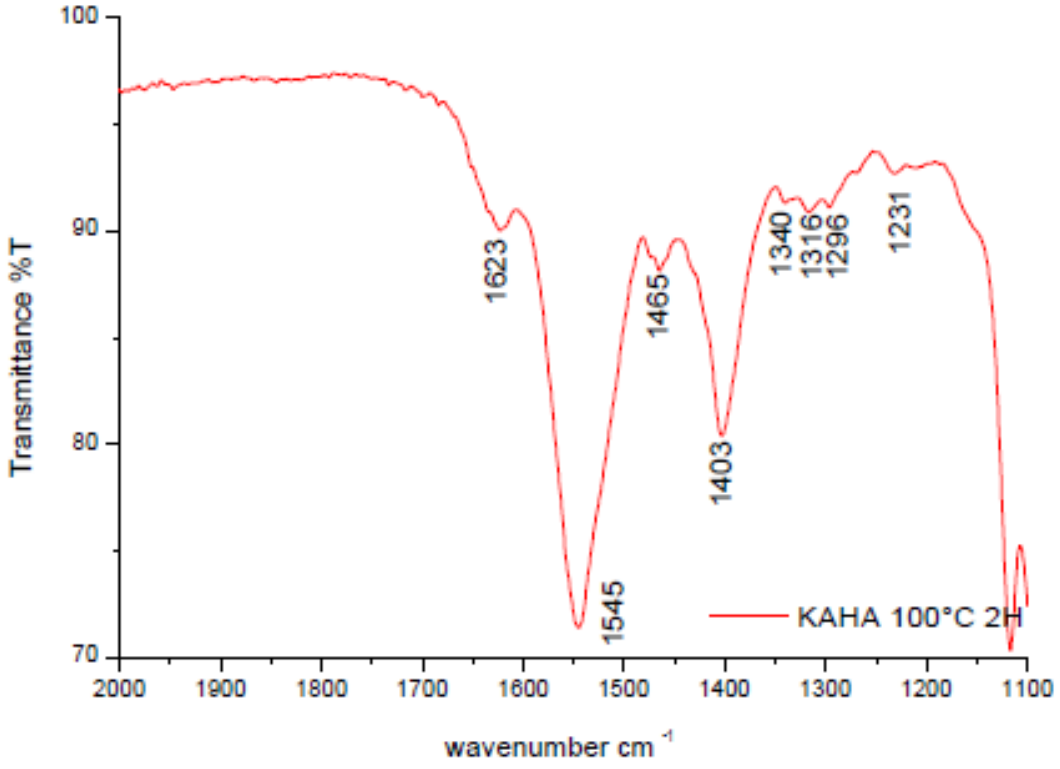

Figure 63 IR study of KAHA100°C 2H in the range 2000-1100 cm^{-1}

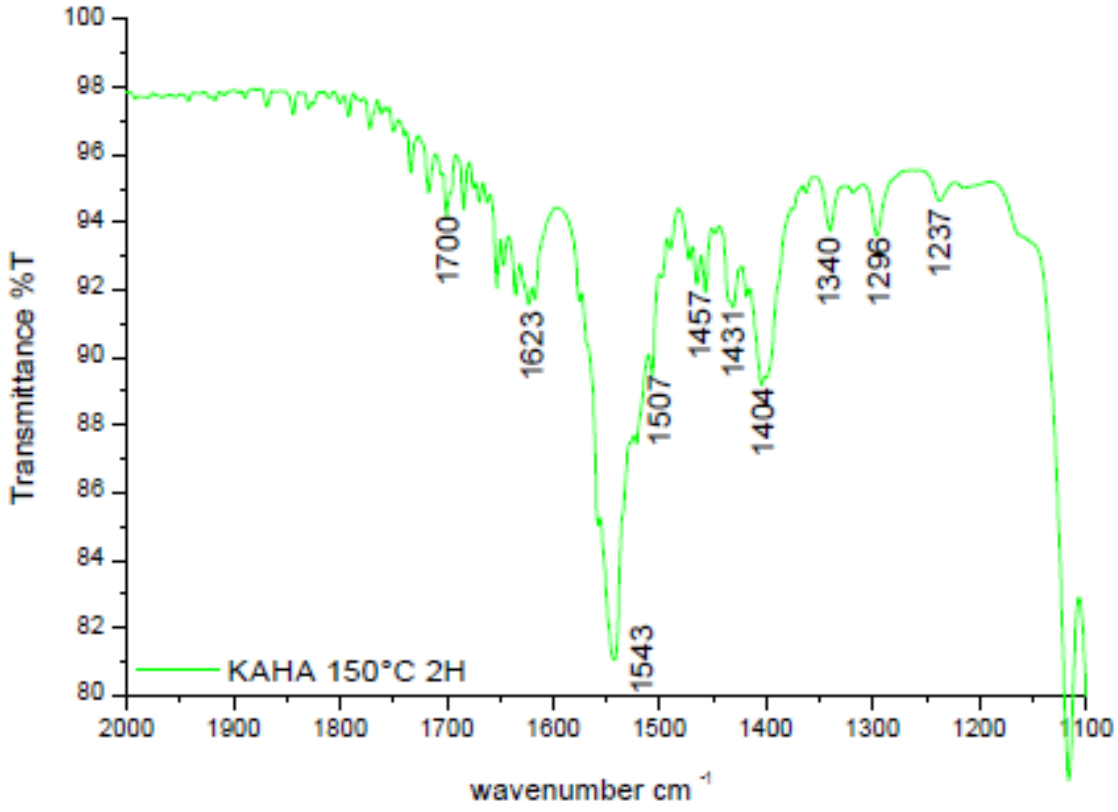

Figure 64 IR study of KAHA150°C 2H in the range of 2000-1100 cm^{-1}

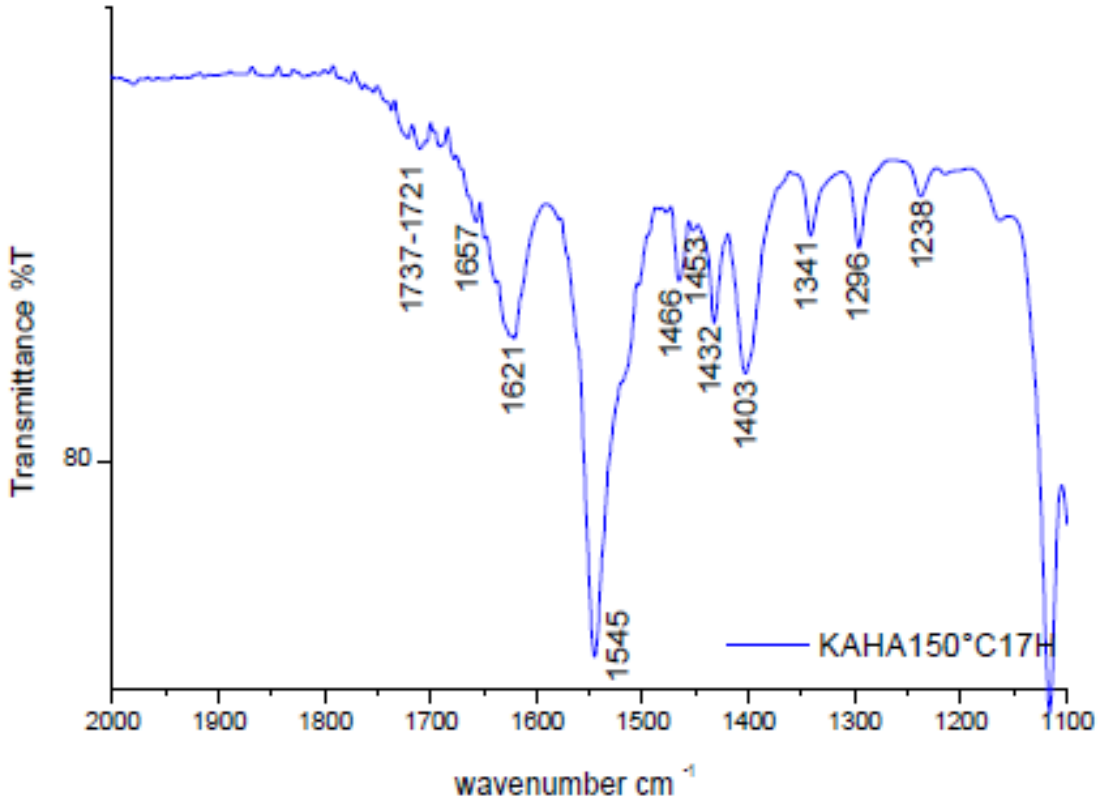

Figure 65 IR spectra of KAHA150°C 17H in the range of 2000-1100 cm^{-1}

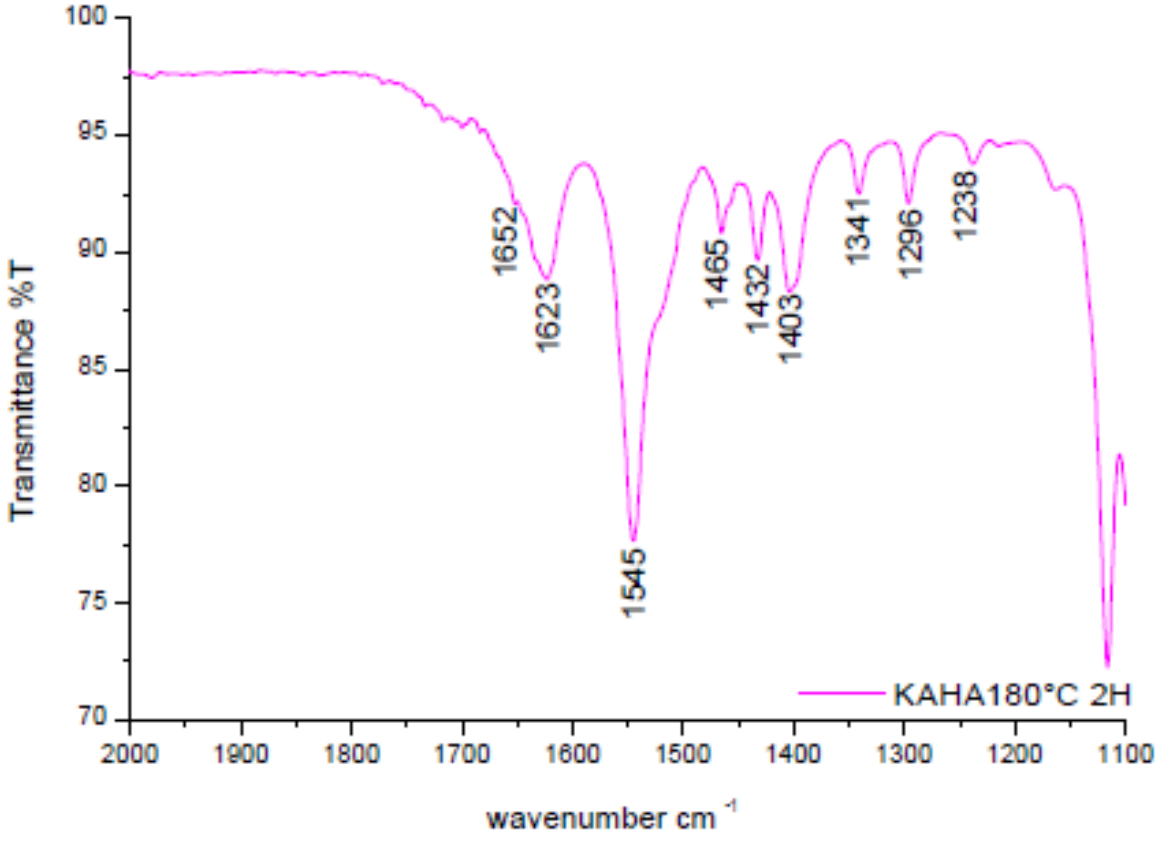

Figure 66 IR spectra of KAHA180°C 2H in the range of 2000-1100 cm^{-1}

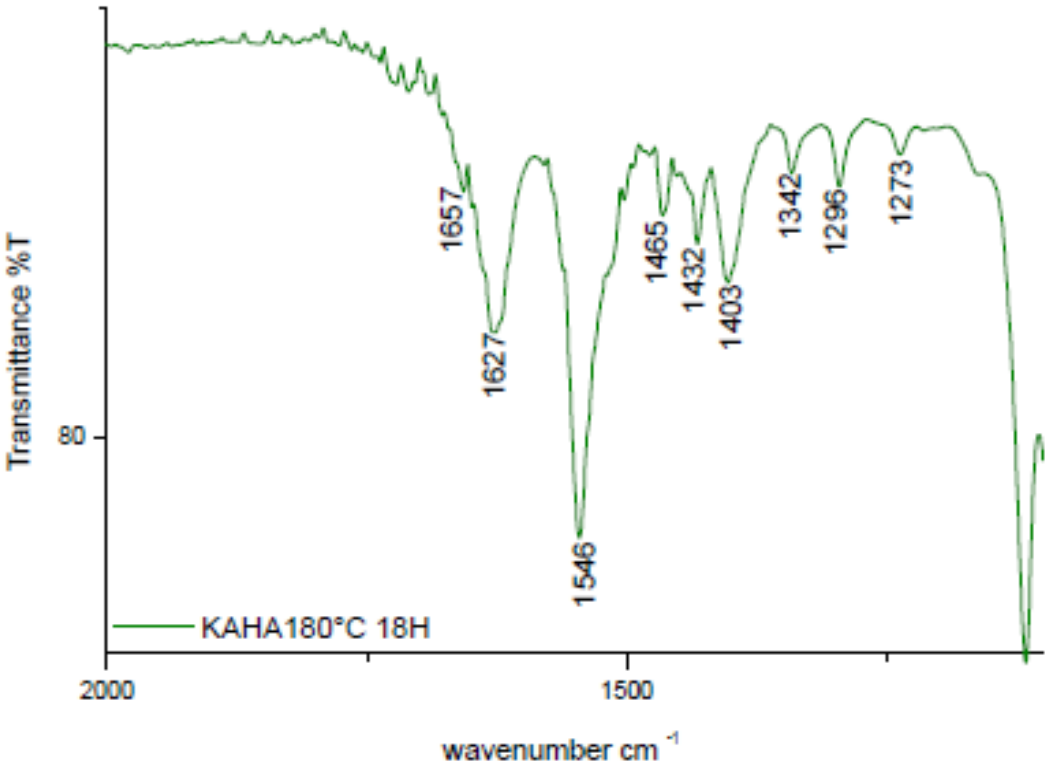

Figure 67 IR spectra of KAHA180°C 18 H in the range of 2000-1100 cm^{-1}

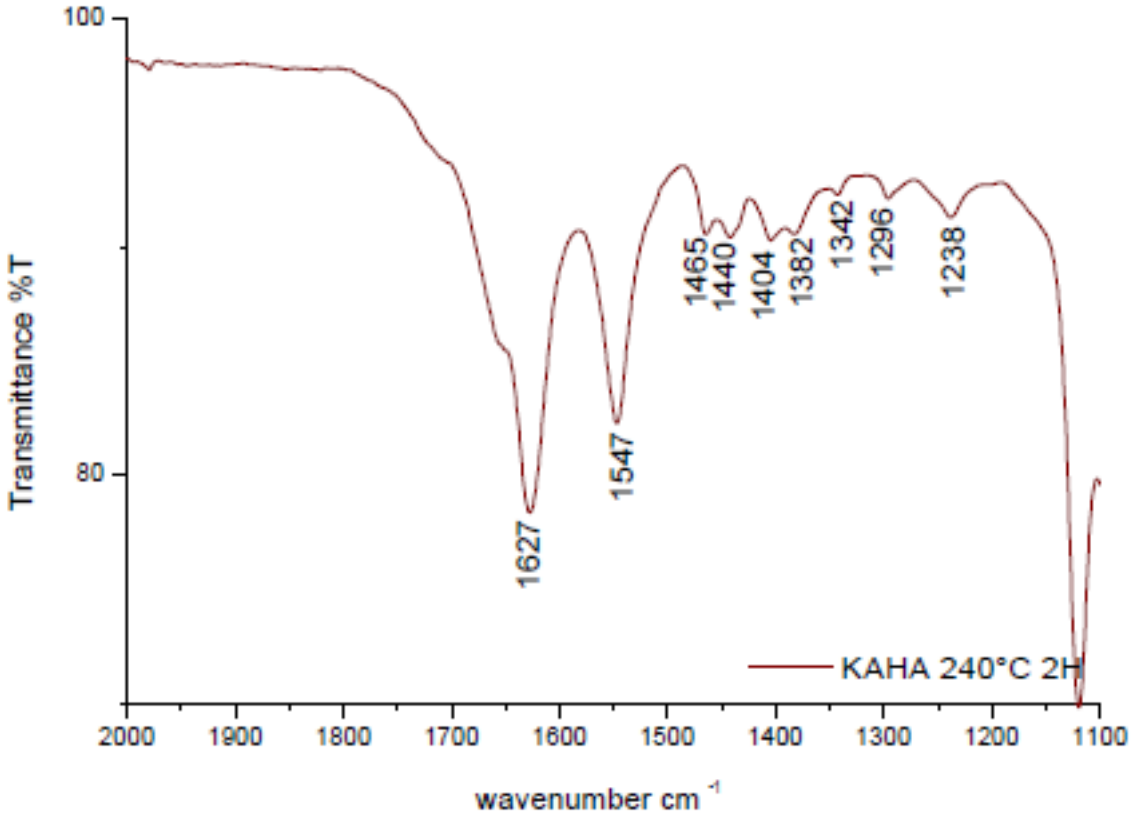

Figure 68 IR study of KAHA 240°C 2H in the range of 2000-1100 cm^{-1}

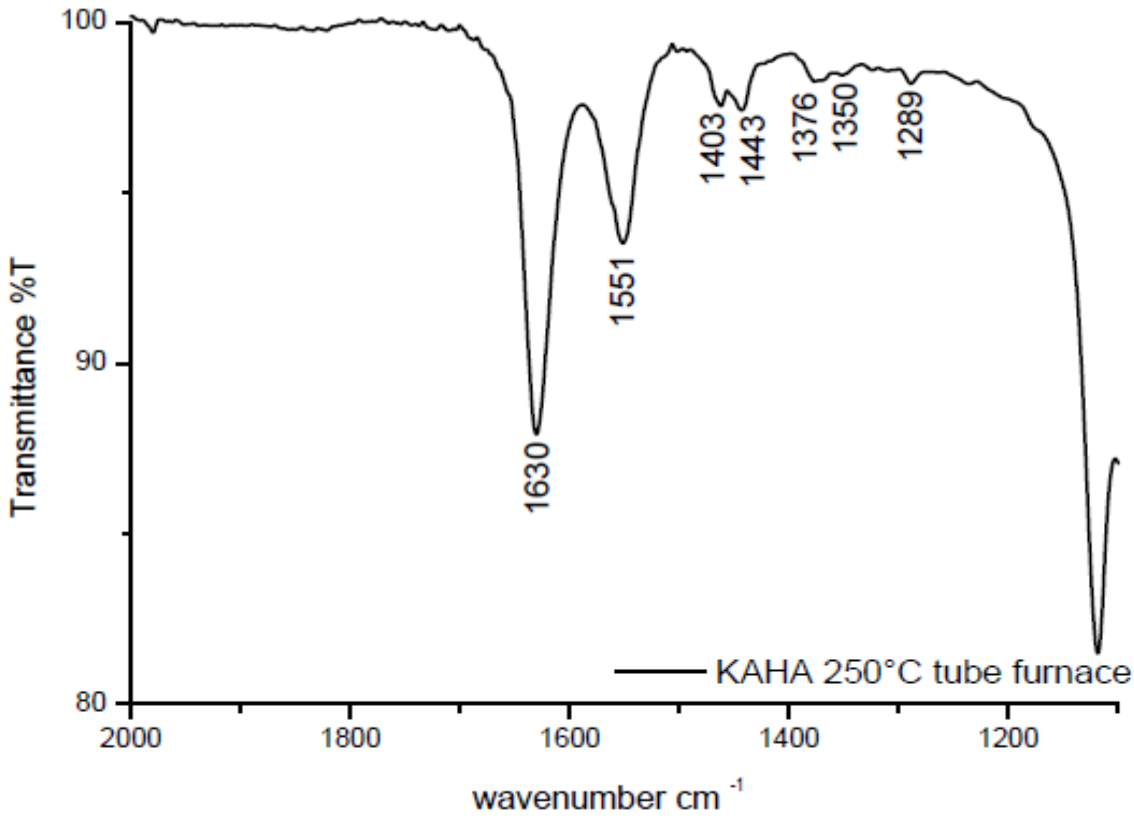

Figure 69 IR spectra of KAHA 250°C tube furnace in the reange of 2000-1100 cm^{-1}

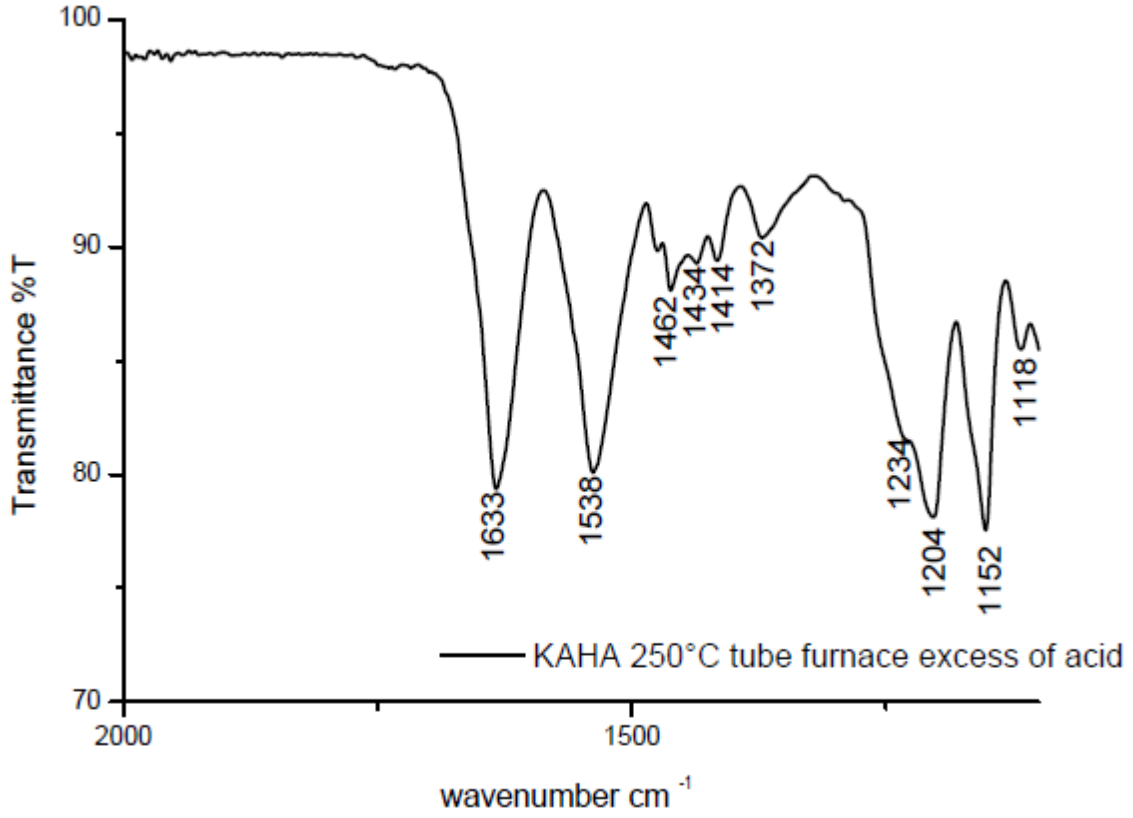

Figure 70 IR study of KAHA 250°Cex with excess of acid in the range of 2000-1100 cm^{-1}

5.4.3 Thermal analysis of AHA-kaolinite series of samples heated under various conditions

The results of thermal analysis prepared for samples heat treated under vacuum conditions may be classified in three groups.

The first group is represented only by KAHA100°C2H samples treated under vacuum at 100°C for 2h. On the TG curve, 4 mass losses are visible, which are also observed on the TG of untreated AHA- kaolinite precursor. The first mass loss is related to the removal of water adsorbed on the kaolinite surface (Hu *et .al.,* 2003). This process is illustrated by the endothermic peak on the DTA curve. The maximum intensity of the external water removal at 48°C is lower than in the case of the untreated precursor. The second and third mass losses are related to the polycondensation of acid between kaolinite layers (Hu *et al.,* 2003), decomposition and volatilization of non polymerized organic molecules and are visualized by endothermic peaks on DTA. On the DTG curve, these processes are visualized by two peaks with maxima at 204°C and 263°C. The peaks in the range of 150°C to 300°C are closer to each other (60°C difference) than in case of untreated precursor (80°C difference). The mass loss related to the first 3 reactions is lower than for the untreated precursor. The fourth mass loss ascribed to the decomposition of nylon 6 and dehydroxylation of kaolinite is connected with an endothermic peak on DTA, in the range of 350°C-550°C and two overlapped peaks on DTG , with maxima at 432°C and 464°C. On the DTA, the exothermic peak at 1009°C is ascribed with recrystallization of mullite.

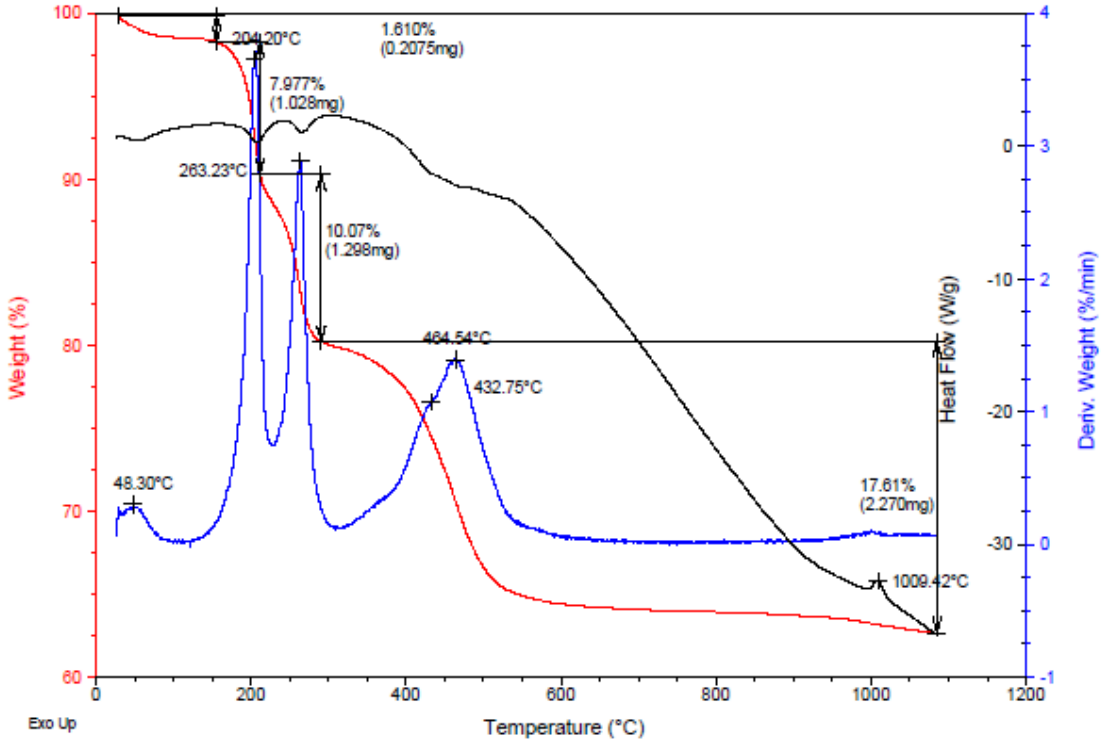

Figure 71 TGA results for KAHA 100°C 2H, TG red line, DTG blue line, DTA black line

The second group of thermal analysis describes the similar behavior of samples heated under vacuum conditions at temperatures 150°C and 180°C for 2h and overnight. The samples KAHA150°C2H, KAHA150°17H, KAHA180°2H and KAHA180°18H will be described together because they are characterized by 3 mass losses.

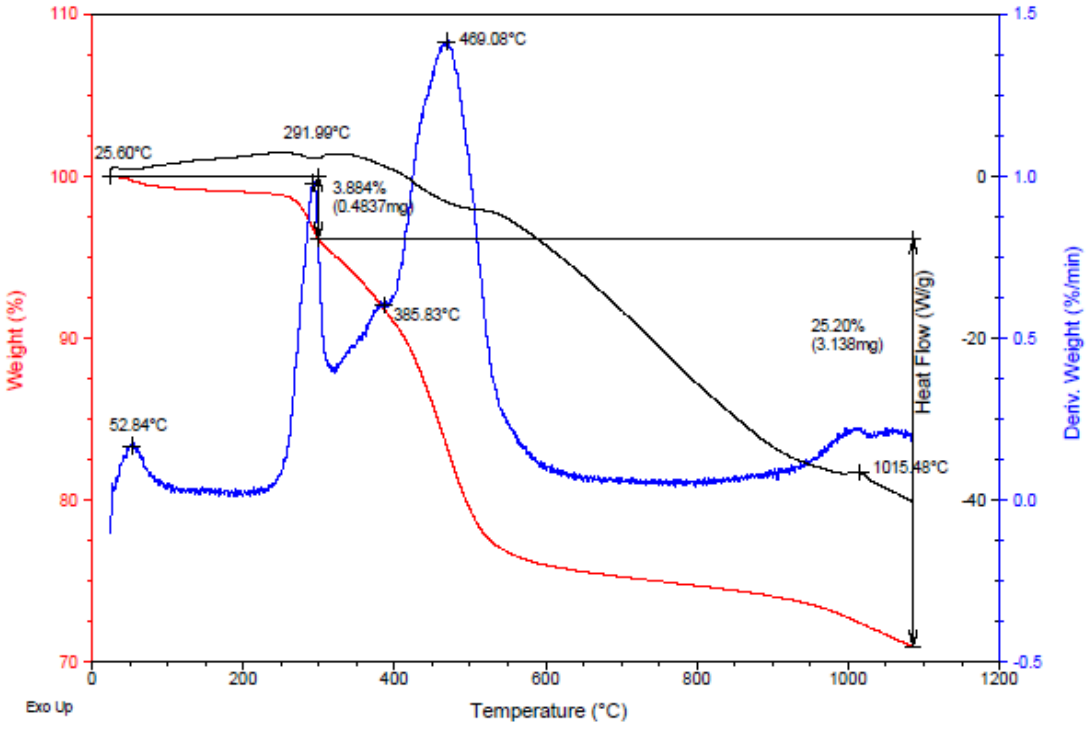

Figure 72 TGA results for KAHA 180°C 2H, TG red line, DTG blue line, DTA black line

For all spectra, the first mass loss is ascribed to evaporation of external layer of water molecules, which is described on the DTA as an endothermic peak, and the DTG maximum for that process is located at a temperature around 45°C for samples heated at 150°C and around 50°C for samples heated at 180°C. The second mass loss for all samples is visualized as an endothermic peak on the DTA with a maximum around 290°C-292°C on DTG. The second mass loss takes place between 270°C and 330°C. In comparison with KAHA100°C2H and the untreated precursor, one major difference is visible. The absence of peaks with a maximum at 198°-204°C,which are related to the polycondensation reaction. It may suggest that, polycondensation of acid was achieved by heat treatment and the second peak at 290°C is ascribed to decomposition and volatilization of parts of the acid chains which were not polymerized and are trapped between kaolinite layers; therefore, they are removed at high temperatures. Moreover, the second mass loss for sample heated up 150°C and 180°C is smaller than the third mass loss for KAHA100°C2H (10%) and directly related to the time and temperature

treatment. For KAHA150°C2H, the second mass loss is 7%, whereas for the sample heated overnight, KAHA150°C17H, the loss of mass is 5%, and respectively 5% and 3.8% for KAHA180°C2H and KAHA180°C18H. The third mass loss is related to the dehydroxylation of kaolinite and the decomposition of nylon 6. Overlapping of two peaks with maxima at 385-387°C and 469-465°C is visible on the DTG curve. The third mass loss is described by the endothermic peak on DTA. The exothermic peaks of all DTA are connected with the changing of the crystalline structure of clay, which is the transformation from kaolinite to mullite.

The third group of thermal analysis made for the sample treated under vacuum conditions is characterized by one major mass loss on TG curve. KAHA240°C2H represents this group. On the DTA curve, 4 endothermic peaks are visible. A DTG maximum at 58°C is related to the loss of externally adsorbed water. A low intensity peak at 290°C from DTG, ascribed to the decomposition of non polymerized organics, is represented by a small endothermic peak on the DTA. Two overlapped peaks on DTG with maxima at 375°C and 463°C are attributed with the decomposition of nylon and dehydroxylation of kaolinite. Exothermic peak on DTA around 1000°C is ascribed to the recrystallization of aluminosilicate.

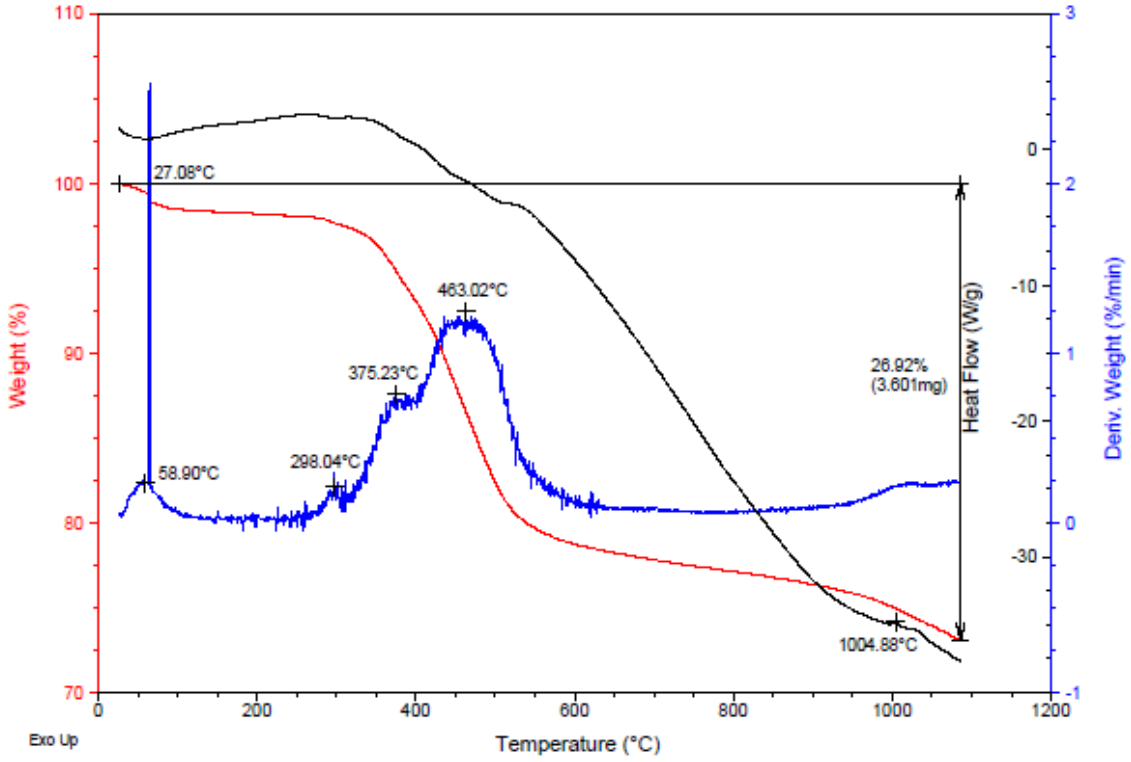

Figure 73 TGA results for KAHA 240°C 2H , TG red line, DTG blue line , DTA black line

The sample treated under nitrogen conditions is characterized by one major mass loss between 375°C and 600°C, with a maximum on the DTG at 461°C, which is attributed with an asymmetric endothermic peak on DTA. The mass loss is assigned to kaolinite dehydroxylation and nylon-6 decomposition. Total mass loss for the sample treated under nitrogen is smaller than for sample KAHA240°C, which is indicative of the best polymerization condition.

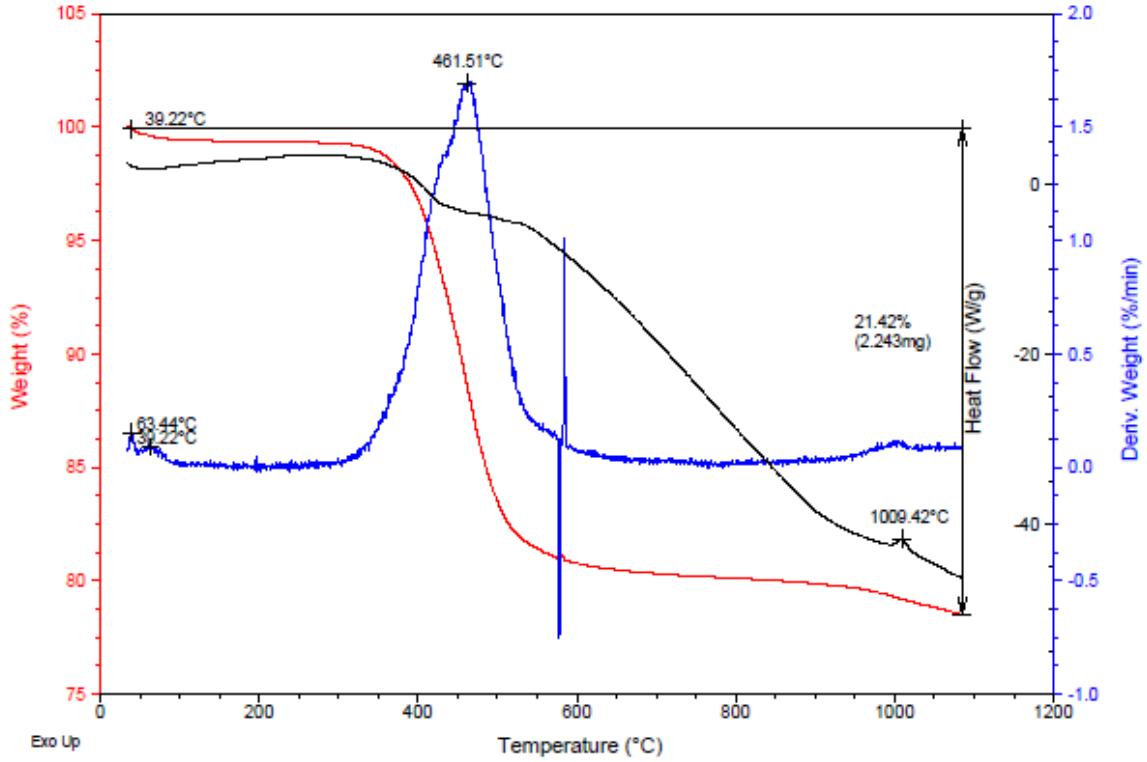

Figure 74 TGA results for KAHA 250°C sample , TG red line, DTG blue line, DTA black line

5.4.4 IR-TGA analysis of KAHA polymerization process

Simultaneous measurements of TGA and IR allow one to characterize the process of the polymerization of pure 6-aminohexanoic acid (AHA), kaolinite- 6-aminohexanoic acid precursor (KAHA) and the precursor heated up to 150°C (KAHA150°C17H). The differences between the behaviors of the 3 compounds are visible on the 3D IR diagrams. The samples were combusted under air for 20 minutes, while the temperature increased up to 1100°C.

As a standard for the comparison of the polymerization process of heated and non heated KAHA precursors, pure 6-aminohexanoic acid was used.

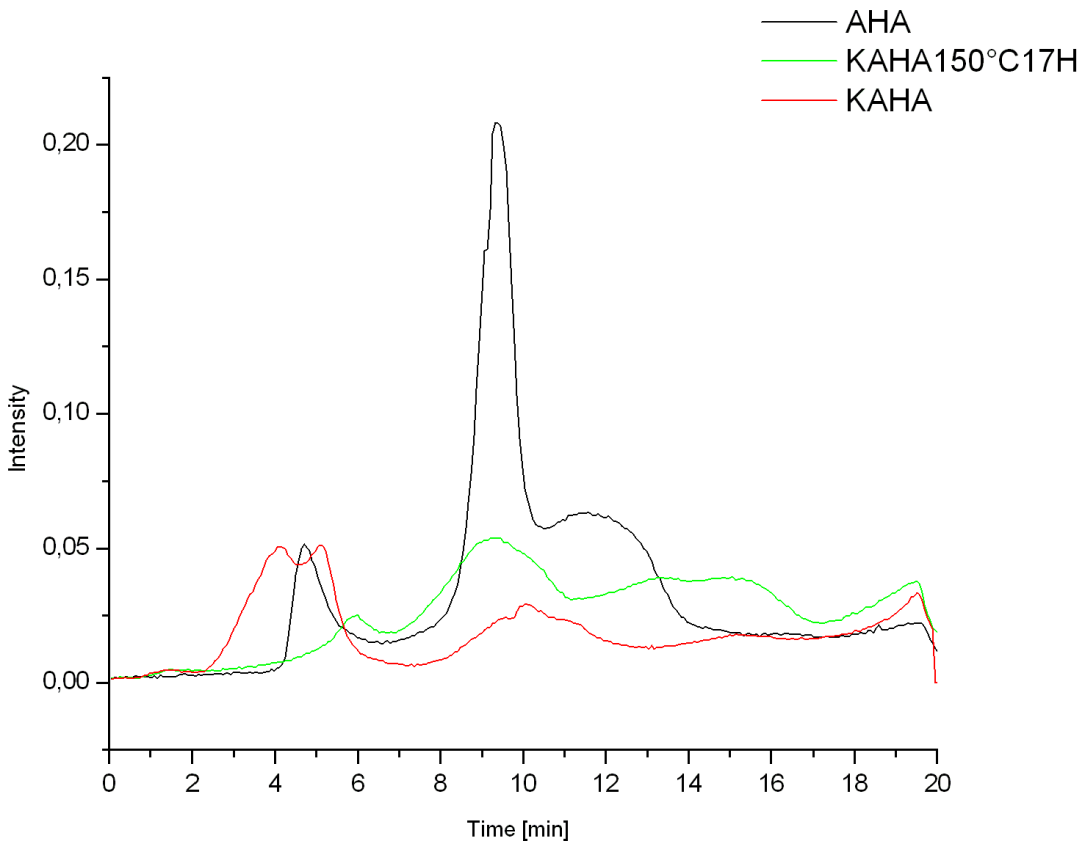

Figure 75 The diagram of the processes progress comparison for sample heated in TGA –IR

In the 3D IR diagram of heat- treated AHA, two major process are visualized by the appearance of peaks on the timeline of the process. The first stage is attributed with

polymerization of the AHA and represented on the IR spectra by a broad valence OH band in a range 3800-3400 cm^{-1}, ascribed to acid and also the presence of water (Mayo *et .al.,* 2004). Partial volatilization of AHA before and during polymerization is visualized by an appearance of aliphatic valence C-H band (2850-2970 cm^{-1}).The first stage of reaction is connected with polymerization around 200-250°C, which takes place between the 4th and 5th minute of the experiment. Around the 10^{th} minute of heating, the decomposition process of AHA is visualized by the appearance of peaks related to the decomposition, like the asymmetric stretching band of CO_2 (Mayo *et .al.,* 2004) at 2200-2300 cm^{-1}. Also, bands ascribed to the N-H bonding around 1180-1360 cm^{-1} are present. The presence of intensive valence band C=O and deformation N-H band around 2000-1500 cm^{-1} is evidence of the decomposition and volatilization of AHA.

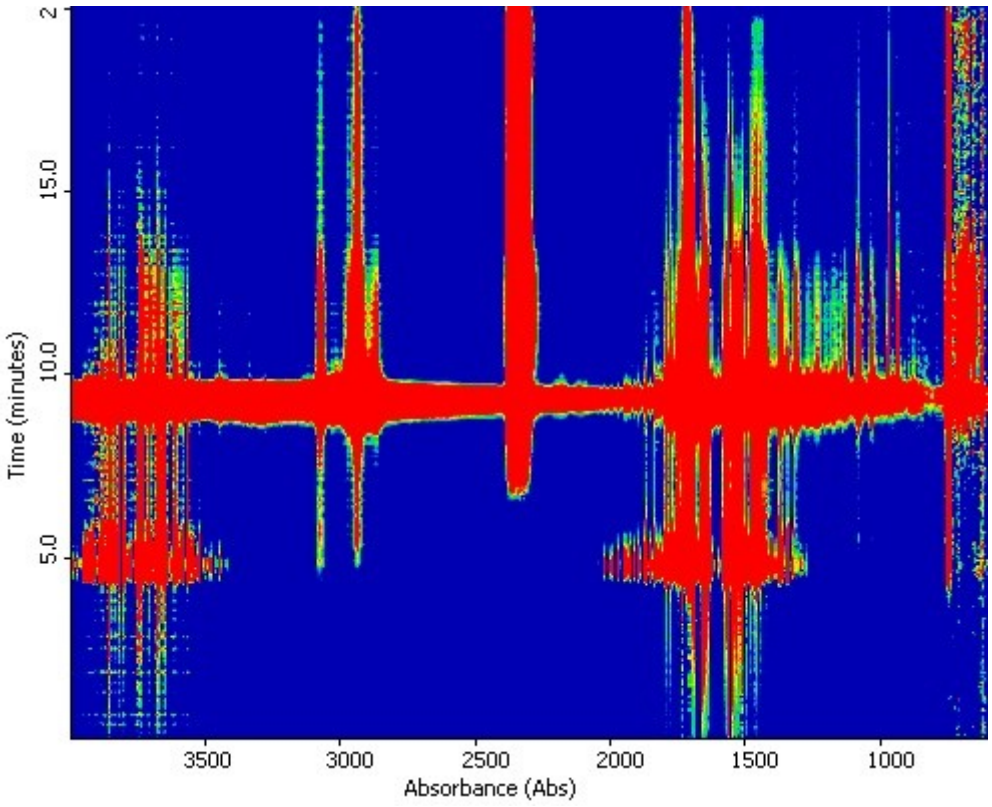

Figure 76 2D diagram for AHA, absorbance vs. time

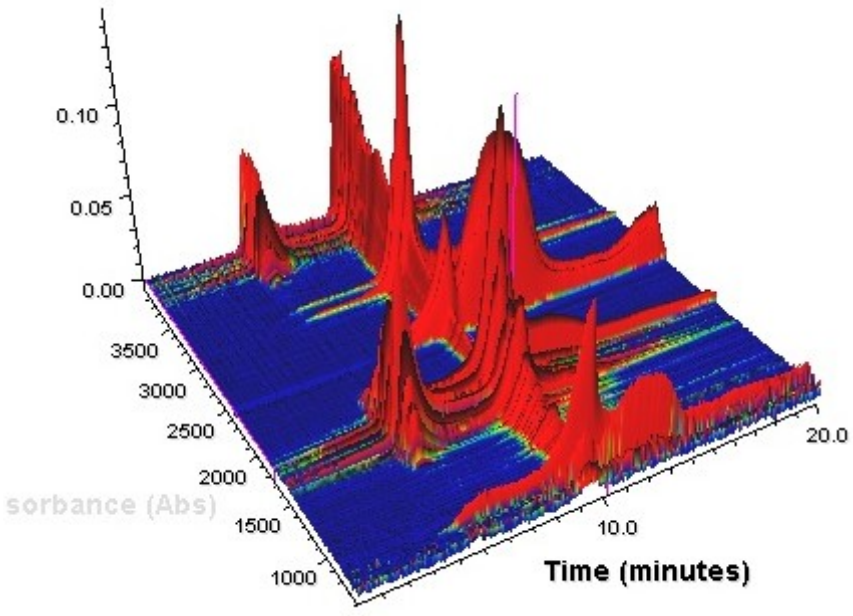

Figure 77 3D diagram of the process of AHA heating in TGA-IR

Four major peaks are visible on the timeline of the heating experiment with kaolinite-AHA precursor. In the 4th minute at around 200°C, there are peaks related to the OH bond at 3800-3400 cm^{-1}, ascribed to the water adsorbed by precursor on the external surface (Mayo *et .al.,* 2004). Also, the volatilization of AHA from the external surface of kaolinite is represented by peaks which appeared at around the 5th minute of the experiment. In comparison with pure AHA, the intensity of bands related to valence aliphatic carbon around 2850-2970 cm^{-1} (Mayo *et .al.,* 2004) in kaolinite –AHA is higher. It may be connected with an existence of an external layer of AHA which surrounds kaolinite plates, even though the precursor was washed by ethanol twice. Around the 10th minute, decomposition of polymer is attested by the appearance of CO_2 which is removed from the structure (Kim *et al.,* 2009). The fourth peak at around the 20th minute is also connected with removal of CO_2 from the system. The reason may be related to the CO_2 molecules trapped in the kaolinite interlayer space, therefore higher temperatures are required to remove trapped molecules.

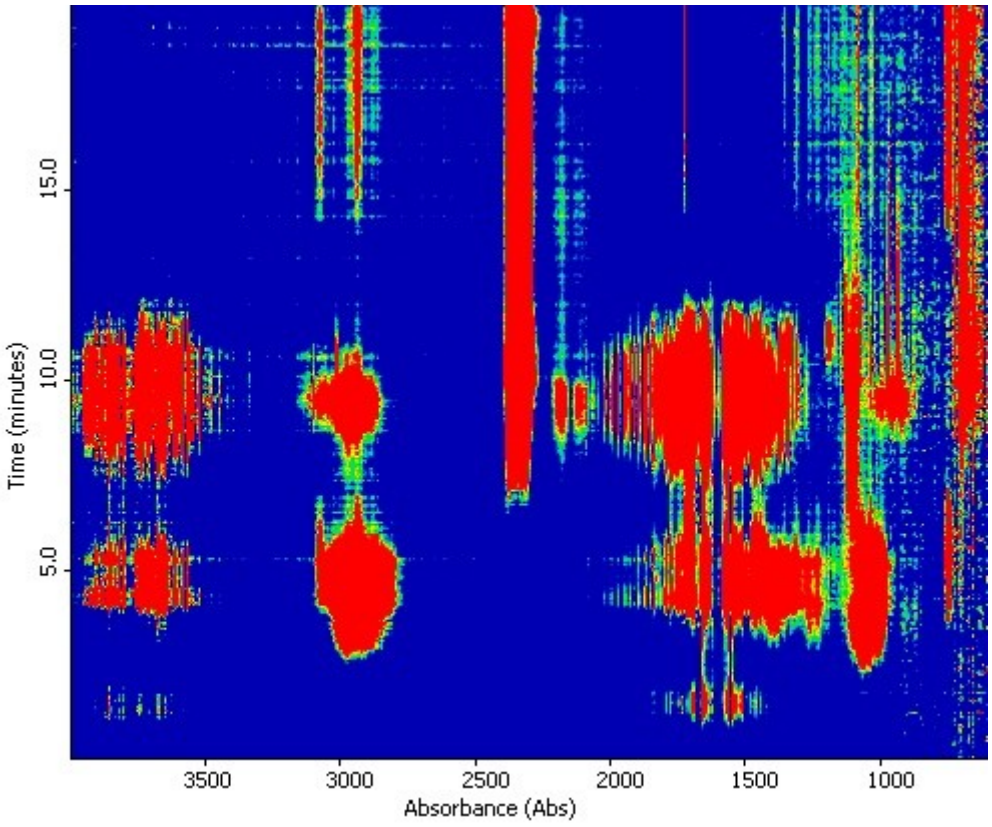

Figure 78 2D diagram of kaolinite-AHA illustrated absorbance bands during the time

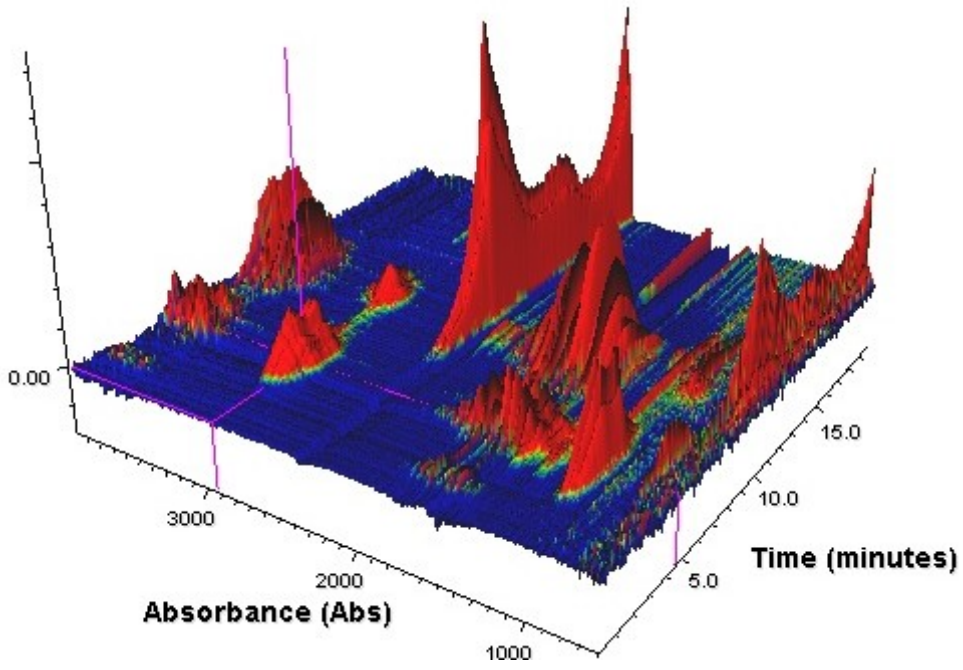

Figure 79 3D diagram of kaolinite-AHA sample heated in TGA-IR

Sample KAHA150°C17H heat-treated under the same conditions as the kaolinite-AHA precursor and AHA, is characterized by four events during the whole experimental

procedure. The first event with a maximum at the 6th minute of heating is associated with OH valence band ascribed to the water molecules above 3500 cm^{-1} and band from valence aliphatic carbon at 2850-2970 cm^{-1}. The lower intensity of the aliphatic band at the polymerization temperature of AHA is observed in the first event. It may be ascribed to the previous polymerization of AHA in the kaolinite-AHA during heating in the vacuum oven. The second episode is connected with the decomposition of obtained nylon at around 500°C. It is significant that there is a decrease of the intensities of bands ascribed to the N-H bonds around 1100 cm^{-1} compared to kaolinite-AHA. During the heating progress and kaolinite dehydroxylation, CO_2 produced due to the decomposition of polymer is removed from the structure of mineral.

The comparison of the intensities of a peak related to CO_2 for KAHA and heated KAHA150°C17H may be an indicator of polymerization of AHA during treatment in the vacuum oven. For KAHA, polymerization takes place during the experimental heating which is confirmed by similarities between 3D spectra of KAHA and AHA. Moreover, the intensities of the peaks connected with water versus CO_2 peaks in KAHA150°C17H are smaller than for KAHA and AHA samples, which is also an attestation of a previous polymerization process in the KAHA150°C17H sample.

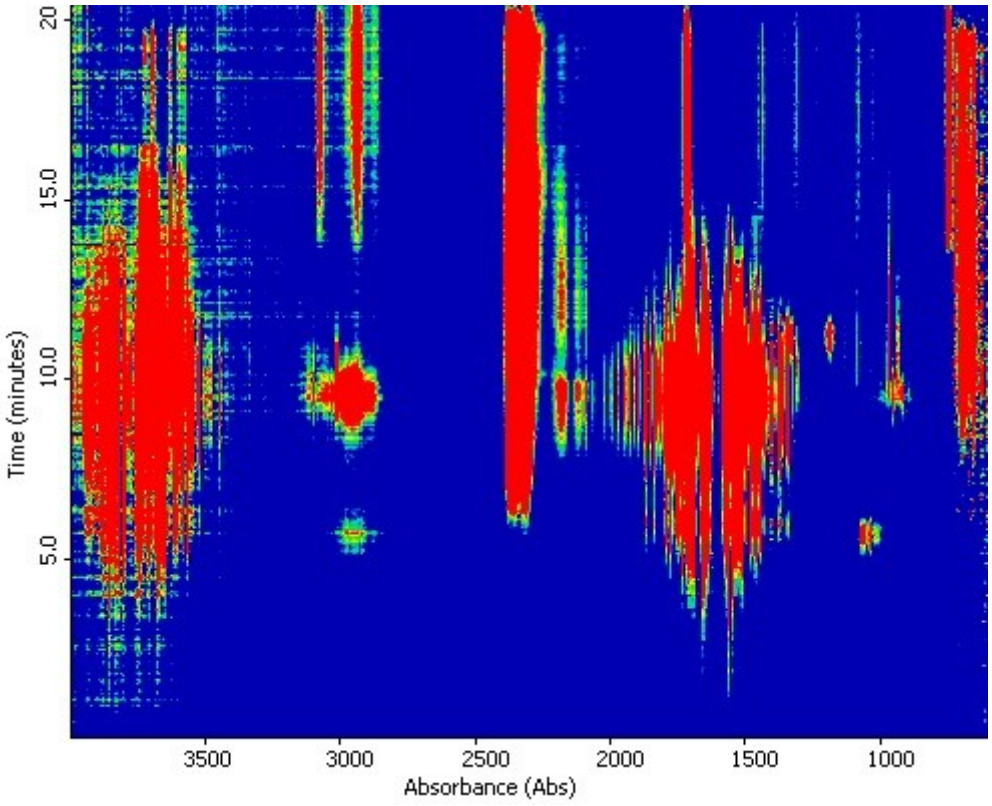

Figure 80 2D diagram of KAHA150°C 17 H sample illustrated appearing of the band during the time of the heating process

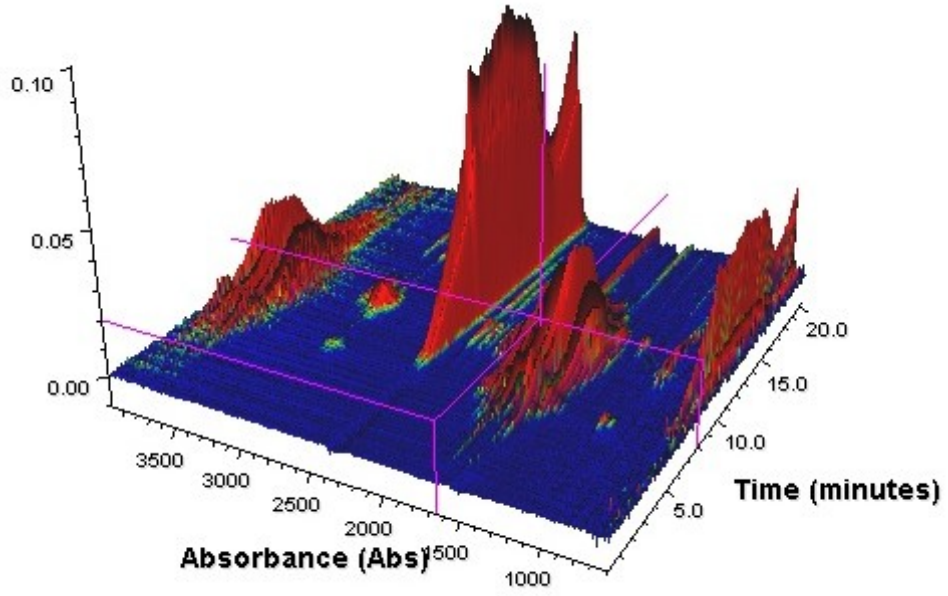

Figure 81 3D diagram of the KAHA150°C 17H heated in TGA-IR

5.4.5 NMR study of samples heated in various conditions

Four NMR spectra have been recorded for samples heated under various conditions. Three samples, KAHA150°C17H, KAHA 180°C2H and KAHA240°C2H, were polymerized under vacuum conditions. For comparison, the sample KAHA250°Cex produced in the tube furnace under a nitrogen flow is investigated.

The ^{29}Si CP/MAS NMR study of the samples polymerized under vacuum conditions is a good illustration of the progress of the process. The spectrum of KAHA150°C17H is characterized by splitting of the signals for two values, -91.05 p.p.m and -91.70 p.p.m, which may be attributed with hydrogen bonding. The signal at -91.70 p.p.m is shifted by 0.13 p.p.m in comparison with untreated AHA-kaolinite precursor. Matsumura *et al.,* (2001) connected that shift to appearance of polymers in the interlayer space of kaolinite. For the sample KAHA180°C2H also, two signals on the ^{29}Si CP/MAS NMR spectra are present at -90.98 p.p.m and -91.78 p.p.m. The small shift in signals assigned to heat treated AHA for KAHA150°C17H and KAHA180°C2H are present. Probably, the nature of the interaction between Si and interlayer guest molecules for both samples are similar. On the KAHA240°C 2H spectra of ^{29}Si only one resonance at -91.74 p.p.m is present. That may be assigned to the nature of interaction between products obtained due to polymerization of AHA and the silicate sheets. The sample polymerized under nitrogen flow, KAHA250°Cex, is characterized by one signal on the ^{29}Si CP/MAS NMR spectra at -92.35 p.p.m which is shifted downfield with comparison to the samples treated under vacuum condition.

On the ^{13}C CP/MAS NMR spectrum of sample KAHA150°C17H, two signals related with carbonyl groups are visible. The signal at 186.75 p.p.m is more intense than 176.60 p.p.m. The signal at 186.75 p.p.m may be attributed to the carbonyl group from AHA. The shift in resonance by 5.6 p.p.m, in comparison to unheated AHA intercalated

in the kaolinite interlayer may be related with the perturbation of molecules during the heating. The signal at 176.60 p.p.m is related with the carbonyl group of nylon 6. The deviation in the chemical shift from the bulk nylon with signal at 171.1 p.p.m (Okada *et al.,* 1989) may be ascribed to the unique interaction between OH and carbonyl groups in nylon 6 with kaolinite. A similar peculiar chemical shift (177.1 p.p.m) was reported by Matsumura *et al.,* (2001). The carbonyl group signals for KAHA180°C2H sample are shifted in comparison with KAHA150°C17H to frequencies of 186.83 p.p.m and 176.86 p.p.m. The intensity of the signal related with nylon 6 is higher for KAHA180°C2H than for KAHA150°C17H. Two signals related with carbonyl groups are visible on the ^{13}C CP/MAS NMR KAHA240°C2H spectra at 187.00 p.p.m and 177.78 p.p.m. Intensity of both signals is similar, which may be related with progress of polymerization of AHA in the kaolinite interlayer space. For the sample KAHA250°Cex polymerized under nitrogen flow, only one signal, which is assigned to carbonyl group, is shifted to 172.54 p.p.m. On the ^{13}C CP/MAS NMR spectra of KAHA150°C17H and KAHA180°C2H, signals at 50.71 p.p.m and 50.83 p.p.m are respectively present, which are assigned to CH_3 groups from methanol preintercalated to kaolinite. This signal is absent in the spectra of KAHA240°C2H and KAHA250°Cex.

On all of the ^{13}C CP/MAS NMR spectra of samples polymerized under vacuum conditions, chemical shifts at 37.06 p.p.m (KAHA150°C17H); 37.02 p.p.m (KAHA180°C2H); 37.53 p.p.m (KAHA240°C2H) are observed. Those signals are attributed to the methylene group bonded to carbonyl group and are consistent with the results obtained by Matsumura et al. (2001). Moreover, those signals are not related with 6-aminohexanoic acid because the untreated precursor AHA-kaolinite is characterized by signals related with this specific methylene group at 39.31 p.p.m. Also on the spectra of KAHA250°Cex, the signal ascribed to the methylene group bonded to

carbonyl group is shifted to lower frequency, 36.4 p.p.m, which is in agreement with values for AHA heated at 250°C reported by Matsumura *et al.,* (2001), and shifted by 1-2 p.p.m, in comparison to the values reported by Okada *et al.,* (1989) for two different crystalline form of nylon 6. The signals related to the methylene group bonded to NH group are present on all of the spectra heated under vacuum conditions. Chemical shifts attributed with that type of carbon are located at 40.79 p.p.m (KAHA150°C17H), 40.72 p.p.m (KAHA180°C2H) and 41.15 p.p.m (KAHA240°C2H) which is consistent with values for nylon 6 proposed by Okada *et al.,* (1989). On the spectra of AHA-kaolinite, the intercalated compound of this signal is not detected. Matsumura *et al.,* (2001) reported the appearance of signal related with this methylene group at 40.0 p.p.m. On the spectra of KAHA250°Cex, overlapping of signals around 40 p.p.m is visible. For all heat treated samples also, signals ascribed to methylene group bonded to each other are located at different frequencies than for non-treated AHA-kaolinite precursor. All samples treated under vacuum conditions are characterized by signals around 28 p.p.m which are shifted to lower frequencies with an increase in the temperature; for KAHA150°C17H, signals at 28.80 p.p;m are shifted to 28.75 p.p.m (KAHA180°C2H) and 28.64 p.p.m for KAHA240°C2H. The signal at 30.09 p.p.m for KAHA150°C17H is shifted by 0.1 p.p.m to higher frequencies for KAHA180°C which is consistent with Matsumura et al., (2001) data for AHA heated at 250°C. The shift of this signal for the sample treated under nitrogen conditions (KAHA250°Cex) to 29.55 p.p.m is consistent with Okada *et al.,* (1989). Resonance present at 24.71 p.p.m for KAHA150°C17H is shifted to 24.63 p.p.m for KAHA180°C2H and 26.07 p.p.m for KAHA250°Cex which is in agreement with Matsumura *et al.,* (2001).

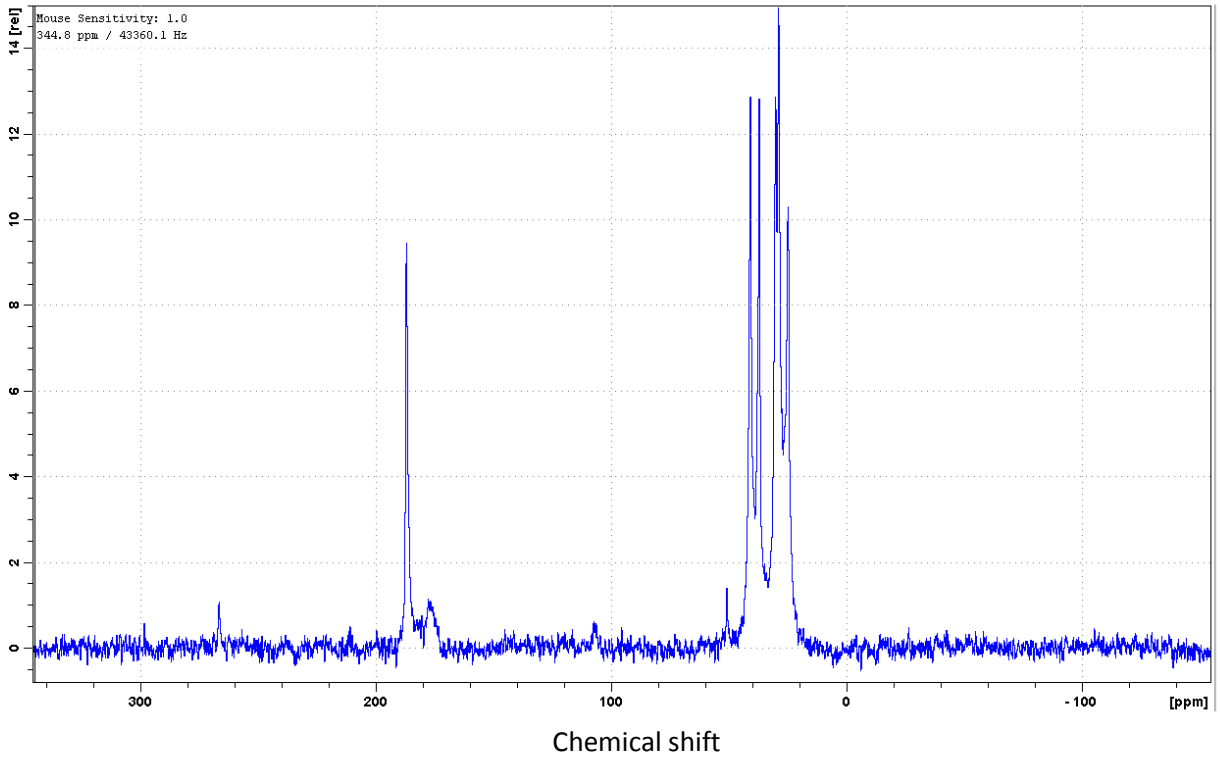

Figure 82 ^{13}C MAS NMR of KAHA 150°C 2H

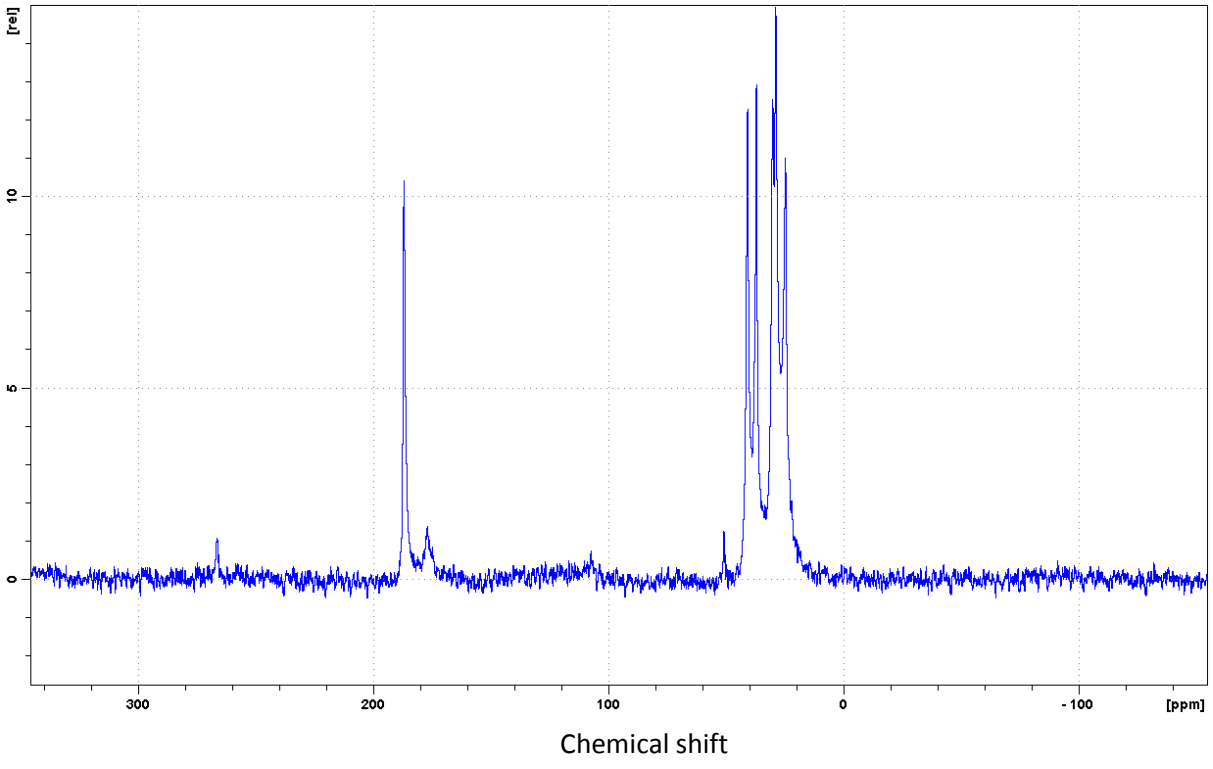

Figure 83 ^{13}C MAS NMR spectra of the KAHA 180°C 2H

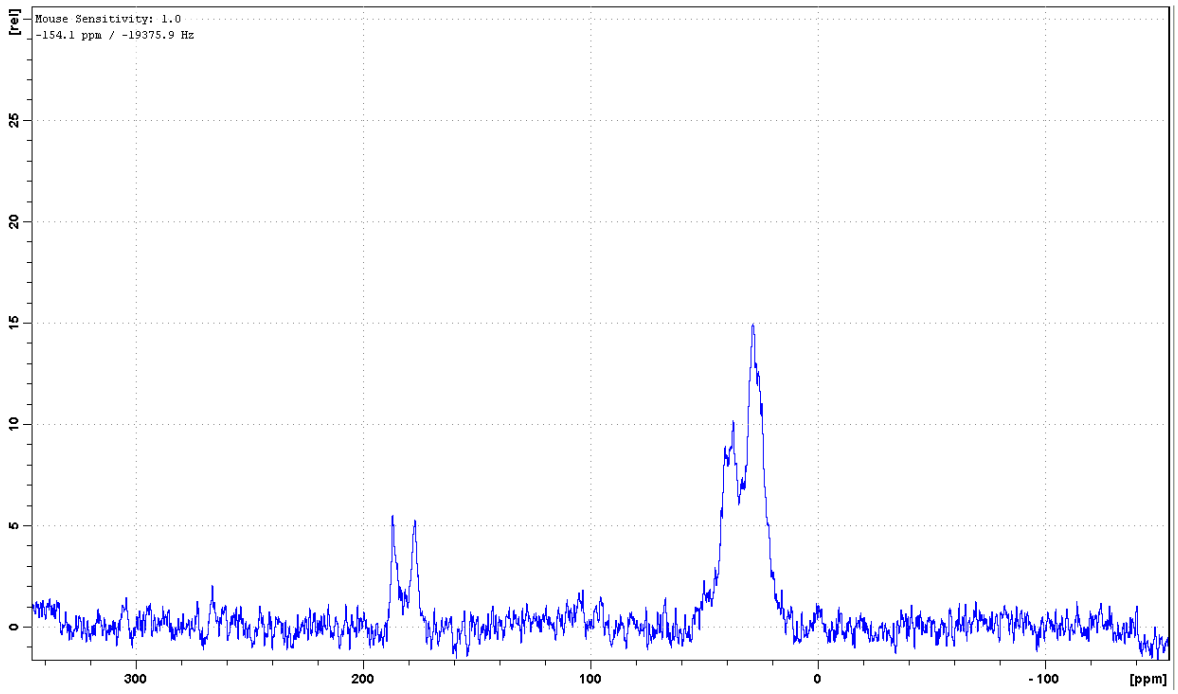

Figure 84 ^{13}C MAS NMR spectra of KAHA 240°C 2H

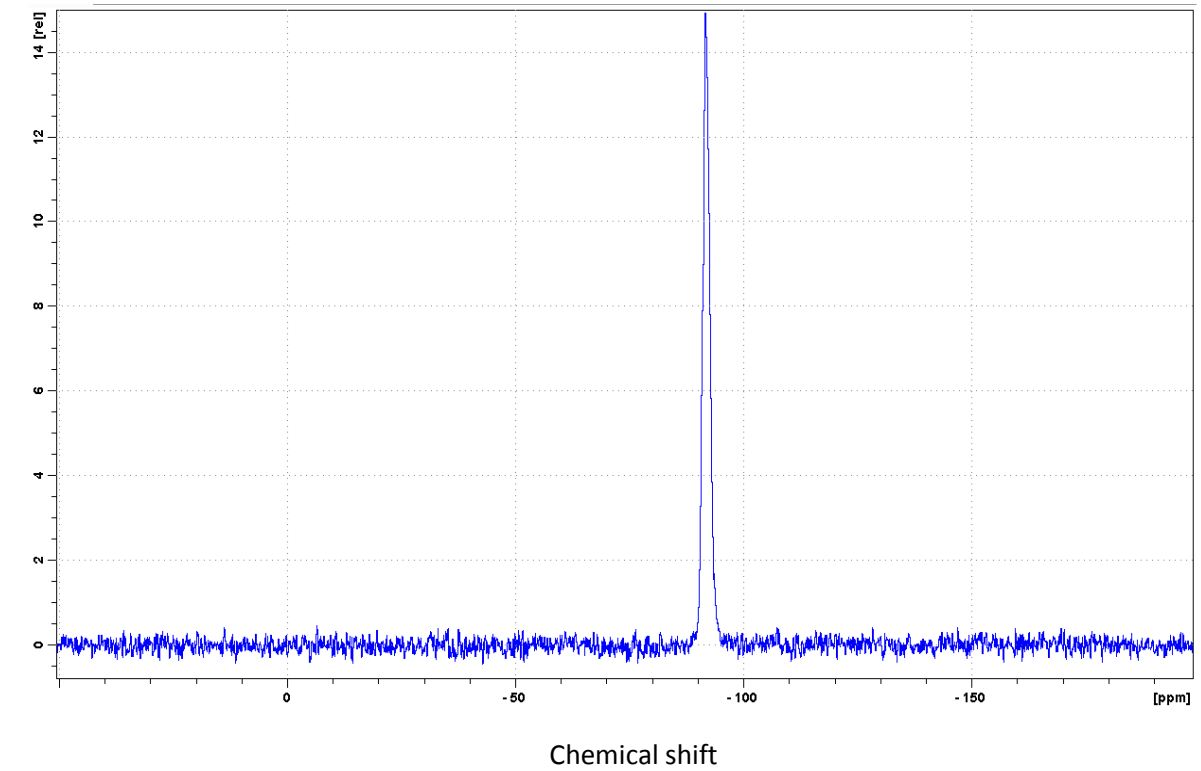

Figure 85 ^{29}Si MAS NMR spectra of KAHA 150°C 2H

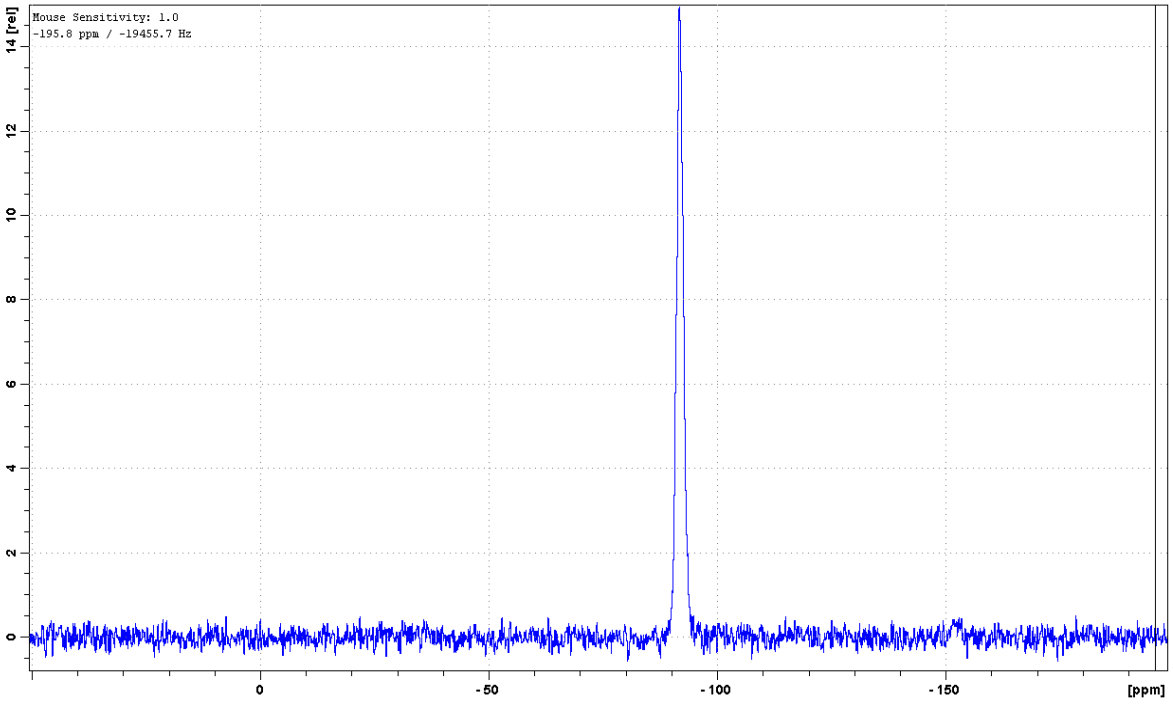

Figure 86 ^{29}Si MAS NMR spectra of KAHA 180°C 2H

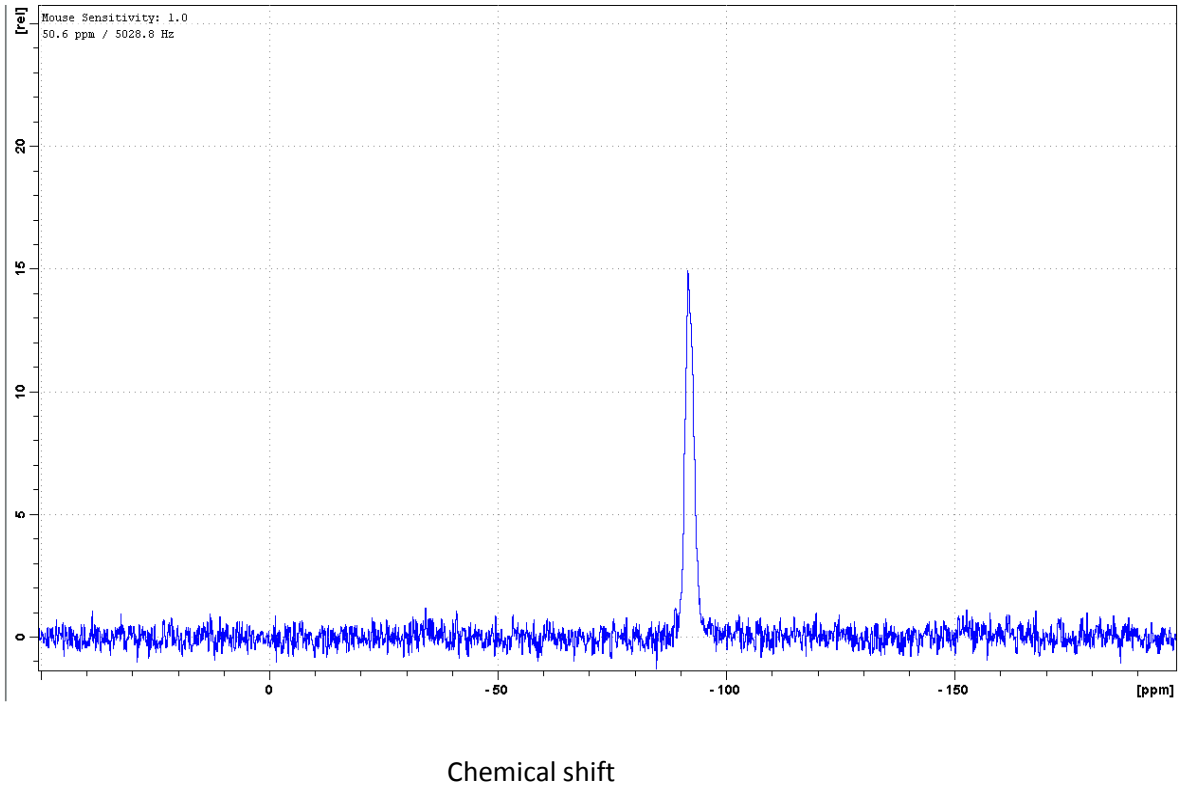

Figure 87 ^{29}Si MAS NMR of KAHA240°C 2H

5.4.6 SEM investigation in heat treated kaolinite-KAHA samples

A detailed investigation was made of the heat treated kaolinite-AHA samples. The images of composites obtained after different time durations of treatment under various conditions are presented here.

The images of pure unheated kaolinite-AHA precursor plays the role of reference for heat treated samples. In image A of the washed kaolinite-AHA precursor, mineral plates are characterized by bimodal distribution of the sizes of the plates. Most of kaolinite plates are characterized by diameter size ranging from 0.5 µm to 0.1 µm. Also, on the picture, bigger plates with diameter of 1µm and more are noticed. The orientation of kaolinite plates in the space may be described as an aggregation. The edges of kaolinite plates are slightly scrolled.

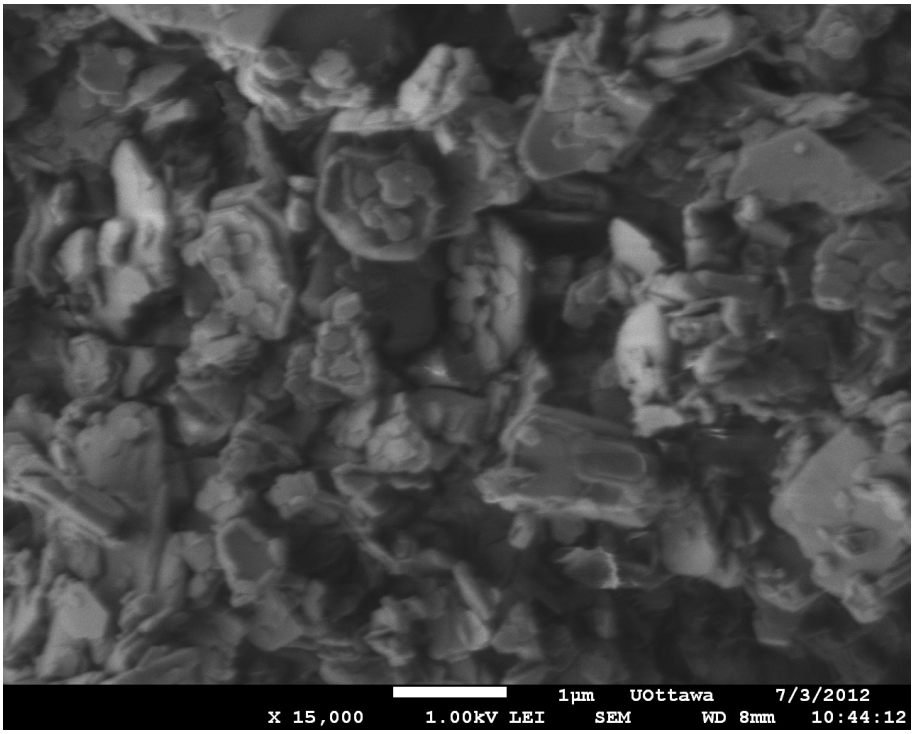

Figure 88 IMAGE A of the pure kaolinite-AHA

The image B is a representation of the structure of the KAHA150°17H sample. Bimodal distribution of kaolinite plate diameters is also characteristic of the heat treated sample. Majority of plates have diameters smaller than 1µm, but some plates with larger sizes

are present. The composite is made of organic molecules located between kaolinite interlayer space and aggregated mineral filler. Some of the plates are scrolling, which is visible on the picture B1.

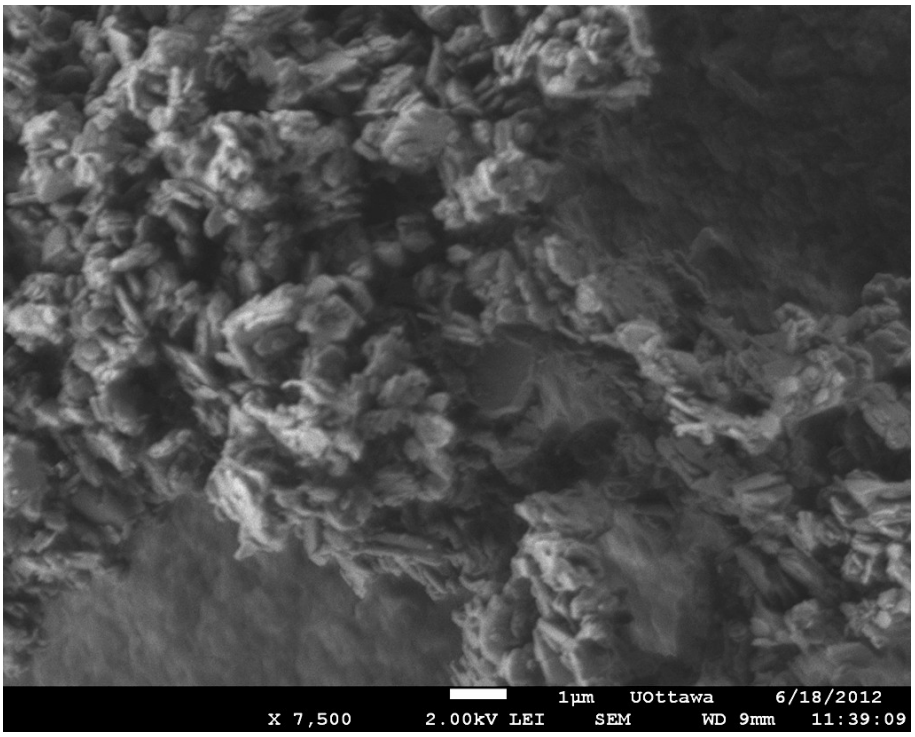

Figure 89 IMAGE B of thestructure of KAHA150°C 17H

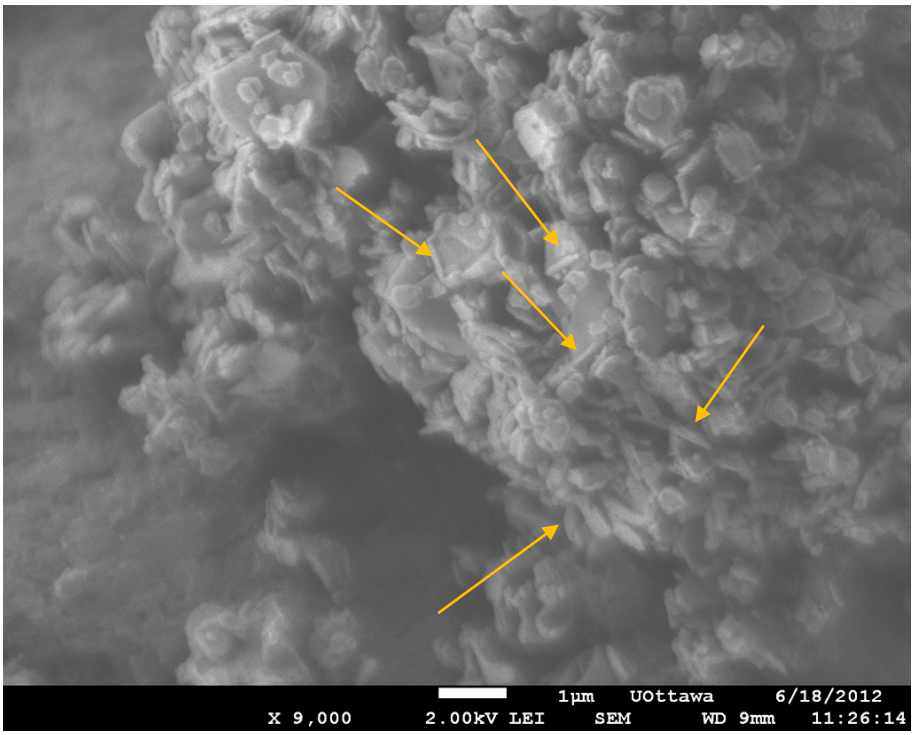

Figure 90 IMAGE B1 with scrolling plate lates

The structural character of the sample heated up to 240°C for 2h under vacuum conditions (KAHA240°C2H) is comparable to the samples described above. Bimodal distribution of kaolinite plates is noticed on the images C and C1. However a different arrangement is observed. The plates with diameters smaller than 1µm are located between two parallel, bigger plates of kaolinite, which is visualized on the upper right part of image C and also in the central part of this picture. This is in contrast to the samples heated at lower temperatures and untreated, where the absence of scrolling edges of kaolinite plates is significant. Therefore, the presence of possible nanoscrolls in the image C1 may be related with previous modification of kaolinite stabilized by heat treatment.

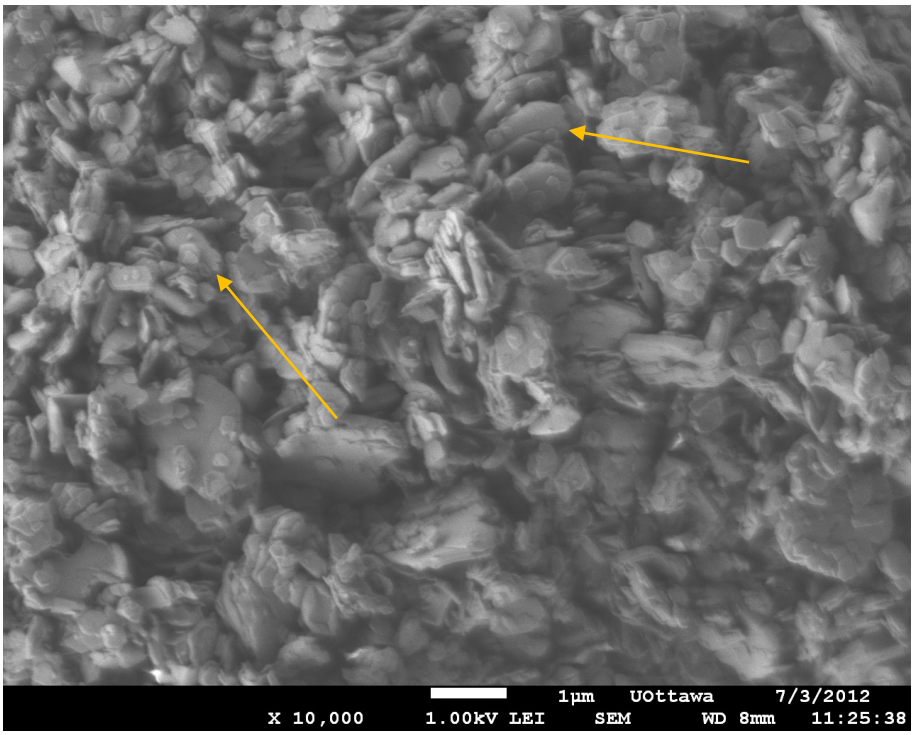

Figure 91 IMAGE C; KAHA 240°C 2H

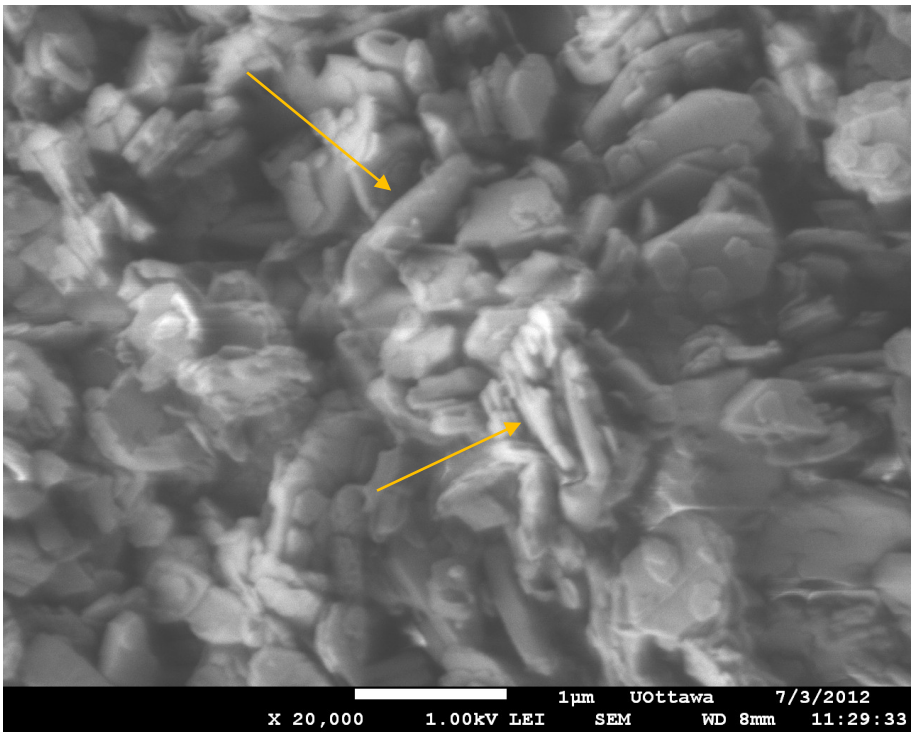

Figure 92 IMAGE C1; scrolls presented in KAHA 240°C 2H sample

On the image D, the structure of the composite prepared under nitrogen flow in a tube furnace (KAHA250°C2H) is presented. Similarities between samples KAHA240°C2H

and KAHA250°C2H are noticed. In case of samples heated up to 250°C, scrolling of kaolinite plates are visible on the left part of image D. Moreover, some possible nanoscrolls are also observed and indicated by arrows on image D1. In the center of image D, organic matter is noticeable as fibrous matter. The same features of nylon are presented on image E, which show 6-aminohexanoic acid polymerized in the tube furnace at 250°C. Delamination of kaolinite plates in the polymer produced by heat treatment wasn't observed, but the presence of nylon 6 between the kaolinite interlayer space is confirmed by XRD, NMR and TGA, and FTIR studies.

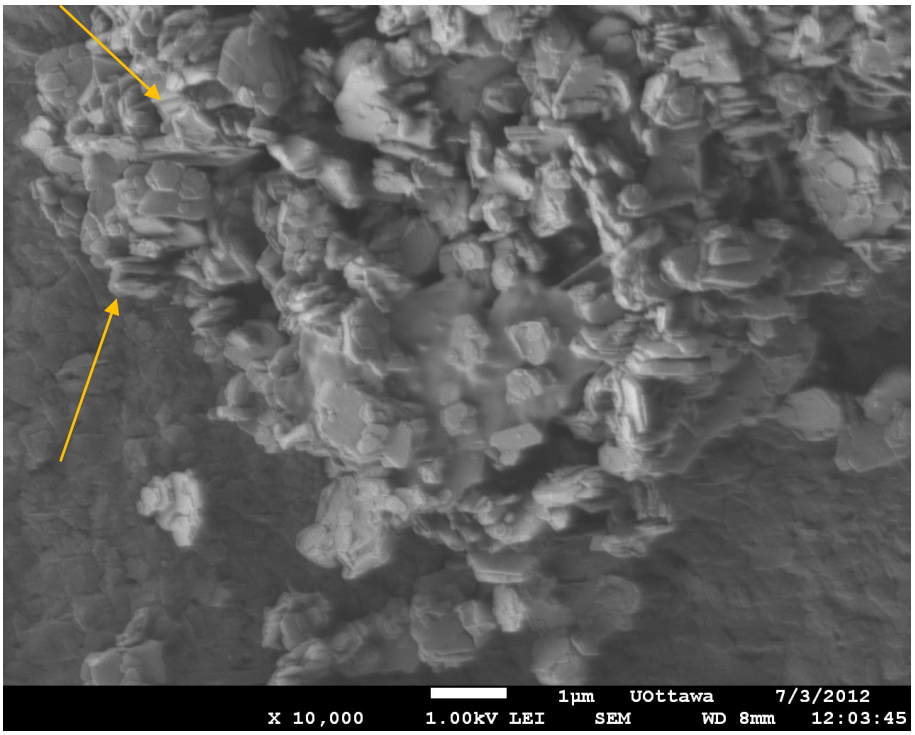

Figure 93 IMAGE D; sample KAHA 250°C 2H

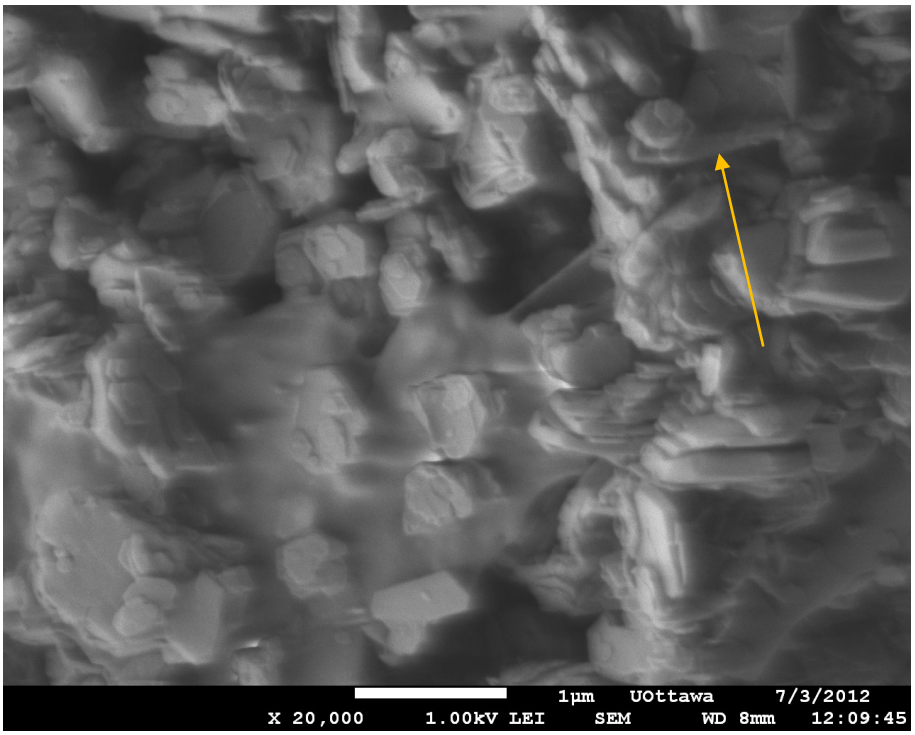

Figure 94 IMAGE D 1; The sample KAHA 250°C 2H magnified 20000 times

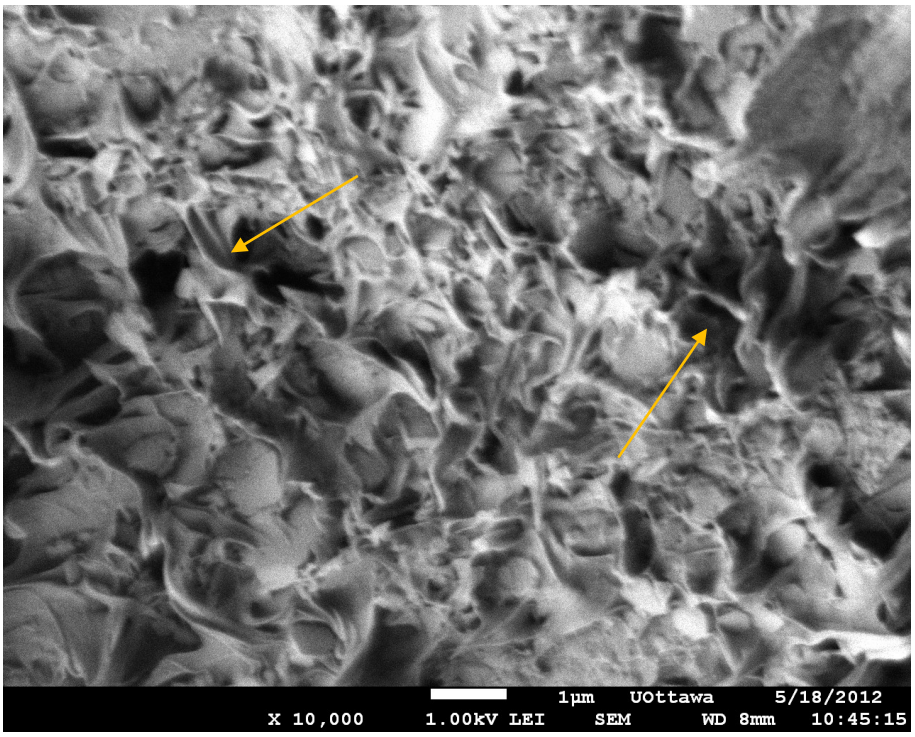

Figure 95 IMAGE E ;6-aminohexanoic acid heated up to 250°C in the tube furnace.

5.5 Conclusions

The preparation of kaolinite-nylon 6 nanocomposites is confirmed by series of measurements. XRD results for the whole series of samples show slight differences in basal spacing of the obtained composites. Therefore, additional studies of IR spectra of heated material were necessary. Based on the appearance of amide bands and an increase in their intensity with time and temperature of treatment, the preparation of nylon clay nanocomposites was confirmed. Also, the results of TGA-IR investigations of heat treated kaolinite AHA precursor were indicative of the polymerization which occurred during heating in the vacuum oven under temperatures lower than 250°C. Series of NMR spectra of samples heated under vacuum conditions are characterized by the evolution of carbonyl bonds assigned to nylon. With increasing temperature, the intensity of chemical shifts associated with polymers grew in comparison to 6-aminohexanoic acid. Comparable TGA results for vacuum oven heated sample (KAHA240°C2H) and tube furnace heated sample may be an indication of the polymerization of kaolinite-AHA precursor under both conditions. On the SEM pictures of the samples heated under vacuum conditions, deformation of planar hexagonal plates of kaolinite are observed. In the same pictures, scrolling of the plates was noticed.

The polymerization process of nylon in the kaolinite interlayer space was confirmed by the obtained results. Also, progress of the reaction was shown by series of samples heated to increasing temperatures, with the first dimers or oligomers created under temperatures lower than the temperature of nylon polymerization at 250°C. First, changes in the structure of organic molecules are reported at the temperature of 100°C, which is associated with new basal spacing of the material investigated by XRD. Moreover, when the temperature is increased up to 150°C, NMR, IR and TGA-IR results attest to the structural changes in the organic molecules, which are related to the

addition of monomers to a chain. Complete polymerization take place in the temperature above 200°C.

6. General conclusions

The modification of kaolinite strongly depends on the chemical properties of the mineral. Very strong interactions between adjacent octahedral and tetrahedral sheets of the kaolinite layers bring some difficulties to the intercalation process, in comparison to the smectite group. Also, the almost neutral charge of kaolinite is responsible for the absence of interlayer cations which support the introduction of molecules in the interlayer space of smectites. In comparison to other clays, kaolinite has low specific surface areas. Therefore, the chemical modification of kaolinite is a more complex process than that of smectites.

The intercalation of ε- caprolactam, 6 –aminohexanoic acid and sarcosine in the kaolinite structure is confirmed by series of measurements by XRD, TGA, NMR, and FTIR. All of the chemical components were introduced to the kaolinite structure through DMSO precursor and methoxy kaolinite. Future work on kaolinite- sarcosine has to be made because this component can be very attractive in pharmaceutical applications, especially for the controlled release of sarcosine from pills used in schizophrenia treatments. Therefore, the optimization of the intercalation procedures of sarcosine in the kaolinite structure has to be made. Also, adjusting the optimal ratio between organics and clays are one of the major issues in this field of study.

In the polymerization experiment, it was shown that 6-aminohexanoic acid is a precursor which may be polymerized in the kaolinite interlayer spaces, under controlled conditions. Therefore, an intense study based on this precursor was made. The application of various experimental conditions showed that the produced nylon-6 kaolinite nanocomposites are characterized by a monolayer arrangement of the polymer in the interlayer space of kaolinite, independently from the applied conditions. Also, it was shown in the TGA results that the preparation of nylon-6 nanocomposite under

various conditions corresponds to different DTG peaks. This could be related to the progressive polymerization of 6-aminohexanoic acid with temperature. During these procedures, under various atmospheres, broad varieties of components may be created. Therefore, a future investigation by mass spectrometry should be done to compare differences in the polymerization process.

7 Bibliography

1) Ahmadi S.J., Huang Y.D.,Li W., (2004). Review Synthetic routes, properties and future applications of polymer-layered silicate nanocomposites, *Journal of Materials Science* vol.39 pp.1919 – 1925.

2) Akiba E., Hayakawa H., Hayashi S., Miyawaki R., Tomura S., Shibasaki Y., Izumi F., Asano H., and Kamiyama T. 1997. Structure refinement of synthetic deuterated kaolinite by Rietveld analysis using time-of-flight neutron powder diffraction data. *Clays Clay Min. 45:781-788*.

3) Balan E., Delattre S., Guillaumet M., Salje E., (2010) Low-temperature infrared spectroscopic study of OH-stretching modes in kaolinite and dickite, *American Mineralogist*, Volume 95, pages 1257–1266.

4) Balan E.,Saitta A.M, Mauri F.,Calas G., (2001). First-principles modeling of the infrared spectrum of kaolinite, *American Mineralogist,* Volume 86, pages 1321–1330.

5) Bergaya F., Theng B.G.K., Lagaly G (Eds)(2006). Handbook of Clay Science, Amsterdam: Elsalvier Science

6) Bhattacharya S.N., Kamal M.R., Gupta R.K.,(2008). Polymeric Nanocomposites: Theory and Practice, Hanser Verlag,- 383 pages

7) Brigatti M., F., Galan E., Theng B. G. K., (2006). Structures and mineralogy of clay minerals. In Bergaya F., Theng B.G.K., Lagaly G (Eds). Handbook of Clay Science pp 19-85, Amsterdam: Elsalvier Science

8) Carretero M., I., Pozo M., (2009). Clay and non-clay minerals in the pharmaceutical industry Part I. Excipients and medical applications, *Applied Clay Science*

9) Carretero, M. I., Lagaly, G.,(2007). Introduction clays and health: An introduction *Applied Clay Science* 36,pp. 1–3.

10) Chen J.S.,(1994). NMR Study of 8-Caprolactam in various Solvents Graphical Determination of Monomer Shift, Dimer Shift and Dimerization Constant from the Dilution Shift Data , J. *Chem. Soc. Faraday Trans*., vol. 90(5), pp. 717-720.

11) Cho J.W., Paul D.R., (2001) Nylon 6 nanocomposites by melt compounding, *Polymer* 42 pp. 1083-1094.

12) Chung, F. H. (1974). Quantitative interpretation of X-ray diffraction patterns of mixtures. I. Matrix flushing method for quantitative multicomponent analysis. *Journal of Applied Crystallographic.* v.7, p.519-525

13) Codish S., Abu-Shakra M., Flusser D., Friger M., Sukenik S., (2005). Mud compress therapy for the hands of patients with rheumatoid arthritis, *Rheumatol Int* 25, pp. 49–54.

14) Davis R.D., Jarrett W.L., Mathias L.J.,(2001). Solution 13C NMR spectroscopy of polyamide homopolymers (nylons 6, 11, 12, 66, 69, 610 and 612) and several commercial copolymers, *Polymer* vol.42 pp. 2621–2626.

15) Do C.H., Pearce E.M., Bulkin B.J.,(1987). FT- IR Spectroscopic Study on the Thermal and Thermal Oxidative Degradation of Nylons. *Journal of Polymer Science: Part A: Polymer Chemistry* , Vol 25, pp 2409- 2424.

16) Elbokl T.A., Detellier C.(2008). Intercalation of cyclic imides in kaolinite. *J Colloid Interface Sci.* 15;323(2):338-48.

17) Elbokl T.A., Detellier C., (2009) Kaolinite-poly(methacrylamide) intercalated nanocomposite via in situ polymerization, *Canadian Journal of Chemistry* 87pp. 272-279

18) European Medicines Agency Pre-authorisation Evaluation of Medicines for Human Use; Guideline on the specification limits for residues of metal catalysts, (2007). London, (http://www.ema.europa.eu/docs/en_GB/document_library/Scientific_guideline/2009/09/WC500003587.pdf http://www.ema.europa.eu/docs/en_GB/document_library/Maximum_Residue_Limits_-_Report/2009/11/WC500012645.pdf)

19) Fakhfakh E., Chakroun I., Chaari I., Medhioub M., López-Galindo A., Rocha F., Gomes C., Kooli F., Zargouni F., Jamoussi F., (2005). Chemical and physical characterization of some Tunisian smectite for human healing use, *Acta Geodyn. Geomater*., Vol.2, No.2 (138), pp.39-45.

20) Fang X., Simone C.D., Vaccaro E., Huang S.J., Scola D.A., (2002). Ring-Opening Polymerization of -Caprolactam and-Caprolactone via Microwave Irradiation, *Journal of Polymer Science: Part A: Polymer Chemistry,* Vol. 40, pp. 2264–2275.

21) Fischer C., Carreira E.M., (2001). Direct Addition of TMS-acetylene to Aldimines Catalyzed by a Simple, Commercially Available Ir(I) Complex, *Org. Lett.*, 3 (26), pp 4319–4321.

22) Flego C., Dalloro L.,(2003). Beckmann rearrangement of cyclohexanone oxime over Silicalite-1: an FT-IR spectroscopic study, *Microporous and Mesoporous Materials* vol. 60 pp.263–271.

23) Fornesa T.D., Yoona P.J., Hunterb D.L., Keskkulaa H., Paula D.R., (2002). Effect of organoclay structure on nylon 6 nanocomposite morphology and properties, *Polymer* 43 pp. 5915–5933.

24) Frost R.L., (1997). The structure of the kaolinite minerals — a FT-Raman study, *Clay Minerals* vol.32, pp. 65–77.

25) Gardolinski J. E. F. C., Lagaly G., (2005), Grafted organic derivatives of kaolinite: II.Intercalation of primary n-alkylamines and delamination, *Clay Minerals* 40, pp. 547-556

26) Gardolinski J. E., Carrera L. C. M., Cantao M. P., Wypych F., (2000) Layered polymer-kaolinite nanocomposites, *Journal of Materials Science* 35 pp.3113 – 3119

27) Gardolinski J., F., E., C., (2005). Interlayer grafting and delamination of kaolinite. PhD Thesis University in Kiel.

28) Gomes C., (2002). Argilas. Aplicações na Indústria, O Liberal Câmara de Lobos, Madeira,

29) Gomez-Zavaglia A., Fausto R.,(2003). Low-temperature solid-state FTIR study of glycine, sarcosine and N,N-dimethylglycine: observation of neutral forms of simple a-amino acids in the solid state, *Phys. Chem*., 5, pp. 3154–3161.

30) Gottlieb H. E., Kotlyar V., Nudelman A., (1997). NMR Chemical shifts of Common Laboratory Solvents as Trace Impurities. *J. Org. Chem* vol 62, pp 7512-7515.

31) Greenler R.G., (1962). Infrared study of the adsorption of methanol and ethanol on alumina oxide. *J. Chem. Phys*. 37: 2094-2100.

32) Hayash S.,(1997). NMR study of dynamics and evolution of guest molecules in kaolinite/Dimethyl Sulfoxide intercalation compound, *Clays and Clay Minerals*, Vol. 45, No. 5, pp 724-732.

33) Hayashi S., Ueda T., Hayamizu K., Akiba E.,(1992), NMR Study of Kaolinite. 2H, 27Al, and 29Si Spin-Lattice Relaxations, *J. Phys. Chem*.,96, pp. 10928-10933.

34) Hu Y., Wang S., Ling Z., Zhuang Y., Chen Z., FanW.,(2003) Preparation and Combustion Properties of Flame Retardant Nylon 6/Montmorillonite Nanocomposite, *Macromol. Mater. Eng.,* 288, No. 3

35) Ilczyszyn M., Godzisz D., Ilczyszyn M.M.,(2003). Sarcosine_/maleic acid (1:1) crystal: structure, 13C NMR and vibrational properties, protonation character, *Spectrochimica Acta Part A* vol. 59 pp. 1815-1828.

36) Itagaki T., Komori Y., Sugaharaa Y., Kuroda K., (2001) Synthesis of a kaolinite–poly(b-alanine) intercalation compound, *J. Mater. Chem*., 11, pp; 3291–3295

37) Johnson C.T., Kogel J.E., Bish D.L., Kogure T.; Murray H.H., (2008).Low-temperature FTIR study of kaolinite minerals group, *Clays and Clay Minerals,* Vol. 56, No. 4,pp. 470–485.

38) Johnson C.T., Sposito G., Bocian D.F., Birge R.R., (1984). Vibrational Spectroscopic Study of the Interlamellar Kaolinite-Dimethyl Sulfoxide Complex, *J. Phys. Chem*. Vol.88, pp. 5959-5964.

39) Kawasumi M., (2004). The Discovery of Polymer – Clay Hybrids. *Journal of Polymer Science: Part A : Polymer Chemistry*, Vol 42, pp 819- 824.

40) Kim K.J., Lee J.S., Prabu A.A., KimT.H.,(2009). Preparation and Characterization of Nylon 6/Organoclay Nanocomposite Filament Fibers, *Polymer Composites* pp. 265- 273.

41) Kim M.,Quintiere J.G., (2007).Predicting polymer burning using TGA/DSC, Proceedings of the 5th International Seminar on Fire and Explosion Hazards, Edinburgh, UK.

42) Komori Y., Matsumara A., Itagaki T., Sugahara Y., Kuroda K., (1999). Preparation of a kaolinite-.EPSILON.-caprolactam intercalation compound. *Clay Sci* ; VOL.11;NO.1;pp.47-55.

43) Komori Y., Sugahara Y., Kuroda K. (1999), Intercalation of alkylamines and water into kaolinite with methanol kaolinite as an intermediate, *Applied Clay Science* vol.15 pp. 241–252

44) Krištofič M., Karabcová N., Alexy P.,. RybaJ., Vassová I., (2005) Modification of PA 6 by Comonomers and Layered *Silicate,FIBRES & TEXTILES in Eastern Europe*, Vol. 13, No. 6 (54)

45) Legido, J.L., Medina, C., Mourelle, M.L., Carretero, M.I., Pozo, M.,(2007). Comparative study of the cooling rates of bentonite, sepiolite and common clays for their use in pelotherapy. *Applied Clay Science* 36, 148–160

46) Letaief S., Detellier C., (2011), Application of thermal analysis for the characterization of intercalated and grafted organo-kaolinite nanohybrid materials, *J Therm Anal Calorim* 104,pp. 831–839

47) Letaief S., Detellier C.,(2007), Functionalized nanohybrid materials obtained from the interlayer grafting of aminoalcohols on kaolinite, *Chem. Commun*., pp. 2613–2615

48) Letaief S., Detellier C.,(2009) Functionalization of the interlayer surfaces of kaolinite by alkylammonium groups form ionic liquids, *Clays and Clay Minerals*, Vol. 57, No. 5,pp. 638–648.

49) Letaief S., DetellierC., (2007), Nanohybrid materials from the intercalation of imidazolium ionic liquids in kaolinite, *J. Mater. Chem*., ,17, pp. 1476–1484.

50) Letaief S., DetellierC.,(2009) Clay-Polymer Nanocomposite Material from the Delamination of Kaolinitein the Presence of Sodium Polyacrylate, *Langmuir*, 25(18) pp. 10975–10979.

51) Letaief S., DetellierC.,(2005) Reactivity of kaolinite in ionic liquids: preparation and characterization of a 1-ethyl pyridinium chloride–kaolinite intercalate, *Journal of Materials Chemistry* 15, pp. 4734–4740.

52) Letaief,S., Leclercq J., Liu Y., Detellier C.,(2011) Single Kaolinite Nanometer Layers Prepared by an In Situ Polymerization Exfoliation Process in the Presence of Ionic Liquids, *Langmuir* 2011, 27, pp. 15248–15254.

53) Li Y., Sun D., Pan X., Zhang B., (2006). Kaolinite intercalation precursors, *Clays and Clay Minerals* v. 57 no. 6 p. 779-786.

54) Liu L., Qi Z., ZHU Q., (1999) Studies on Nylon 6/Clay Nanocomposites by Melt-Intercalation Process, *Journal of Applied Polymer Science*, Vol. 71, pp. 1133–1138/

55) Ma C., Eggleton R., A.;(1999). Cation Exchange Capacity of kaolonite; *Clays and Clay Minerals,* Vol.47, No. 2,

56) MacKenzie K.J.D., Smith M.E.,(2002) Multinuclear Solid-State Nuclear Magnetic Resonance of Inorganic Materials, Elsevier, 26 avr. 2002 - 748 pages.

57) Madejova J., Komadel P., (2001). Baseline studies of The Clay Minerals Society Source Clays Infrared methods, *Clays and Clay Minerals*, Vol. 49, No. 5, pp. 410–432.

58) Matsumura A., Komori Y., Itagaki T., Sugahara Y., Kuroda K.,(2001) Preparation of a Kaolinite–Nylon 6 Intercalation Compound, *Bull. Chem. Soc. Jpn.*, 74, pp. 1153—1158.

59) Matusik J., (2010). Minerals from kaolinite group as the precursors of mineral nanotubes. PhD Thesis AGH University of Science and technology in Cracow. (In polish)

60) Matusik J., Gawel A., Bahranowski K., (2012). Grafting of metanol in dickite and intercalation of hexylamine. *Applied Clay Science* vol 56, pp 63-67.

61) Matusik J., Scholtzová E., Tunega D., (2012). Influences of synthesis conditions on the formation of a kaolinite-mathanol complex and simulationof its vibrational spectra, *Clays and Clay Minerals* v. 60 no. 3 p. 227-239.

62) Mayo D.W., Miller F.A., Hannah R.W., (2003).Course Notes on the Interpretation of Infrared and Raman Spectra, John Wiley & Sons, Inc. Hoboken, New Jersey.

63) Migas A., (2008). Reologia ceramicznych zawiesin tiksotropowych, AGH Krakow PhD thesis

64) Miller J.V., Bartick E.G., (2001). Forensic Analysis of Single Fibers by Raman Spectroscopy, *Applied Spectroscopy*, Volume 55, Number 12, pp. 1729-1732.

65) Morel R., (1996). Les sols cultivés. Lavoisier, Paris.

66) Mosad, A., Natarajan S., (1989). Crystal and Molecular Structure of Sarcosine. *Acta Chem. Scan.* Vol 43, pp 1004-1006.

67) Murakami J., Itagaki T., Kuroda K.,(2004). Synthesis of kaolinite-organic nanohybrids with butanediols, *Solid State Ionics Volume* 172, Issues 1–4, 31, Pages 279–282.

68) Nihal Tünzun F.,(2008). Effect of the Activator Type and Catalyst/Activator Ratio on Physical and Mechanical Properties of Cast PA-6, *Polymer-Plastics Technology and Engineering,* 47: pp. 532–541.

69) Okada A., Kawasumi M., Tajima I., Kurauchi T., Kamigaito O., (1989). A Solid state NMR Study on Crystaline Forms of Nylon 6. *Journal of Applied Polymer Science*, Vol. 37, pp 1363- 1371.

70) Olejnik, S., Aylmore, L. A. G., Posner, A. M. and Quirk, J. P. (1968) Infrared spectra of kaolin mineral dimethyl- sulfoxide complexes: *J. Phys. Chem.* 72, 241-249.

71) Olejnik, S., Posner, A. M. and Quirk, J. P. (1970) The intercalation of polar organic compounds into kaolinite: *Clay Mineral*s 8, 421~434.

72) Olejnik S., Posner A.M., Quirk J.P.,(1971) The IR spectra of interlamellar kaolinite amide complexes—I.The complexes of formamide, N-methyl-formamide and dimethylformamide, *Clays and Clay Minerals, Vol. 19, pp. 83-94.*

73) Pais J., Cunha P., P., Legoinha P., (2010) Litostratigrafia do Cenozóico de Portugal. In Neiva, J. M.C., Ribeiro, A., Victor, L. M., Noronha, F. & Ramalho, M. (edit.*) Ciências Geológicas: Ensino e Investigação*.Vol. I: 365-376.

74) Pereira, D. I., (1997). Sedimentologia e Estratigrafia do Cenozóico de Trás-os-Montes oriental (NE Portugal).Dissertação doutoramento, Univ. Minho.

75) Pinnavaia T.J., Beall G.W.(2000) *Polymer-Clay Nanocomposites* (Wiley Series in Polymer Science),John Wiley and Sons, England, 349 pages.

76) Raupach M., Barron P.F., Thompson J.G.,(1987). Nuclear Magnetic Resonance, Infrared, and X-RAY powder diffraction study of Dimethyl Sulfoxide and Dimethyl Selenoxide intercalates with kaolinite, *Clays and Clay Minerals*, Vol. 35, No. 3, pp 208-219.

77) Ray S.S., Okamoto M., (2003). Polymer/layered silicate nanocomposites: a review from preparation to processing*, Prog. Polym. Sci.* 28 pp. 1539–1641.

78) Rebelo M., Gonçavles P., Silva E., Rocha F.,(2005). Some Portuguese clay sediments used as raw materials for curative clay pastes: A study of physical and technological properties, *Acta Geodyn. Geomater.*, Vol.2, No.2 (138), 151-155

79) Rebelo M., Viseras C., López-Galindo A., Rocha F., Ferreira da Silva E., (2007). Minerals and clay minerals in medical geology-*Applied Clay Science* 36,4–21

80) Rebelo M., Viseras C., López-Galindo A., Rocha F., Ferreira da Silva E.,(2011). Rheological and thermal characterization of peloids made of selected Portuguese geological materials, *Applied Clay Science,*

81) Rebelo M., Viseras C., López-Galindo A., Rocha F., Ferreira da Silva E.;(2010). Characterization of Portuguese geological materials to be used in medical hydrology; *Applied Clay Science* 51, 258–266

82) Rotter G., Ishida H., (1992). FTIR Separation of Nylon- 6 Chain conformations: Clarification of the Mesomorphous and γ- Crystalline Phases; *Journal of Polymer Science: Part B: Polymer Physics* , Vol 30 , pp 489-495.

83) Ruiz-Hitzky, E., Van Meerbeek, A., 2006. Clay mineral- and organoclay–polymer nanocomposite. In: Bergaya, F., Theng,B.K.G., Lagaly, G. (Eds.), Handbook of Clay Science, Developments in Clay Science, vol. 1. Elsevier, Amsterdam, pp. 583–621

84) Sato H., Ohtani H., Harada R., Tsuge S., Kato M., Usuki A., (2006). Polymer/silicate Interaction in Nylon 6-Clay Hybrid Studied by Temperature Programmed Pyrolysis Techniques. *Polymer Journal* Vol 38, No 2 pp 171-177.

85) Sato M., (1999). Preparation of kaolinite – amino acid intercalates derived from hydrated kaolinite. *Clay and Clay Minerals* Vol. 47 No.6 pp 793-802.

86) Schmid-Wendtner M., H., Korting H., C.,(2006). The pH of the skin surface and its impact on the barrier function. *Skin Pharmacol. Physiol*., Vol. 19,

87) Summa V., Tateo F., (1998).The use of pelitic raw materials in thermal centres: mineralogy, geochemistry, grain size and leaching tests. Examples from the Lucania area(southern Italy); *Applied Clay Science* 12, 403–417.

88) Sun D., Li Y.,Zhang B., Pan X., (2010). Preparation and characterization of novel nanocomposites based on polyacrylonitrile/kaolinite, *Composites Science and Technology* Volume 70, Issue 6, June 2010, Pages 981–988

89) Tunney J. J., Detellier C., (1996), Chemically modified kaolinite. Grafting of methoxy groups on the interlamellar aluminol surface of kaolinite, *J. Mater. Chern*., 6(lo), pp; 1679-1685.

90) Tunney J.J., Detellier C.,(1996) Aluminosilicate Nanocomposite Materials. Poly(ethylene glycol)-Kaolinite Intercalates, *Chem. Mater*. 8,pp. 927-935.

91) TunneyJ.J.,Detellier C., (1994). Preparation and characterization of two distinct ethylene glucol derivatives of kaolinite, *Clays and Clay Minerals*, Vol. 42, No. 5, pp 552-560.

92) Turhan Y., Dogan M., Alkan M., (2010). Poly(vinyl chloride)/Kaolinite Nanocomposites: Characterization and Thermal and Optical Properties, *Ind. Eng. Chem*. Res. Vol. 49, pp. 1503–1513.

93) Unal H., Fındık F., Mimaroglu A., (2003). Mechanical behavior of nylon composites containing talc and kaolin, *Journal of Applied Polymer Science,* Volume 88, Issue 7, pages 1694–1697.

94) Usuki A., Kojima Y., Kawasumi M., Okada A., Fukushima Y.,Kurauchi T., Kamigaito O., (1993) Synthesis of nylon 6-clay hybrid, *J. Mater. Res*., Vol. 8, No. 5,

95) Uvdal K., Bodö P., Ihs A., Liedberg B., Salaneck W.R.,(1990). X-ray photoelectron and infrared spectroscopy of glycine adsorbed upon copper. *Journal of Colloid and Interface Science* Volume 140, Issue 1, Pages 207–216.

96) Veniale F., Bettero A., Jobstraibizer P., G., Setti M., (2007). Thermal muds: Perspectives of innovations, *Applied Clay Science* 36 , 141–147

97) Wada K., (1961). Lattice expansion of kaolin minerals by treatment with potassium acetate: *Am. Mineral*. 46,pp. 78-91.

98) Wada K., (1965). Intercalation of water in kaolin minerals: *Am. Min- eral*.80, pp.924-941.

99) Wang M.S., Pinnavaia T.J., (1994) Clay-Polymer Nanocomposites Formed from Acidic Derivatives of Montmorillonite and an Epoxy Resin, *Chem. Mater*.,6, pp.468-474.

100) Yariv S., Lapides I., Nasser A., Lahav N., Brodsky I., Michaelian K.H.,(2000). Infrared study of the intercalation of Potassium Halides in kaolinite, *Clays and Clay Minerals*. 48 no. 1p. 10-18.